Journal of Materials Chemistry C

REVIEW

View Article Online
View Journal

Cite this: DOI: 10.1039/d5tc01861g

A guide to mastering multi-resonance thermally activated delayed fluorescence: from challenges to strategies for high-performance OLEDs†

P. Keerthika, [b] Venkatramaiah Nutalapati*[bc] and Rajendra Kumar Konidena *[a]

Over the last decade, there has been a considerable upsurge in the development of organic emitters that produce narrowband emission and can utilize triplet excitons without relying on metal-containing components, thereby significantly advancing OLED technology. In particular, boron (B)- and heteroatom-doped polycyclic nanographenes with multi-resonance thermally activated delayed fluorescence (MR-TADF) have emerged as promising emitters. Compared with conventional donor–acceptor (D–A) TADF emitters, MR-TADF materials offer several advantages, including sharp emission spectra (a full width at half maximum of ≤40 nm), high photoluminescence efficiency, and small singlet–triplet energy gaps, making them strong contenders for next-generation OLEDs. Recently, MR-TADF emitters have demonstrated device efficiencies that surpass those of traditional TADF and phosphorescent emitters. However, several interconnected challenges persist, such as limited color tunability, sluggish exciton up-conversion rates, aggregation-induced quenching, efficiency degradation at high brightness, and limited operational lifetimes. These obstacles are often intertwined owing to fundamental "trade-offs" in material properties. Overcoming them requires precise molecular engineering and mastering material design. This review systematically examines the progress in B-based MR-TADF emitters, with a particular focus on molecular design strategies tailored to address these limitations. This study categorizes by emission color to aid the development of high-performance, full-color MR-OLEDs and concludes by outlining the current challenges and potential directions for future research on MR-TADF emitter development.

Received 9th May 2025,
Accepted 24th June 2025

DOI: 10.1039/d5tc01861g

rsc.li/materials-c

1. Introduction

Since the pioneering work of Tang and Van Slyke in 1987,[1] organic light-emitting diodes (OLEDs) have attracted considerable attention from academia and industry.[2–10] Today, OLEDs are widely employed in advanced display panels and solid-state lighting systems, largely owing to their intrinsic advantages over conventional lighting technologies. These advantages include low manufacturing costs, lightweight and flexible form, wide viewing angles, high contrast ratios, and low power consumption.[11–13] Central to the performance of OLEDs are organic emitters, which govern essential parameters such as emission color, spectral purity, charge transport characteristics, device efficiency, and operational stability.[14–22] Therefore, a comprehensive understanding of the structure–property relationships in organic emitters is crucial for the rational design of high-performance emitters.[23–25] Under electrical excitation, organic emitters generate excitons in a 1 : 3 ratio of singlets to triplets, as dictated by spin statistics.[26–31] First-generation fluorescent emitters, which rely solely on singlet excitons for radiative recombination, are inherently limited to an internal quantum efficiency (IQE) of 25%, typically translating to external quantum efficiencies (EQEs) of approximately 5%.[32–34] To circumvent this efficiency obstacle, second-generation phosphorescent emitters based on heavy-metal complexes were introduced.[35] These materials benefit from strong spin–orbit coupling (SOC), enabling the radiative utilization of triplet excitons and achieving near-unity IQE and EQEs exceeding 20%.[33,35–40] However, the reliance on scarce and potentially toxic noble metals such as iridium and platinum poses significant challenges in terms of sustainability, cost, and environmental impact.[41,42] Consequently, recent research efforts

[a] Department of Chemistry, Indian Institute of Technology-Patna, Bihta campus, Daylpur, Daulatpur, Patna, Bihar-801103, India. E-mail: rajsan@iitp.ac.in, rkonidena531@gmail.com
[b] Department of Chemistry, Faculty of Engineering and Technology, SRM Institute of Science and Technology, Kattankulathur, Chennai-603203, India. E-mail: venkatrv1@srmist.edu.in
[c] Centre for Interdisciplinary Research (CIDR), SRM University AP, Amaravati, Andhra Pradesh 522 240, India

† Electronic supplementary information (ESI) available. See DOI: https://doi.org/10.1039/d5tc01861g

have shifted toward the development of purely organic emissive emitters capable of accessing triplet excitons through alternative mechanisms, offering a more sustainable pathway toward next-generation OLED technologies.

In this regard, Adachi *et al.* introduced thermally activated delayed fluorescence (TADF) emitters, which have since become prominent candidates for next-generation OLEDs. TADF materials are capable of harvesting triplet excitons by converting them into emissive singlet excitons *via* reverse intersystem crossing (RISC), thereby enhancing device efficiency without relying on heavy metals (Fig. 1).[26,28–30,33,35,43–45] Efficient RISC depends on a small energy gap (ΔE_{ST}) between the lowest singlet (S_1) and triplet (T_1) excited states. To achieve this, typical TADF molecular designs adopt a twisted D–A architecture, which spatially separates the highest occupied molecular orbital (HOMO) and lowest unoccupied molecular orbital (LUMO), thereby reducing their overlap and minimizing ΔE_{ST}.[46–55] While this design strategy has enabled notable improvements in efficiency compared to traditional phosphorescent emitters, it also introduces several challenges. The reduced HOMO–LUMO overlap lowers the oscillator strength (f), resulting in slower radiative decay rates (k_r) and diminished photoluminescence quantum yield (PLQY), ultimately constraining the EQE in devices. Additionally, due to their emission from charge transfer (CT) states, conventional D–A TADF emitters tend to produce broad emission spectra, with FWHM values typically ranging from 70 to 100 nm.[56,57] This broad emission undermines color purity, complicates device architecture, and limits their suitability for high-definition display applications.[27,58–68] The importance of spectral precision has become more pronounced with the introduction of the BT.2020 color gamut standard by the International Telecommunication Union Radiocommunication

P. Keerthika

P. Keerthika received her Master's degree (MSc) in general chemistry from Annamalai University, Chidambaram, Tamil Nadu, India, in May 2022. Currently, she is pursuing her PhD in chemistry from SRM Institute of Science and Technology (SRMIST), Kattankulathur, Chennai, India, under the joint supervision of Dr Rajendra Kumar Konidena, Department of Chemistry, IIT-Patna, and Dr Venkatramaiah Nutalapati, SRMIST. Her current research work focuses on the design and synthesis of triplet harvesting deep-blue organic emitters for OLEDs.

Venkatramaiah Nutalapati

Dr Venkatramaiah Nutalapati obtained his PhD from Pondicherry University, India. He was a Post-Doctoral Fellow at the Indian Institute of Science (IISc), Bangalore, India (2011–2012), and a FCT post-doctoral fellow at the University of Aveiro, Portugal (2012–2016). Following Research Associate work at the Indian Institute of Science (IISc), Bangalore, India (2016–2017), he joined as Research Assistant Professor in the Department of Chemistry, SRM Institute of Science and Technology (SRMIST), in 2017 later promoted to Research Associate Professor at SRMIST from 2021. Recently, he moved to Centre for Interdisciplinary Research (CIDR), SRM University AP, Amaravati, Andhra Pradesh. He is an author of more than 152 research articles with an h-index of 28. His major research interests include supramolecular chemistry, OLEDs, photochemistry/photophysics of organic chromophores, and (chemo)sensors.

Rajendra Kumar Konidena

Dr Rajendra Kumar Konidena is an accomplished chemist with a strong academic and research background in organic chemistry and functional materials. He earned his Master of Science (MSc) in Organic Chemistry from Vellore Institute of Technology (VIT), Vellore, India, in 2012. He then pursued his doctoral studies at IIT-Roorkee, where he completed his PhD in 2017 under the guidance of Prof. K. R. Justin Thomas. Following his PhD, from 2018 to 2020, Dr Konidena undertook a postdoctoral fellowship sponsored by the NRF at Sungkyunkwan University, South Korea, in the research group of Prof. Jun Yeob Lee, focusing on advanced organic emitters for optoelectronic applications. He then joined the Technical University of Dresden, Germany, for a six-month postdoctoral stint. In July 2021, Dr Konidena began his tenure as a Research Professor at Kyung Hee University, Korea, a role he held until March 2022. Subsequently, he moved to Kyushu University, Japan, where he served as a JSPS Postdoctoral Fellow until April 2023. Returning to India, he worked as Research Assistant Professor at SRMIST for one year. In May 2024, Dr Konidena joined the Department of Chemistry at IIT-Patna as Assistant Professor. His research interests lie in the design and development of innovative organic functional materials for applications in optoelectronics and biomedical sciences.

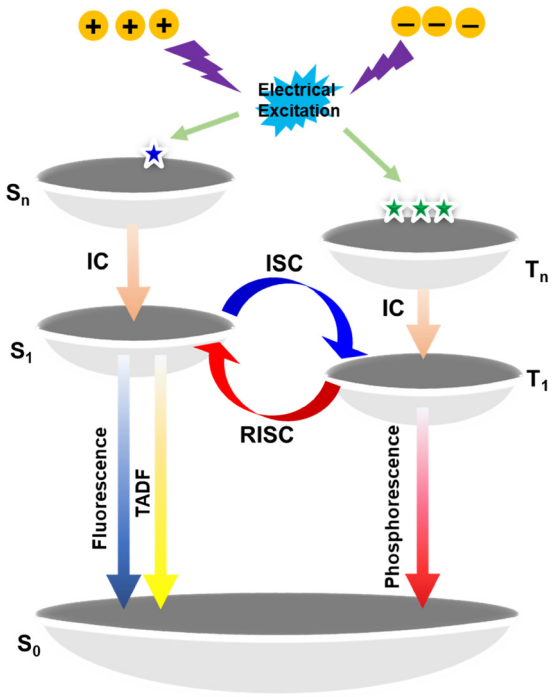

Fig. 1 Emission mechanism of different generation emitters.

Sector (ITU-R) in 2012, which specifies precise commission Internationale l'Éclairage (CIE) coordinates for red (0.708, 0.292), green (0.170, 0.797), and blue (0.131, 0.046) emission.[68] Meeting these stringent color requirements necessitates the development of high-efficiency narrowband emitters. Significant research efforts have been directed toward designing TADF materials with sharp emission profiles to address the inherent limitations of conventional D–A architectures and facilitate their integration into high-performance full-color OLEDs.

In this regard, Hatakeyama *et al.* introduced a novel emitter design strategy based on MR-TADF, which has since attracted widespread attention.[69–71] MR-TADF materials leverage complementary resonance effects between electron-donating heteroatoms and electron-accepting boron (B) atoms within a rigid nano-graphitic framework (Fig. 2). This innovative molecular architecture localizes the HOMO and LUMO on adjacent *ortho*- and *para*-carbon atoms of the aromatic core, resulting in spatially separated frontier orbitals and a small ΔE_{ST}, which is a prerequisite for RISC-based efficient triplet exciton harvesting. The highly rigid and planar structure of these molecules also suppresses vibrational relaxation, resulting in narrowband emission with FWHM values typically below 40 nm and PLQYs approaching unity. A representative MR-TADF emitter, **ν-DABNA**, exhibited exceptional blue emission with a FWHM of approximately 14 nm and an EQE nearing 34%, marking a significant leap in OLED emitter design.[72] This success catalysed the development of a wide array of MR-TADF compounds incorporating various heteroatoms, such as nitrogen, oxygen, sulfur, and carbonyl groups, as well as nitrogen-containing polycyclic aromatic hydrocarbons (PAHs). According to display standards established by the National Television System Committee (NTSC) and ITU-R, full-color high-definition OLED displays require precise red, green, and blue emissions. However, the weak CT nature inherent to MR-TADF structures, arising from their atomically localized HOMO and LUMO, poses a significant challenge in achieving red-shifted emission beyond the blue-green spectral region.[77–142] In particular, MR-TADF

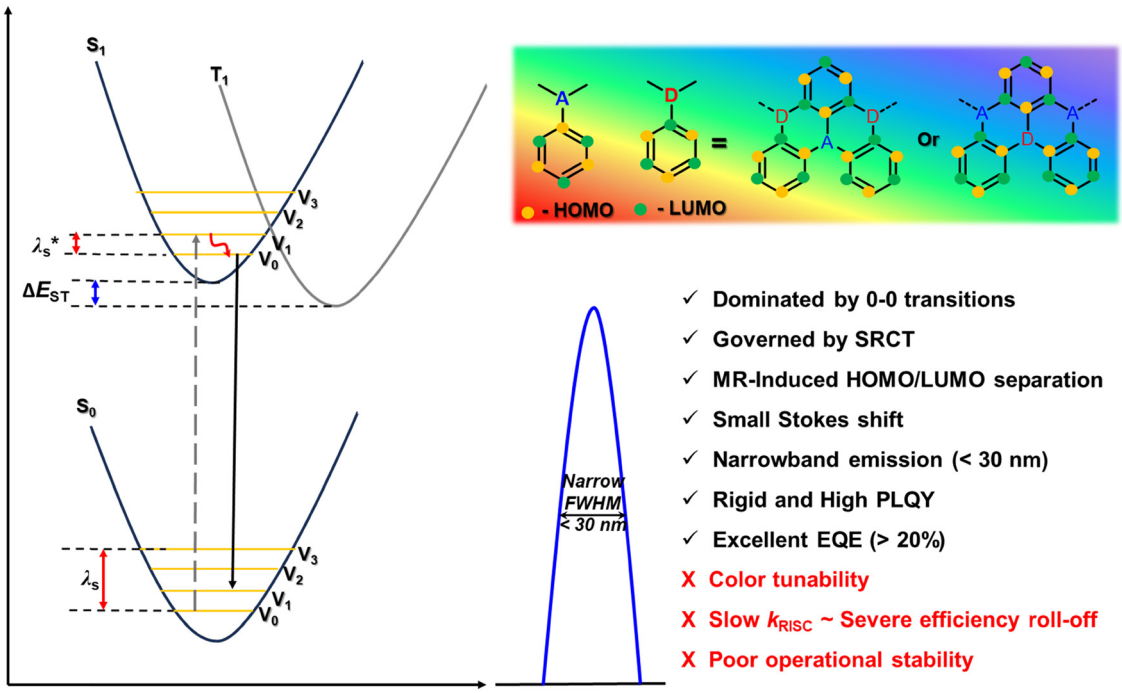

Fig. 2 Narrowband emission principle of MR-TADF emitters.

emitters with emission wavelengths beyond 550 nm and narrowband characteristics remain scarce, partly due to the limited flexibility in molecular design, the weak short-range CT (SRCT) character, and synthetic complexity.[142–178] This underscores a pressing need for innovative molecular engineering strategies capable of extending MR-TADF emission into the longer-wavelength (green-red) region while maintaining narrowband emission. Additionally, despite notable improvements in color purity and efficiency, MR-TADF emitters often exhibit relatively slow RISC rates ($k_{RISC} \approx 10^{-4}$ s^{-1}), which can lead to exciton accumulation, bimolecular quenching, and EQE roll-off under high-brightness conditions-factors that limit device performance in practical applications. This review provides a comprehensive overview of the recent advancements in the design of MR-TADF emitters, focusing on strategies for modulating the emission color across the visible spectrum and enhancing the RISC dynamics. Emitters are categorized by emission wavelength, and key molecular design principles, photophysical characteristics, and corresponding device performances are critically analysed. The review concludes with a discussion on the current limitations and emerging opportunities for achieving efficient, long-wavelength MR-TADF materials suitable for next-generation OLED technologies.

2. Challenges and strategies for blue MR-TADF emitters

The development of narrowband MR-UV emitters with short-wavelength (<400 nm) and FWHM <50 nm is a key challenge. Recently, Xu *et al.* synthesized new UV MR-emitters based on carbazole as the donor and phosphine oxide (P═O) as the acceptor, resulting in **CzP2PO** and ***t*BcZP2PO**.[177] The compounds exhibited a narrowband UV emission with a peak wavelength of <390 nm, FWHM of <35 nm and a high PLQY of 62% due to the synergistic MR effects of P═O and N-atoms. The combination of the steric and electronic effects of P═O simultaneously modulates the MR-effect and intermolecular interactions, resulting in P═O and N embedded PAH based OLEDs exhibiting efficient EQE (≤15.1%) and high color purity ($CIE_y \sim 0.04$).

In 2016, Hatakeyama *et al.* introduced an enticing molecular design involving the strategic substitution of B and O atoms within a rigid tricoordinate framework. This concept laid the foundation for the rapid development of MR-TADF materials incorporating B and various heteroatoms. Among these, emitters containing B/N have attracted significant attention owing to their unique electronic structure. The distinct resonance interactions between N and B enable the precise localization of the HOMO and LUMO on specific atoms within the molecular framework, thereby reducing the ΔE_{ST} and promoting efficient TADF behaviour. In their initial work, Hatakeyama *et al.* reported two B/N-based MR-TADF emitters, **DABNA-1** and **DABNA-2**, which exhibited emission red-shifted relative to their B,O-analog.[71] This shift is attributed to the stronger electron-donating character of nitrogen than that of oxygen. **DABNA-2** displayed a greater bathochromic shift due to the presence of phenyl and diphenylamine substituents, which act as auxochromes and further extend conjugation. Unlike conventional donor–acceptor TADF emitters, both **DABNA-1** and **DABNA-2** exhibited remarkably narrow emission profiles, with a FWHM of approximately 33 nm, indicative of high color purity. The measured ΔE_{ST} values for **DABNA-1** and **DABNA-2** were 0.18 eV and 0.14 eV, respectively, which are sufficiently small to facilitate RISC. Both compounds exhibited short τ_d and respectable RISC rates: 93.7 μs/9.9 × 10^3 s^{-1} for **DABNA-1** and 65.3 μs/14.8 × 10^3 s^{-1} for **DABNA-2**. These emitters were incorporated into OLED devices using an mCBP host matrix. The **DABNA-1**-based device emitted deep-blue light with a peak wavelength of 459 nm, a FWHM of 28 nm, and CIE coordinates of (0.13, 0.09). It achieved a maximum EQE of 13.5% and a current efficiency (CE) of 10.6 cd A^{-1}. Meanwhile, the **DABNA-2**-based device demonstrated superior performance, with a peak EQE of 20.2% and CE of 21.1 cd A^{-1} reflecting nearly complete exciton utilization and an estimated IQE approaching 100%. Notably, despite its red-shifted emission, **DABNA-2** maintained an impressively narrow FWHM (28 nm), comparable to that of **DABNA-1**. These findings underscore the strong potential of B/N-based MR-TADF materials in achieving high-efficiency, color-pure OLEDs, particularly in the blue emission range.

The same group introduced an advanced molecular design by incorporating two B and four N atoms into a rigid polycyclic framework, resulting in the MR-TADF emitter **ν-DABNA**.[72] This molecule exhibited an ultra-narrow blue emission centered at 468 nm in toluene, with an exceptionally small FWHM of only 14 nm, among the sharpest emissions reported for organic emitters. In the solid state, **ν-DABNA** maintained a small ΔE_{ST} of just 17 meV, enabling efficient triplet harvesting *via* RISC. Photophysical characterization revealed a PLQY of approximately 82%, along with τ_p/τ_d of 4.1 ns and 4.1 μs, respectively, indicative of a fast and effective RISC process. When integrated into an OLED device as the emissive material, **ν-DABNA** delivered outstanding performance, including high efficiency and minimal efficiency roll-off at high brightness. The device exhibited EL at 469 nm with a FWHM of 18 nm and CIE color coordinates of (0.12, 0.11), reflecting excellent color purity in the deep-blue region. These results highlight **ν-DABNA** as a benchmark MR-TADF emitter for achieving ultra-narrowband blue OLEDs with high efficiency and stability.

Subsequently, the same group reported a new MR-TADF emitter, **ν-DABNA-O-Me**,[73] in which an oxygen atom replaces the nitrogen atom present in the original **ν-DABNA**. This structural modification led to an ultrapure deep-blue emission in the solid state, with a peak emission wavelength of 464 nm and a narrow FWHM of 24 nm. The compound also exhibited high PLQY and efficient RISC. The enhanced RISC rate is primarily attributed to the restricted π-conjugation of the HOMO, which increases the energy gap between the HOMO and LUMO compared to the parent compound. Therefore, a larger frontier orbital separation is achieved, further optimizing the MR-TADF characteristics. When integrated into an OLED device, **ν-DABNA-O-Me** displayed EL at 465 nm with an

impressively narrow FWHM of 23 nm and CIE coordinates of (0.13, 0.10), indicating excellent color purity. The device also achieved a high EQE of 29.5%. Notably, compared to **ν-DABNA**, this derivative exhibited significantly reduced efficiency roll-off and improved operational stability, making it a promising candidate for high-performance blue OLED applications.

Naveen *et al.* developed three MR-TADF emitters, ***m*-ν-DABNA**, **4F-ν-DABNA**, and **4F-*m*-ν-DABNA**, by incorporating methyl groups at positions *para* to the B atoms and fluorine atoms at the *ortho* positions relative to N-atoms.[74] These structural modifications altered the electronic distribution, resulting in an increased bandgap due to the combined electron-donating and electron-withdrawing effects. As shown in Fig. 3, the compounds displayed deep-blue emission with peak emission wavelengths at 464, 457, and 455 nm for ***m*-ν-DABNA**, **4F-ν-DABNA**, and **4F-*m*-ν-DABNA**, respectively. They also exhibited excellent photophysical properties, including a PLQY of approximately 90% and a small $\Delta E_{ST} < 0.07$ eV, which facilitated efficient k_{RISC}. OLED devices fabricated with these emitters demonstrated outstanding performance, showing emission wavelengths/FWHM/EQE/CIE coordinates of 471 nm/18 nm/36.2%/(0.122, 0.12) for ***m*-ν-DABNA**, 464 nm/18 nm/35.8%/(0.13, 0.08) for **4F-ν-DABNA**, and 461 nm/18 nm/33.7%/(0.13, 0.06) for **4F-*m*-ν-DABNA**.

To enhance the color purity of **ν-DABNA**, Yasuda *et al.* introduced a series of ultrapure blue MR-TADF emitters, **BOBO-Z**, **BOBS-Z**, and **BSBS-Z**, by substituting the intra-cyclic nitrogen atoms with less electron-rich O and/or S atoms.[75] This structural modification led to a notable blue shift in their emission wavelengths in solution: **BOBO-Z** (441 nm), **BOBS-Z** (453 nm), and **BSBS-Z** (460 nm), compared to 468 nm for **ν-DABNA**. These materials retained sharp emission profiles with FWHM values ranging from 15 to 21 nm. The simulated CIE coordinates for **BOBO-Z** (0.15, 0.03), **BOBS-Z** (0.15, 0.06), and **BSBS-Z** (0.14, 0.07) align well with UHD display standards, indicating their potential for high-color-purity applications. In doped thin films (3 wt% in mCBP), these compounds showed deep-blue emission at 445 nm for **BOBO-Z**, 457 nm for **BOBS-Z**, and 464 nm for **BSBS-Z**. Notably, the S-containing compounds exhibited significantly higher k_{RISC} rates, 8.6×10^5 s^{-1} for **BOBS-Z** and 1.6×10^6 s^{-1} for **BSBS-Z**, which are approximately 2.4 and 4.2 times faster, respectively, than that of **ν-DABNA** (3.3×10^5 s^{-1}), likely due to the heavy atom effect. PLQYs were also improved in the S-containing compounds, with **BOBS-Z** and **BSBS-Z** achieving 94% and 93%, respectively, compared to 76% for **BOBO-Z**. OLED devices fabricated using these emitters exhibited high-performance metrics, including narrowband emission with FWHM values of 18 nm (**BOBO-Z**), 23 nm (**BOBS-Z**), and 22 nm (**BSBS-Z**), peak λ_{EL} at 445, 456, and 463 nm, and CIE coordinates of (0.15, 0.04), (0.14, 0.06), and (0.13, 0.08), respectively. These devices also achieved impressive EQE_{max} values of 13.6% for **BOBO-Z**, 26.9% for **BOBS-Z**, and 26.8% for **BSBS-Z**.

Wang *et al.* recently introduced a series of blue MR-TADF emitters, including **NBN**, ***t*BuNBN**, **SeNBN**, and **Se*t*BuNBN**.[76] By incorporating selenium (Se) at the *para*-position relative to the

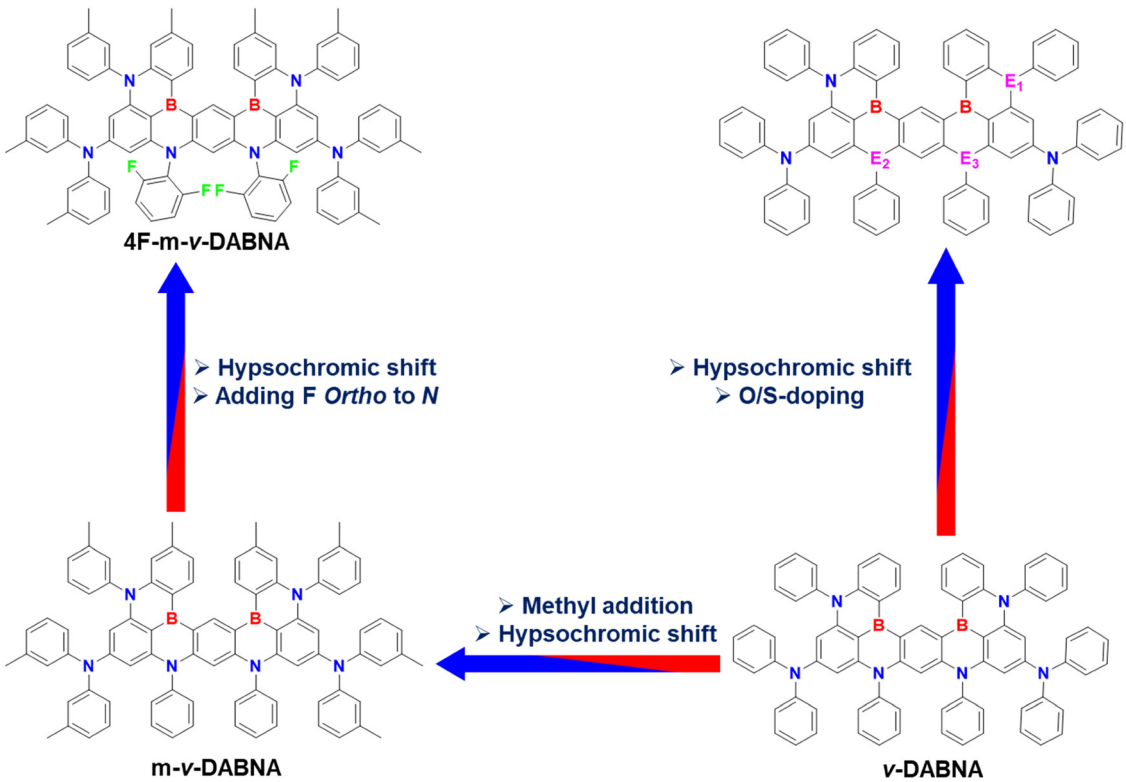

Fig. 3 Tuning the emission of **ν-DABNA** *via* chemical modifications.

B-atom in the core structures of **NBN** and ***t*BuNBN**, the resulting Se-containing derivatives exhibited a blue-shifted, narrowband emission along with enhanced SOC. Photophysical studies showed emission peaks and FWHMs of 477 nm (25 nm) for **NBN**, 489 nm (23 nm) for ***t*BuNBN**, 470 nm (24 nm) for **SeNBN**, and 481 nm (23 nm) for **Se*t*BuNBN**. Notably, the introduction of Se significantly boosted the RISC rates from 0.2×10^5 s^{-1} (**NBN**) and 0.1×10^5 s^{-1} (***t*BuNBN**) to 3.34×10^5 s^{-1} (**SeNBN**) and 2.30×10^5 s^{-1} (**Se*t*BuNBN**). OLED devices incorporating **SeNBN** and **Se*t*BuNBN** demonstrated impressive electroluminescent performance, with narrowband blue emission (FWHM of 29 nm and 25 nm, respectively), peak wavelengths near 480 nm, and EQE_{max} of approximately 25.5%. The inclusion of Se also helped minimize efficiency roll-off, contributing to overall improved device stability and performance.

Hatakeyama *et al.* synthesized the extended hetero-helicene **V-DABNA-Mes**, which consists of three B atoms and six N atoms, using a one-step borylation reaction.[77] The electronic interaction between the N- and B-atoms imparts an MR character to **V-DABNA-Mes**, resulting in a narrow PL emission with a peak at 484 nm. This emission is red-shifted compared to the parent compound, ***ν*-DABNA**, owing to the extended π-skeleton. **V-DABNA-Mes** exhibited an improved MR effect, with a narrow ΔE_{ST} of 0.04 eV, a short τ_d of 2.39 μs, and a k_{RISC} of 4.4×10^5 s^{-1}, outperforming the parent structure. The solution-processed OLED device based on **V-DABNA-Mes** exhibited EL with a peak emission wavelength of 480 nm, a FWHM of 27 nm, CIE coordinates of (0.09, 0.21), an EQE of 22.9%, and a CE of 26.7 cd A^{-1}.

Kim *et al.* developed a pure blue MR-TADF emitter, ***m*BP-DABNA-Me**, by introducing *meta*-xylenyl and *meta*-phenylphenylamine substituents into the DABNA core.[78] These modifications effectively reduced aggregation-induced quenching and prevented isomer formation. The emitter exhibited narrow blue emission with a peak wavelength of 464 nm, a FWHM of 28 nm, and an impressively high PLQY of 97%. OLED devices incorporating ***m*BP-DABNA-Me** demonstrated excellent performance, achieving an EQE_{max} of 24.3%, a CE of 24.3 cd A^{-1}, and blue EL with CIE coordinates of (0.124, 0.140). The EL spectrum remained highly stable even at doping concentrations above 20%, which was attributed to the suppression of intermolecular interactions by the incorporated bulky substituents.

Lee *et al.* developed ***t*-DABNA**, a *tert*-butyl-substituted derivative of **DABNA-1**, to reduce aggregation-induced emission quenching.[79] This modification resulted in a 5 nm red shift in emission and a slightly lower ΔE_{ST} of 0.17 eV while maintaining a long τ_d of 83.3 μs. When evaluated as dopants in a DPEPO host, ***t*-DABNA** and **DABNA-1** achieved EQE_{max} values of 25% and 18.7%, respectively. However, both suffered from significant efficiency roll-off due to the extended τ_d. To address this, **DMAC-DPS** was introduced as an assistant dopant, which effectively suppressed triplet exciton accumulation. This approach improves the device performance by maintaining a τ_d of 83.3 μs and increasing the k_{RISC} to 2.44×10^3 s^{-1}. Notably, the operational lifetime of the ***t*-DABNA**-based devices improved significantly by nearly tenfold when using the assistant dopant, compared to devices based solely on the DPEPO host. Furthermore, ***t*-DABNA** and **DABNA-1** were successfully applied as fluorescent dopants to mitigate triplet exciton quenching. When anthracene-based ADN, a wide band-gap host, was employed, back energy transfer helped lower the triplet exciton density. Under these conditions, ***t*-DABNA** and **DABNA-1** delivered EQE_{max}/CE values of 31.4%/13.0 cd A^{-1} and 13.5%/10.6 cd A^{-1}, respectively, confirming the enhanced efficiency and triplet management of the modified system.

Subsequently, the same group introduced a new blue MR-TADF emitter, ***t*-DABNA-d*t*B**, by incorporating di-*tert*-butylbenzene substituents into the ***t*-DABNA** core.[80] This structural modification effectively suppressed quenching processes by limiting intermolecular interactions (Chart 1). The emitter displayed a high PLQY and a narrow emission bandwidth with a FWHM of approximately 22 nm. In OLED applications, ***t*-DABNA-d*t*B** achieved an EQE of 11.4%, with an operational lifetime (LT_{95}) of 208 hours at 1000 cd m^{-2}, and exceeding 10 000 hours at 100 cd m^{-2}. It emitted a pure blue light at 471 nm, with a CIE_y coordinate of ∼0.13. Notably, in a tandem OLED configuration optimized with this emitter, the device reached an EQE above 25% and an extended LT_{95} of over 500 hours at 1000 cd m^{-2}, demonstrating both high efficiency and excellent operational stability (Table S2, ESI†).

Su *et al.* developed two multi-resonant TADF emitters, **IDAD-BNCz** and **TIDAD-BNCz**, using a sterically hindered donor decoration strategy.[81] This approach introduced rigid and bulky IDAD and TIDAD units, which effectively suppressed ACQ without promoting intermolecular vibrations or non-radiative relaxations, thereby maintaining high luminescence efficiency even at elevated doping levels. Additionally, the electron-donating nature of the IDAD and TIDAD groups elevated the CT state energy, contributing to an enhanced RISC rate (Fig. 4). Both emitters displayed blue emission with peak wavelengths of 489 nm (FWHM ∼ 23 nm) for **IDAD-BNCz** and 488 nm (FWHM ∼ 22 nm) for **TIDAD-BNCz**, accompanied by near-unity **PLQYs**. When applied in OLED devices, they emitted sky-blue light with EL peak wavelengths of 492 nm and FWHMs of 29 nm (**IDAD-BNCz**) and 30 nm (**TIDAD-BNCz**). These devices delivered exceptional performance, with EQE values ranging from 29.6% to 31.3% for **IDAD-BNCz** and 30.9% to 34.3% for **TIDAD-BNCz** as the dopant concentration increased from 3 wt% to 20 wt%. Notably, the devices also exhibited minimal efficiency roll-off, highlighting their potential for high-performance, stable blue OLED applications.

Wang *et al.* employed a peripheral cladding design strategy by introducing diphenylamine and *t*Bu groups into the **DABNA-1** framework, forming a B–π–N architecture aimed at achieving narrowband deep-blue TADF emission while suppressing intermolecular interactions and concentration quenching.[82] The resulting compounds (**PAB**, **2tPAB**, and **3tPAB**) exhibited deep-blue emission, with **PAB** emitting at 449 nm, while **2tPAB** and **3tPAB** exhibited red-shifted emissions at 456 nm. All compounds maintained narrow spectral profiles with FWHM values ranging from 23 to 26 nm, PLQYs between 60% and 74%, and short τ_d of 55–74 μs. These features were attributed to an

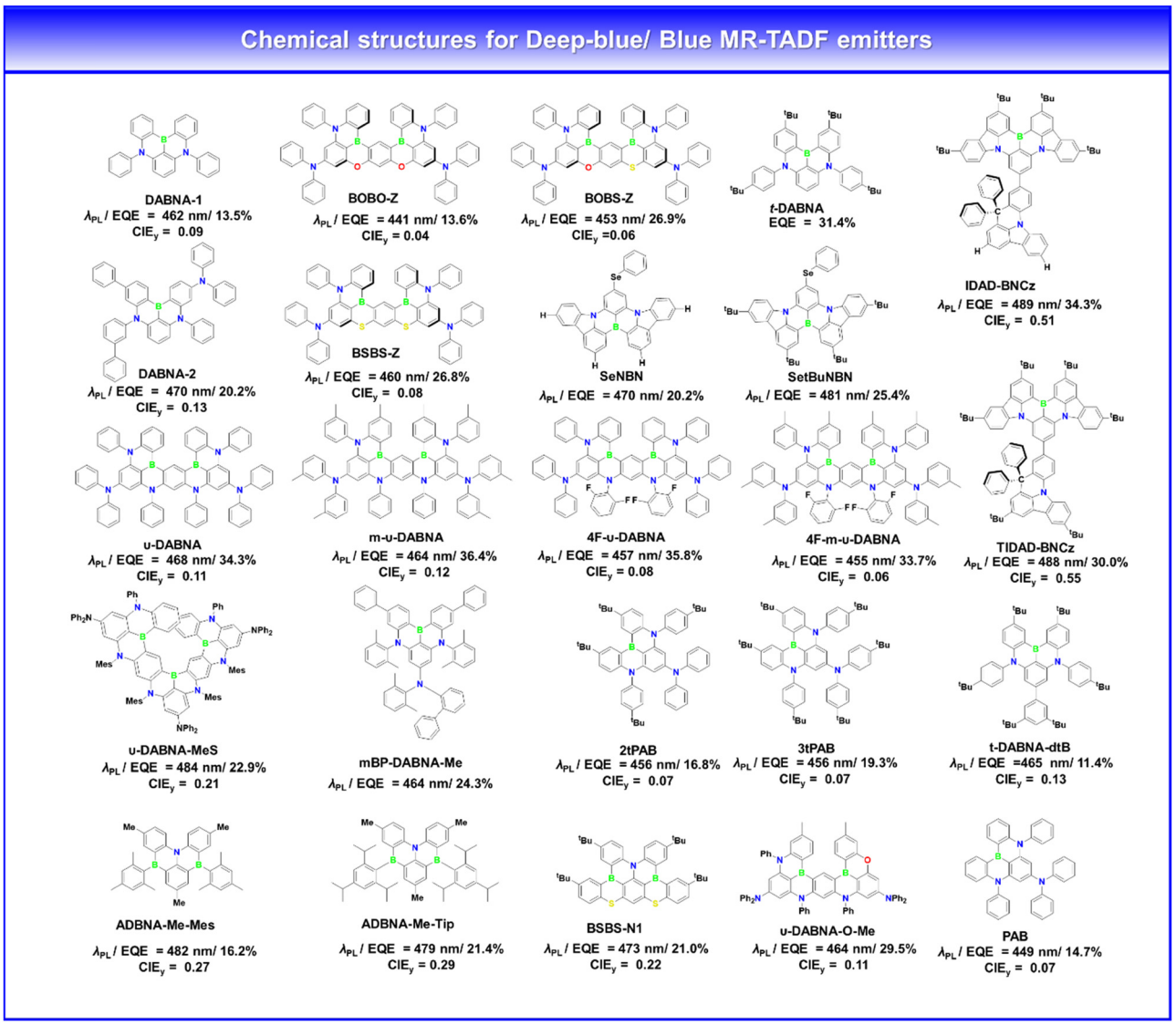

Chart 1 Chemical structure of blue MR-TADF emitters.

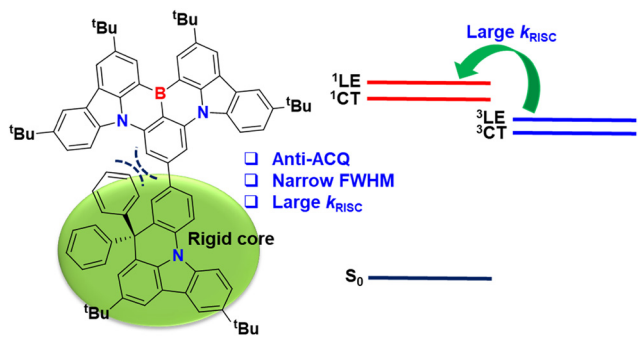

Fig. 4 MR-TADF emitter with synergetic steric hindrance and excited state modulation.

increased ΔE_{ST}, which in turn reduced the RISC rate compared to the parent compound **DABNA-1** (Table S1, ESI†). OLED devices fabricated using these emitters produced deep-blue EL at 456 nm (**PAB** and **2tPAB**) and 460 nm (**3tPAB**), with FWHMs of 31 nm, 27 nm, and 26 nm, respectively, and consistent CIE coordinates of (0.14, 0.07). In terms of performance, **PAB** achieved an EQE of 14.7%, CE of 10.4 cd A^{-1}, and PE of 7.1 lm W^{-1}; **2tPAB** delivered 16.8%, 11.8 cd A^{-1}, and 8.0 lm W^{-1}; and **3tPAB** delivered 19.3%, 34.4 cd A^{-1}, and 10.2 lm W^{-1}, respectively. The incorporation of *t*Bu groups provided peripheral shielding that significantly improved device performance and emission stability.

Hatakeyama *et al.* developed two novel MR-TADF emitters, **ADBNA-Me-Mes** and **ADBNA-Me-Tip**, each featuring a molecular structure comprising two boron atoms and one nitrogen atom.[83] These ADBNA-based compounds exhibit photophysical properties comparable to the well-known **DABNA-1**, delivering narrowband blue emissions with peak wavelengths of 482 nm (FWHM ∼ 34 nm) for **ADBNA-Me-Mes** and 479 nm (FWHM ∼ 33 nm) for **ADBNA-Me-Tip**, along with high PLQYs of 88.9% and 87.6%, respectively. OLEDs incorporating these materials

as the emissive layer demonstrated efficient blue emission. The device using **ADBNA-Me-Tip** emitted at 480 nm with a FWHM of 32 nm and achieved an EQE_{max} of 21.4%. Similarly, the **ADBNA-Me-Mes**-based device emitted at 481 nm, also with a FWHM of 32 nm, and reached an EQE_{max} of 16.2%. These results highlight the potential of ADBNA-type structures for high-efficiency, narrowband blue OLED applications.

Yasuda *et al.* designed a nanographitic fused-nonacyclic π-system, named **BSBS-N1**, incorporating multiple N, O, and S atoms as an MR-TADF emitter.[84] The structure features phenothiaborin subunits with two S atoms, which were intended to enhance the multi-resonance effect through interactions with adjacent nitrogen atoms due to their electron-rich nature. This design also leveraged the heavy atom effect of sulfur to boost the k_{RISC} rate. Photophysical characterization showed that **BSBS-N1** emits narrow sky-blue fluorescence, with a peak emission at 473 nm and a FWHM of 21 nm in toluene. A slightly red-shifted emission was observed at 478 nm in the solid film state, with an FWHM of 24 nm and a high PLQY of 89%. The compound also exhibited a notably high RISC rate of $1.9 \times 10^6\ s^{-1}$, attributed to its ΔE_{ST} of 0.14 eV and the presence of sulfur atoms. When used in OLED devices, **BSBS-N1** delivered excellent electroluminescent performance with an EQE of up to 21.0%. However, the devices experienced significant efficiency roll-off at higher brightness levels, likely due to the combination of fast k_{RISC} and limited bimolecular exciton quenching. The EL emission was centered around 478 nm, with a narrow FWHM of 25 nm, underscoring its potential for high-color-purity blue OLEDs.

The same group further explored the impact of heavy atoms on the properties of MR-TADF materials by introducing heteroatoms (N, O, and Se) into the core structure (Fig. 5). They synthesized three new MR-TADF emitters: **CzBO**, **CzBS**, and **CzBSe**.[85] Photophysical analysis revealed that all three compounds emitted in the blue region and exhibited low ΔE_{ST} values, all below 0.16 eV. **CzBSe** demonstrated the fastest k_{RISC} rate of $1.8 \times 10^8\ s^{-1}$, significantly faster than **CzBO** at $0.9 \times 10^4\ s^{-1}$ and **CzBS** at $2.2 \times 10^5\ s^{-1}$, attributed to the strong SOC induced by the Se atom. The OLED devices fabricated using these compounds exhibited promising performance. Of the three emitters, **CzBSe** exhibited the highest EQE_{max} of 23.9%, minimal efficiency roll-off and a CIE_y coordinate of 0.24, highlighting its superior potential for blue OLED applications.

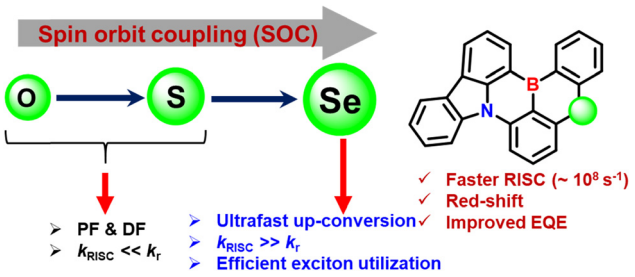

Fig. 5 Effect of heavy atoms on SOC and k_{RISC} of MR-TADF emitters.

Lee *et al.* developed a series of MR-TADF emitters, including **B-O-dpa**, **B-O-Cz**, **B-O-dmAc**, and **B-O-dpAc**, featuring asymmetric molecular structures with B, O and N atoms.[86] The light emission characteristics of these compounds were tailored by substituting the aromatic units attached to the nitrogen atom with **B-O-dpa**, **B-O-Cz**, **B-O-dmAc**, and **B-O-dpAc**. The introduction of a weak electron-donating oxygen atom into the structure resulted in blue emission, with the emission color being influenced by the specific aromatic unit linked to nitrogen. Among the synthesized emitters, **B-O-dpa** exhibited a narrow pure blue emission with a peak wavelength of 443 nm and a FWHM of 28 nm. The acridine-substituted compounds (**B-O-dmAc** and **B-O-dpAc**) demonstrated the advantage of high EQE and low efficiency roll-off, which can be attributed to the accelerated RISC mechanism and weak ICT character. When used in OLED devices, these compounds exhibited satisfactory performance in the DPFPO host. Specifically, the **B-O-dpa** emitter achieved an EQE_{max} of 16.3%, a deep-blue EL emission with a FWHM of 32 nm, and a CIE coordinate of (0.15, 0.05).

In a continuation of their work, Yang *et al.* introduced a series of MR-TADF emitters, including **CzBNO**, **DMAcBNO**, and **DPACBNO**, following a similar design strategy.[87] These compounds exhibited excellent TADF properties due to the opposing resonance effects of the B, N, and O atoms. All materials exhibited blue emission with narrow FWHM values. The OLED device using the **CzBNO** emitter emitted deep-blue light with a FWHM of 36 nm and achieved a maximum EQE of 13.6%. **DMAcBNO** and **DPACBNO** exhibited higher EQE values of 20.4% and 23.0%, respectively. Sensitizer-assisted devices using **DMAcBNO** and **DPACBNO** achieved EQE values of up to 29.6% with minimal efficiency roll-off.

Subsequently, the same group developed a series of MR-TADF emitters using a peripheral decoration strategy. They synthesized three new emitters, **DPACzBN1**, **DPACzBN2**, and **DPACzBN3**, by incorporating varying numbers of DPA units onto the parent **CzBN** core.[88] These compounds exhibited blue emission with a FWHM of approximately 21 nm in solution but showed a red-shifted emission in doped films. The introduction of DPA units enhanced the PLQY and k_{RISC}, leading to a narrower FWHM in the EL emission as the number of DPA units increased. **DPACzBN3** exhibited the best performance among these emitters, with a deep-blue emission and FWHM of 20 nm. The OLED device made with this emitter emitted light from blue to sky blue and achieved an impressive EQE of 27.7%.

Xu *et al.* developed an ambipolar self-hosted MR-TADF emitter, ***t*CBNDADPO**, by combining **CzBN** with the phosphine oxide-based ambipolar core **DADPO**.[89] This design enhanced the TADF characteristics of ***t*CBNDADPO**, achieving an accelerated k_r of $2.11 \times 10^8\ s^{-1}$ and suppressed k_{nr} (Fig. 6). The emitter displayed a narrow blue emission with a maximum wavelength of 466 nm, an FWHM of 26 nm, a PLQY of 99%, and short τ_p and τ_d values of 2.67 ns and 1.9 μs, respectively. OLED devices with a high doping ratio of 30 wt% achieved an EQE of 30.8%, while non-doped OLEDs reached an EQE of 30%, demonstrating the effectiveness of the self-host strategy for developing efficient host-free MR-TADF emitters.

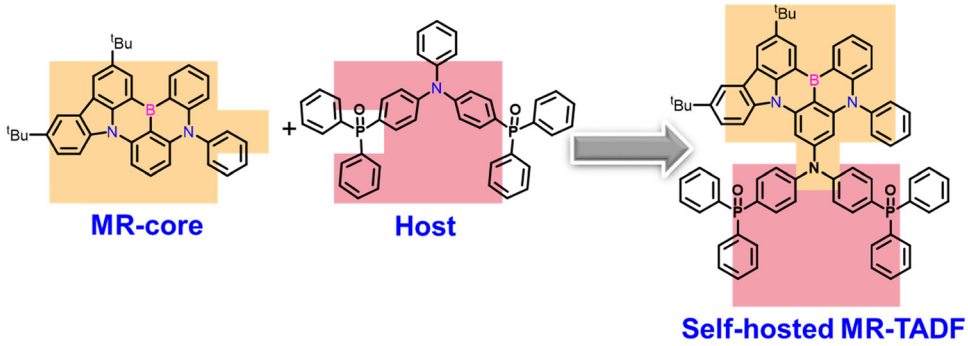

Fig. 6 MR-TADF emitters with a self-hosting strategy.

The same group later reported three blue MR-TADF emitters, **PTZBN1**, **PTZBN2**, and **PTZBN3**, which were developed using the same peripheral modification strategy.[90] By incorporating the DPA unit into the parent compound (**PTZBN2**), the emission wavelengths of the compounds were hypsochromically shifted from 490 nm (**PTZBN1**) to 468 nm (**PTZBN3**). The sulfone group in **PTZBN3** helped control the emission in the narrow deep-blue region, resulting in a high PLQY of 98% and an FWHM of 30 nm. OLED devices based on **PTZBN1**, **PTZBN2**, and **PTZBN3** achieved maximum EQEs of 26.9%, 30.5%, and 19.9%, respectively. The sensitized-TADF device based on **PTZBN2** achieved an EQE_{max} of 34.8%, while the **PTZBN3**-based device exhibited an EL emission at 368 nm with an EQE_{max} of 32.0%, although with efficiency roll-off due to the presence of sulfone.

The same group later developed three deep-blue MR-TADF emitters (**BN1**, **BN2**, and **BN3**) with progressively larger ring-fused structures and increased rigidity.[91] All three emitters exhibited high PLQY values above 90% and an increase in k_{RISC} from **BN1** to **BN3**. These compounds emit deep-blue light with a CIE_y coordinate below 0.08. The OLED device based on **BN3** achieved a maximum EQE of 37.6%, with reduced efficiency roll-off, marking the highest performance reported for deep-blue TADF OLEDs. These results highlight the potential to enhance OLED performance by optimizing the fused π-conjugated skeleton, which improves the RISC process.

Jiang *et al.* introduced a new design using spirobifluorene (SBF) as a building block with an MR-core, resulting in **SF1BN** and **SF3BN** at the C1 or C3 positions.[92] Both emitters exhibited similar photophysical properties, showing narrow bluish-green emission with maximum wavelengths of 493 nm and FWHMs of 23 and 25 nm (Fig. 7). The SBF-substituted derivatives effectively prevented aggregation, even at high doping concentrations, achieving high PLQYs of 93% and 90% for **SF3BN** and

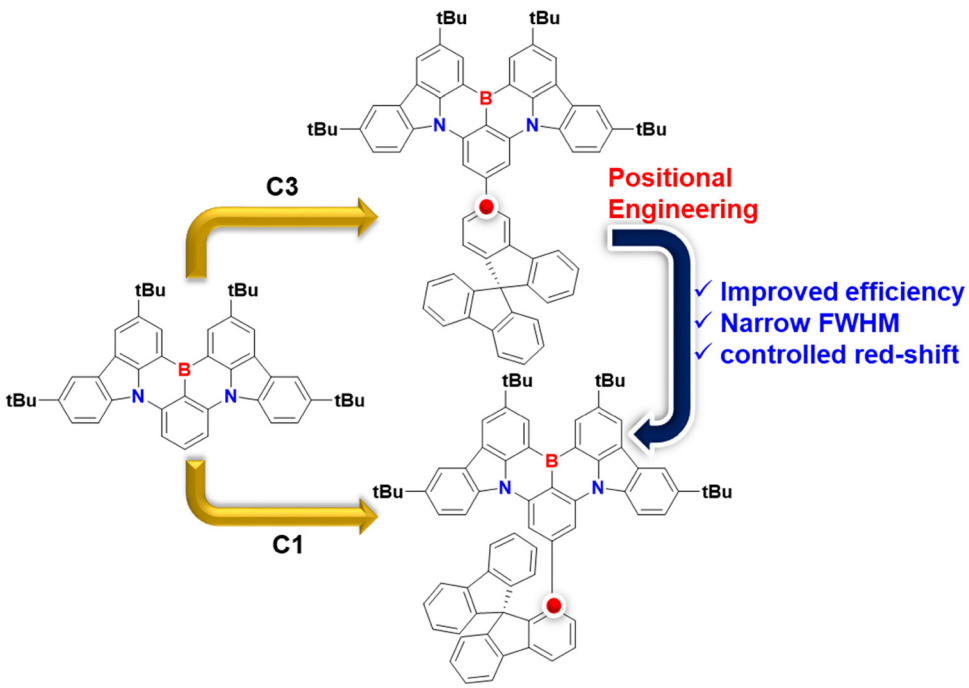

Fig. 7 SBF positional engineering to control emission in the blue region with a narrow FWHM.

SF1BN, respectively. OLED devices based on these emitters demonstrated a 1.5-fold increase in EQE (32–35%) compared to their parent molecule, BNCz.

Kwon *et al.* developed two novel carbazole-fused MR-TADF analogues, ***m*ICZ-DABNA** and **BFCz-DABNA**, using a new design strategy.[93] In this approach, electron-donating groups-N-atoms in ***m*ICZ-DABNA** and O-atoms in **BFCz-DABNA** were introduced at the periphery, inducing an inductive effect that influenced the electron density of the central nitrogen and the bandgap energy. The photophysical properties of these compounds revealed blue emission with maximum wavelengths of 461 nm and 456 nm and FWHMs of 22 nm. Both compounds exhibited high PLQY values of 92.6% and 93.1% for ***m*ICZ-DABNA** and **BFCz-DABNA**, respectively, with a consistent ΔE_{ST} of 0.20 eV. OLED devices based on these compounds demonstrated EL emission at 466 nm with an FWHM of 26 nm, CIE coordinates of (0.13, 0.11), and an EQE_{max} of 26.4% for ***m*ICZ-DABNA**. For **BFCz-DABNA**, the device emitted at 463 nm with a FWHM of 26 nm, CIE coordinates of (0.13, 0.09), and an EQE_{max} of 28% (Chart 2).

Colman *et al.* developed a novel MR-TADF emitter, **NOBNacene**, which features a boron, nitrogen, and oxygen-doped linearly extended ladder-type structure.[94] The **NOBNacene** emission spectra revealed deep-blue emission, with a peak wavelength at 410 nm and a narrow FWHM of 38 nm, resulting in a 71% PLQY film. In solution, **NOBNacene** exhibited a PL maximum at 405 nm, a FWHM of 40 nm, and a PLQY of 33%. Notably, **NOBNacene** displayed a weak TADF characteristic with a τ_d of 1.18 ms and a k_{RISC} of 3.74×10^3 s^{-1}, due to its large ΔE_{ST} of 0.30 eV. OLED devices incorporating **NOBNacene** were fabricated by doping it into either TSPO1 or DPEPO at various concentrations. The TSPO1-based device showed superior performance, achieving an EQE of 11.2% and emitting deep-blue light with CIE coordinates of (0.176, 0.068).

Recently, Adachi *et al.* developed the narrowband deep-blue helical MR-TADF material, ***f*-DOABNA**, by combining the DABNA and DOBNA fragments to achieve a small ΔE_{ST} and a large SOC, enhancing the k_{RISC}.[95] The ***f*-DOABNA** exhibits a small ΔE_{ST} and a π-delocalized structure, resulting in a high SOC of 0.44 cm^{-1}, which leads to a short-delayed fluorescence lifetime and an elevated k_{RISC}. This B, N, and O-doped helicene demonstrated an exceptionally high k_{RISC} compared with other blue MR-TADF materials, with an emission at 442 nm, an FWHM of 18 nm, a PLQY of 93%, and an ΔE_{ST} of 0.08 eV. The reduced ΔE_{ST} resulted in a short τ_d of 1.22 μs and an outstanding k_{RISC} of 1.41×10^6 s^{-1}. The OLED device fabricated with mCP as the host

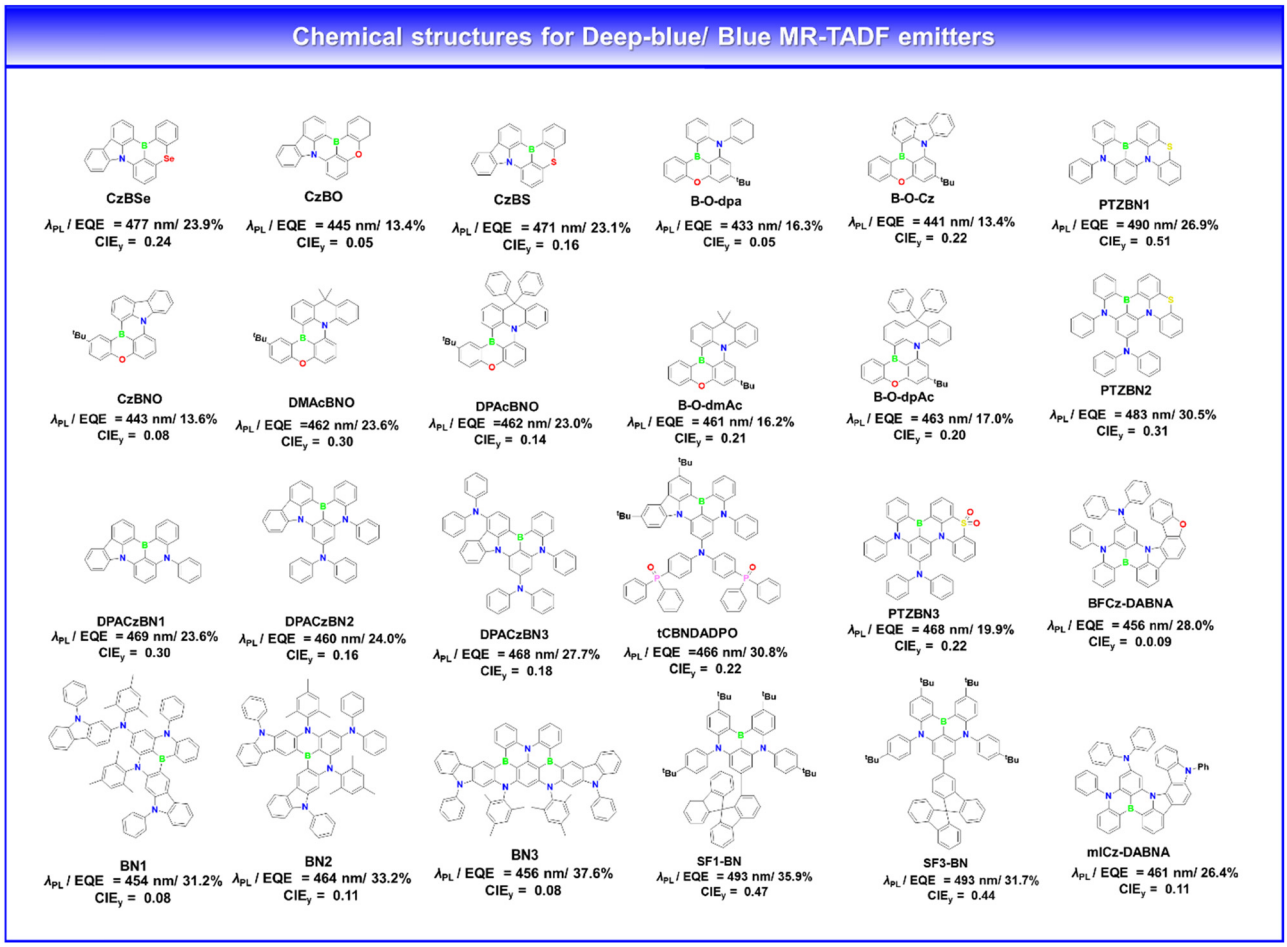

Chart 2 Chemical structure of the deep-blue/blue MR-TADF emitters.

displayed deep-blue emission with a peak wavelength of 445 nm, an FWHM of 24 nm, and CIE(x, y) coordinates of (0.150, 0.04), marking the first MR-TADF material to achieve a CIE$_y$ coordinate of 0.04, with a maximum EQE of 15.9%.

Recently, Zhang *et al.* successfully synthesized three MR-TADF materials referred to as **CFDBO**, **CFDBA**, and **CFDBCz** by incorporating carbazole into BN-PAHs in a single-step borylation reaction with a high yield of 70%.[96] The inclusion of peripheral groups, such as oxygen atoms, diphenylamine, and carbazole units, in these MR-TADF materials effectively suppressed the intermolecular interactions (Fig. 8). The emission wavelengths of **CFDBO**, **CFDBA** and **CFDBCz** were 452, 467 and 479 nm, respectively, with FWHMs of 18, 16 and 18 nm, respectively. Additionally, the PLQY of **CFDBO**, **CFDBA** and **CFDBCz** were 94%, 96% and 96% while τ_p/τ_d of 3.25 ns/60.79 μs, 3.01 ns/70.51 μs and 4.49 nm/32.66 μs, respectively. The corresponding OLED devices show EL emission in the blue region with peak wavelengths (FWHM) of 460 nm (24 nm), 473 nm (21 nm) and 488 nm (22 nm) for **CFDBO**, **CFDBA** and **CFDBCz**, respectively. The OLEDs of **CFDBO**, **CFDBA** and **CFDBCz** exhibited excellent performance with EQEs of 20.7%, 30.9% and 32.4%, respectively.

Kwon *et al.* developed two blue MR-TADF emitters, **TPD4PA** and ***t*Bu-TPAD4PA**, by integrating a rigid oxygen-bridged DOBNA with a PAB unit, resulting in emitters with improved ICT characteristics.[97] Photoluminescence studies indicated that both compounds exhibited deep-blue emissions, with maximum wavelengths of 445 and 451 nm, respectively, and a FWHM of 19 nm. These materials show small ΔE_{STs} of 0.05 eV and 0.06 eV and high PLQY values of 88.1% and 90.3%, respectively, with k_{RISC} around 2.5 × 10^5 s^{-1} for **TPD4PA** and ***t*Bu-TPAD4PA**. OLED devices utilizing **TPD4PA** and ***t*Bu-TPAD4PA** achieved maximum EQEs of 30.7% and 32.5%, respectively. In addition, both devices demonstrated narrowband deep-blue emissions with peak wavelengths at 455 and 460 nm, along with CIE color coordinates of (0.14, 0.06) and (0.14, 0.07), respectively. To the best of our knowledge, this is the first report of a device performance that maintains deep blue color emissions (CIE$_y$ coordinate below 0.07) and a high RISC rate for double boron-embedded low molecular-weight MR-TADF emitters.

Recently, Zhang *et al.* introduced a novel concept utilizing out-of-plane interactions, specifically π–π and lone pair-π-interactions, to create a spatial perturbation (SPPT) aimed at enhancing the TADF performance (Fig. 9). This work resulted in two blue MR-TADF emitters, ***o*-BNPO** and **BNPO**.[98] The ***o*-BNPO** compound exhibits a folded structure that facilitates intramolecular π–π stacking and noncovalent interactions with its DPPO moiety. In contrast, the direct attachment of DPPO to the **D*t*BuCzB** framework in **BNPO** disturbs π-conjugation and diminishes out-of-plane interactions, resulting in weaker SPPT interactions compared with ***o*-BNPO**. Photophysical analysis indicates that both compounds emit blue light, with peak wavelengths of 494 nm (FWHM = 22 nm) for ***o*-BNPO** and 492 nm (FWHM = 22 nm) for **BNPO**, both of which are red-shifted relative to the parent compound, **D*t*BuCzB**. Furthermore, OLED devices incorporating 8 wt% of ***o*-BNPO** and **BNPO** demonstrated similar electroluminescent emissions, with peak wavelengths of 496 nm and FWHM values of 26 nm and 25 nm, respectively. The maximum EQE for the **BNPO**-based device is 24.6%, while ***o*-BNPO** achieves 36.0%, accompanied by reduced efficiency roll-off. The superior device performance of ***o*-BNPO** is attributed to its SPPT effect and the strategic spatial positioning of the DPPO moiety.

Zhang *et al.* developed the MR-TADF emitter **DPMX-CzDABNA**, which features significant steric hindrance for use in white OLEDs.[99] In solution, this compound exhibits a narrow PL emission in the blue region, with a peak wavelength at 471 nm (FWHM ∼ 22 nm). A thin film comprising 15 wt% **DPMX-CzDABNA**:SF3-TRZ demonstrates a narrowband emission at 481 nm and a PLQY of 94.2%. Transient PL studies revealed that the compound has an ΔE_{ST} of 0.11 eV, a τ_d of 14.8 μs, a τ_p of 4.3 ns, and a k_{RISC} of 6.6 × 10^4 s^{-1}. The corresponding OLED devices show nearly identical narrowband EL spectra, peaking at 484 nm with FWHMs of 29 nm. The corresponding CIE coordinates are approximately (0.11, 0.31), placing them in a desirable blue region for achieving high-quality white emission, with a maximum EQE of 24.5%.

Wang *et al.* synthesized two heterocyclic-based MR-TADF molecules, **Py-BN** and **Pm-BN**, by strategically incorporating one or two nitrogen atoms into the HOMO-distributed positions of the central aromatic ring of the BCz-BN skeleton.[100] The introduction of nitrogen atoms stabilized the HOMO energy and facilitated the formation of intramolecular hydrogen bonds, leading to the hypsochromic shift and narrower emission spectra compared to the parent core (Fig. 10). In the

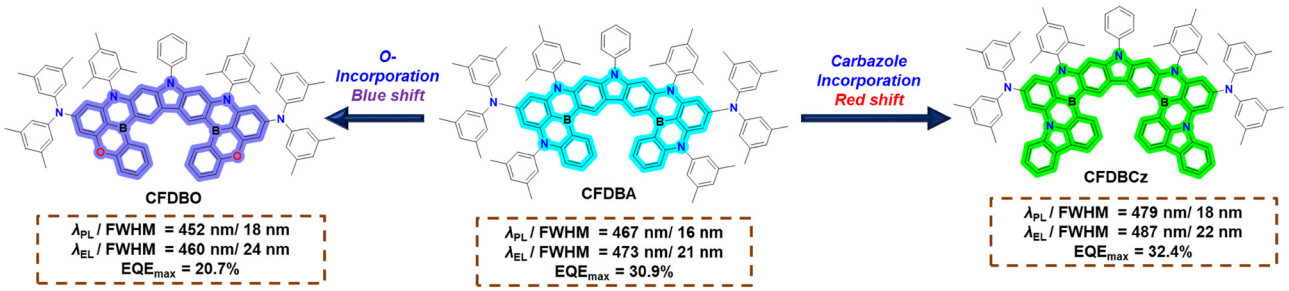

Fig. 8 Carbazole fused dual B,N-based MR-TADF emitters for narrowband emission.

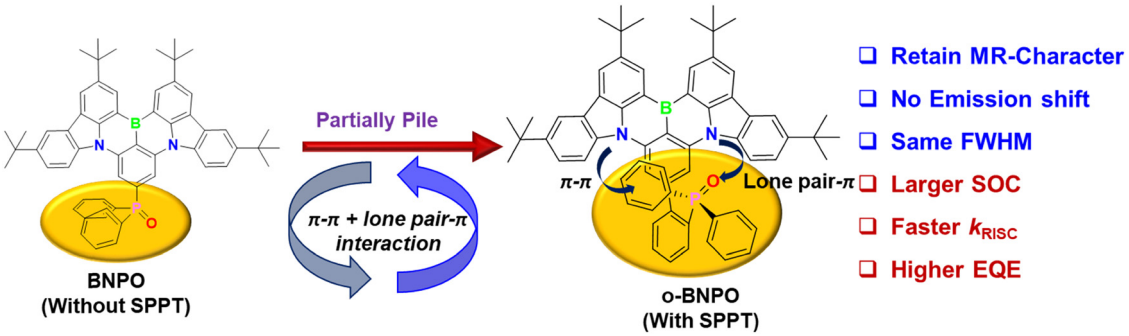

Fig. 9 π–π and lone pair-π interaction strategy to enhance the RISC and SOC of the MR-TADF emitters.

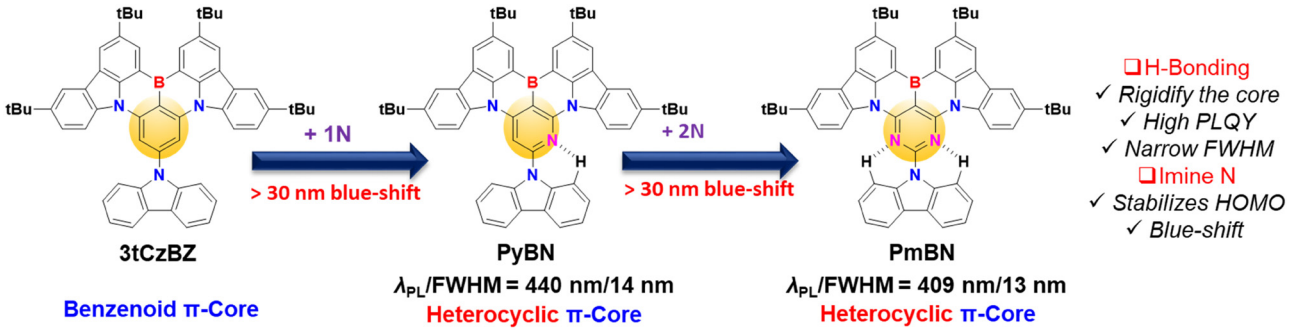

Fig. 10 Incorporation of N-at central π-core to obtain narrowband deep-blue emission.

toluene solution, **Py-BN** and **Pm-BN** displayed narrowband deep-blue emissions with peaks at 440 and 409 nm, and FWHMs of 14 and 13 nm, respectively, along with PLQY values of 93% and 94%. Devices using **Py-BN** and **Pm-BN** emit deep-blue light with maxima at 445 and 415 nm and exceptionally narrow FWHM values of 21 and 24 nm, respectively, with CIE coordinates of (0.153, 0.045) and (0.161, 0.045), respectively, and EQE_{max} of 15.8% and 5.8%, respectively. Notably, the hyperfluorescent OLEDs using **Py-BN** as an emitter achieved a maximum EQE of 27.7% and CIE coordinates of (0.150, 0.052), closely aligning with the BT.2020 blue standard.

Li *et al.* developed three sky-blue MR-TADF emitters- **BNCz-SAF**, **BNCz-DMAC**, and **BNCz-PXZ**, by introducing different donor groups, such as spiroacridine (SAF), acridine (DMAC), and phenoxazine (PXZ), at the *para*-position of the boron atom in the MR core BNCz.[101] All three compounds exhibited similar PL emission wavelengths around 477 nm, with FWHMs of ~22 nm and PLQYs exceeding 82%. The OLEDs based on **BNCz-SAF** and **BNCz-DMAC** show single-band sky-blue emission primarily originating from the MR core, achieving maximum EQEs of 25.3% and 23.8%, respectively, along with narrow FWHMs of 24 and 25 nm. In contrast, the **BNCz-PXZ** device in an mCBP host also exhibited a single-band sky-blue EL with a maximum EQE of 20.93%. When placed in polar solvents or hosts, **BNCz-PXZ** displays dual emission peaks at 484 and 548 nm, resulting in a warm white light emission characterized by CIE coordinates of (0.31, 0.4) and a maximum EQE of 16.4%.

Wong *et al.* developed a deep-blue MR-TADF emitter, **DOBN**, by fusing two O–B–N MR units and making peripheral modifications with strong electron-donating diphenylamine, resulting in hybrid exciton characteristics that combine both long-range and short-range charge transfer.[102] The O–B–N MR units and rigid molecular skeleton favor SRCT characteristics for TADF and narrowband emission, whereas the diphenylamine moiety favors blue-shifted emission and LRCT excitation to promote delayed fluorescence characteristics. As a result, **DOBN** exhibits a narrowband deep-blue emission with a maximum wavelength of 438 nm and a FWHM of 19 nm with a PLQY of 96% in solution. Furthermore, **DOBN** shows a prompt lifetime of 3.2 ns, a delayed lifetime of 21.7 μs and fast k_{RISC} of 7.5×10^4 s^{-1}. The solution-processed OLED based on **DOBN** as the emitter exhibits a deep-blue emission at a wavelength of 447 nm with EQE_{max} of 27.70% and CIE(x, y) of (0.15, 0.03). Furthermore, the vacuum-evaporated hyperfluorescence based on **DOBN** as the emitter exhibits a deep-blue emission at a peak wavelength of 449 nm with EQE_{max} of 35.44% and color coordinates of (0.15, 0.04), respectively.

Huang *et al.* developed two high-performance MR-TADF emitters by peripheral modification of the MR-framework (**DABNA-1**) with an alkyl group, resulting in **IPrBN** and a diarylamino group at the *para*-position of boron, resulting in **IPrBN-*m*CP**.[103] The photophysical properties of these emitters reveal that these compounds show narrowband blue emission with λ_{em}/FWHM of 458 nm/20 nm for **IPrBN** and 452 nm/19 nm for **IPrBN-*m*CP**, along with CIE coordinates of (0.125, 0.094) and

(0.143, 0.047) in the solution state. The narrow FWHM values of the emitters are attributed to the minimal reorganization energies of the excited states. Both compounds show identical ΔE_{ST} of 0.17 eV, which promotes the RISC under ambient conditions *via* LRCT, thus enabling the TADF characteristics. In the solid state, both emitters exhibited blue emission with λ_{em}/FWHM of 462 nm/23 nm for **IPrBN** and 453 nm/22 nm for **IPrBN-*m*CP** in 1% doped films, achieving a PLQY of nearly unity. Corresponding OLEDs were fabricated at different concentrations. Notably, the 10 wt% **IPrBN**-based OLED exhibited narrow blue emission with a maximum EQE of 20.1%. The 10% **IPrBN-*m*CP**-based OLED exhibited an EQE_{max} of 33.4% and excellent color purity with a CIE_y-coordinate of 0.046, satisfying the BT.2020 standard.

Ding *et al.* designed four MR-TADF emitters through peripheral substitution engineering, in which an electron-donating carbazole group is integrated into the [B–N]N parent core *via para*-B–π–N and *meta*-B–π–N conjugations to modulate the electronic excited state and introduce steric hindrance, thereby minimizing the intermolecular interaction and spectral broadening in the solid states. Consequently, a series of blue MR-TADF emitters, namely, **[B-N]N1**, **[B-N]N2**, **[B-N]N3** and **[B-N]N4**, were synthesized.[104] These compounds exhibit narrowband blue emission with wavelengths ranging from 438 to 463 nm, with a FWHM of 16 to 37 nm and PLQY of ~90%. The OLED device based on these emitters exhibits a narrow blue emission. Notably, **[B-N]N2**-based device featuring *para*-B–π–N conjugation achieved an EQE_{max} of 20.3% with a FWHM of 20 nm and CIE coordinates of (0.152, 0.046). This work provides a new B–N embedded framework with superior device performance.

Recently, Zhang *et al.* synthesized an ultra-narrowband blue emitter, **TB-PB**, based on the "SR-CT regulation" design strategy by combining the structural features of **ν-DABNA** and **BBCz-DB**.[105] In this approach, the singular B-based DABNA moiety in **ν-DABNA** is replaced with a double B-conjugated structure of **BBCz-DB**, which expands the SRCT distribution span while increasing the molecular rigidity and D/A strength (Fig. 11). This modification results in a regulated optical bandgap, spectral narrowing and reduced FMO overlap. Therefore, the tetra-borylated, **TB-PB** emitter shows PL emission with a wavelength peak at 473 nm and a FWHM of 12 nm with a PLQY of 99%. The corresponding OLED device shows maximum efficiencies (EQE/CE/PE) of 36.4%/49.1 cd A^{-1}/51.4 lm W^{-1} and blue EL with FWHM of 15 nm. To the best of our knowledge, this is the only compound that shows very narrow emission with a FWHM of 12 and 15 nm in PL and EL emission, respectively.

Cao *et al.* proposed a "9,9′-spirobifluorene (SF)-fused" strategy to develop narrowband deep-blue MR-TADF emitters, by promoting π-electron delocalization and steric shielding, resulting in two regioisomeric emitters, **DB-SF1** and **DB-SF2**.[106] The PL spectra of these compounds show λ_{em} at 457 nm (FWHM ~ 21 nm) for **DB-SF2** and 461 nm (FWHM ~ 22 nm) for **DB-SF1** in the solution state. The blue shift in **DB-SF2** is attributed to the lower reorganization energy between the ground state and the excited state configuration. The presence of sterically hindering groups minimized the molecular

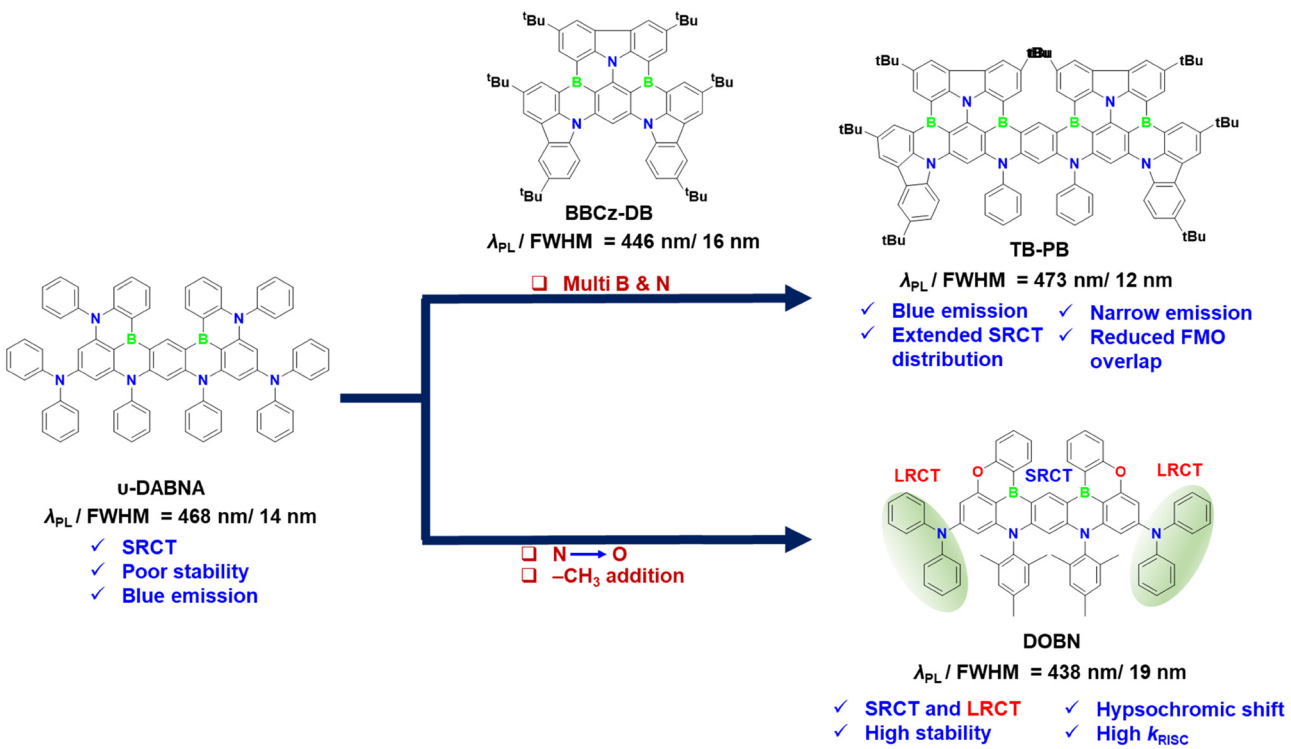

Fig. 11 Design strategy for efficient blue MR-TADF emitters with ultra-narrowband emission.

aggregation, resulting in PLQY values of 81% for **DB-SF1** and 95% for **DB-SF2**. In addition, **DB-SF2** shows low ΔE_{ST} and fast RISC process values of 0.17 eV and 2.4×10^5 s^{-1} compared to **DB-SF1** of 0.20 eV and 1.0×10^5 s^{-1}, respectively. The corresponding non-sensitized OLED device based on **DB-SF1** showed λ_{EL} at 463 nm (FWHM $\sim$ 24 nm) with a maximum EQE of 32.2%, whereas **DB-SF2** showed λ_{EL} at 460 nm (FWHM $\sim$ 20 nm) with a maximum EQE of 39.0%. Moreover, the hyperfluorescent OLED device based on **DB-SF1** and **DB-SF2** exhibited blue emission with EQE_{max} values of 34.2% and 40.4%, respectively, with lower efficiency roll-off.

Li *et al.* synthesized two novel emitters, **NBO-*m*SAF** and **NBO-*p*SAF**, by introducing an electron donor, 10*H*-spiroacridine-9,9′-fluorene (SAF), relative to the *para*-position of the O-atom and the *para*-position of the B-atom in the N/B/O ternary doped asymmetric MR-skeleton.[107] The weak electron-donating strength of the SAF moiety reduces the LRCT effect. Thus, the ^{1}LRCT state is located over the intrinsic ^{1}SRCT state of the MR-core, leading to blue emission. Additionally, the rigid spiro structure of the SAF moiety restricts the structural relaxation and vibrations in the excited state, which contributes to the color purity and high PLQY. The photophysical properties show that both compounds exhibit emission in the blue region, with wavelengths peaking at 458 nm for **NBO-*m*SAF** and 446 nm for **NBO-*p*SAF**, each exhibiting a FWHM of 28 nm in the toluene solution. The k_{RISC} values of 9.5×10^4 s^{-1} and 14.8×10^4 s^{-1} for **NBO-*m*SAF** and **NBO-*p*SAF**, which are 5–10 times larger than the parent compound (NBO). In the corresponding OLED device using 2,6-bis(3-(9*H*-carbazol-9-yl)phenyl)pyridine (26DCzPPy) as a bipolar host, the devices with **NBO-*m*SAF** and **NBO-*p*SAF** achieved EQE_{max} values of 29.5% and 20.5%, respectively. These devices exhibited FWHM values of 28 nm and 26 nm and CIE coordinates of (0.128, 0.114) and (0.147, 0.048), respectively. Furthermore, the hyperfluorescent OLED device exhibited enhanced EQE_{max} values of 25.2% and 26.7% for **NBO-*p*SAF** and **NBO-*m*SAF**, respectively, with suppressed efficiency roll-off.

To enhance the RISC rate for MR-TADF materials, Yang *et al.* developed an effective molecular design strategy by introducing a suitable auxiliary donor into the B/N-based MR-TADF framework (BCzBN). Therefore, a series of phenoxazine functionalized MR-TADF emitters, **CzBN1**, **CzBN2** and **CzBN3**, were synthesized.[108] By altering the number of alkyl substituents, the excited-state energy levels are adjusted, which silently induces an additional intersegmental charge transfer triplet state without impacting the MR character of the lowest singlet excited state, resulting in broad emission. The PL spectra exhibit that all the compounds show blue emission with λ_{max}/FWHM of 471 nm/78 nm for **CzBN1**, 477 nm/75 nm for **CzBN2** and 478 nm/21 nm for **CzBN3**. The compounds showed significant enhancement in k_{RISC} of 206.5×10^4 s^{-1}, 7.8×10^5 s^{-1}, and 3.27×10^5 s^{-1} for **CzBN1-3** compared to BCzBN (1.4×10^4 s^{-1}). Among these emitters, **CzBN3** exhibited rapid radiative decay, a PLQY close to unity, enhanced k_{RISC} and a narrow FWHM. Furthermore, the non-sensitized OLED device based on **CzBN3** exhibited a narrow blue EL emission with EQE_{max} of 36.4% and EQE_{1000} of 30.3%. **CzBN3**-based hyperfluorescent devices exhibited a high EQE_{max} of 42.3% and EQE_{1000} of 34.1% with reduced efficiency roll-off.

To achieve deep-blue emitters with high color purity, high efficiency and concentration quenching, Yang *et al.* developed a molecule with multiple mesityl groups, attached peripherally to the planar double B-embedded MR-framework (Chart 3). Based on this strategy, two emitters were developed, **DBNO** and **DMBNO**, which exhibit blue emission (λ_{PL} $\sim$ 445 nm), small ΔE_{ST} ($\sim$0.18 eV), high PLQY of >90% and a horizontal ratio of emitting dipole orientation ($\Theta_{\parallel}$) exceeding 90% in doped films.[109] The corresponding OLED device with 10 wt% concentration of **DBNO** and **DMBNO** exhibits deep-blue emission peaking at 448 nm and 449 nm with FWHM of 26 nm and 25 nm, maximum EQE of 22.7% and 32.3% along with CIE_y coordinate of 0.47 and 0.46, which exactly matches with BT.2020 blue gamut. To enhance the device performance, they also developed a TADF-sensitizing approach, resulting in an enhanced EQE_{max} of 36.8% with reduced efficiency roll-off even at high brightness.

3. Challenges and strategies for the use of green MR-TADF emitters

Duan *et al.* developed a series of green MR-TADF emitters by modifying the DABNA core. They replaced the diphenylamine unit with a rigid di-*tert*-butylcarbazole, resulting in a new MR-TADF core (**BCz-BN**) (Fig. 12). Substituting this core with either a carbazole donor or a fluorobenzene acceptor at the *para*-carbon of the central phenyl group relative to the B-atom resulted in the formation of **2F-BN**, **3F-BN**, **4F-BN**, and **TCz-BN**.[110] The incorporation of the fluorobenzene group stabilized the LUMO energy and reduced the bandgap, causing a bathochromic shift in the emission. These emitters displayed high PLQY values ranging from 80% to 99% in toluene, with emissions in the green region (λ_{em} $\sim$ 501–503 nm) and narrow FWHM values of 22–25 nm. The ΔE_{ST} values for **2F-BN**, **3F-BN**, and **4F-BN** were 0.16 eV, 0.08 eV, and 0.11 eV, respectively, with τ_d values of 25.9 μs, 16.7 μs, and 19.0 μs, all of which were shorter than that of **TCz-BN**. When used as dopants in the host material mCPCB:35% **5TCzBN**, these emitters showed green emissions with peak wavelengths and FWHM values of 501/40 nm for **2F-BN**, 499/39 nm for **3F-BN**, and 493/32 nm for **4F-BN**. The OLED device based on **2F-BN** emitted pure green light with a CIE_y value of 0.60. These emitters exhibited excellent device performance, achieving EQE values of 22.0%, 22.7%, and 20.9%, respectively, with minimal efficiency roll-off.

Duan *et al.* synthesized **AZA-BN** by fusing aza-aromatics with a B–N skeleton through a one-step multiple cyclization reaction.[111] DFT calculations revealed that the aza-aromatics contributed to multiple resonance interactions, while the incorporation of the fused aza-cyclic system into the MR core enhanced π-conjugation (Chart 4). The studies also confirmed the hybridized multi-resonance and charge transfer (HMCT) concept, which helped optimize the HOMO–LUMO

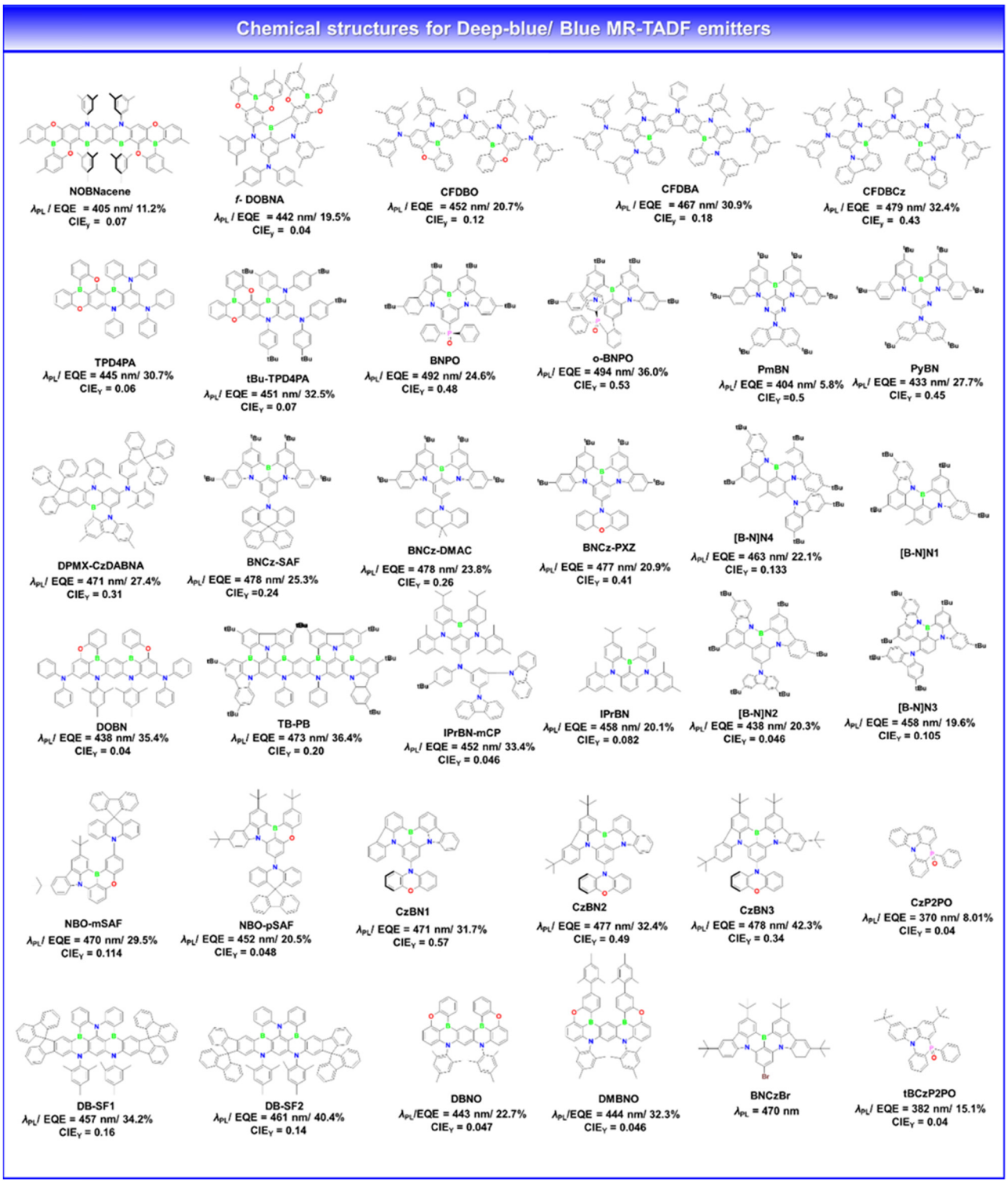

Chart 3 Chemical structure of the deep-blue/blue MR-TADF emitters.

distributions, improve the ICT character, and stabilize the S_1 state energy. **AZA-BN** demonstrated pure green emission with a peak wavelength of 522 nm and a narrow FWHM of 28 nm, achieving an impressive PLQY of 99.7% in toluene. In an mCBP-doped film, the compound emitted at a peak wavelength of 528 nm with a FWHM of 36 nm. OLED devices based on **AZA-BN** emitted green light with a peak wavelength of 527 nm and an FWHM of 30 nm. The device achieved a maximum EQE of 28.2% and a peak efficiency of 121.7 lm W^{-1}, with CIE coordinates of (0.27, 0.69).

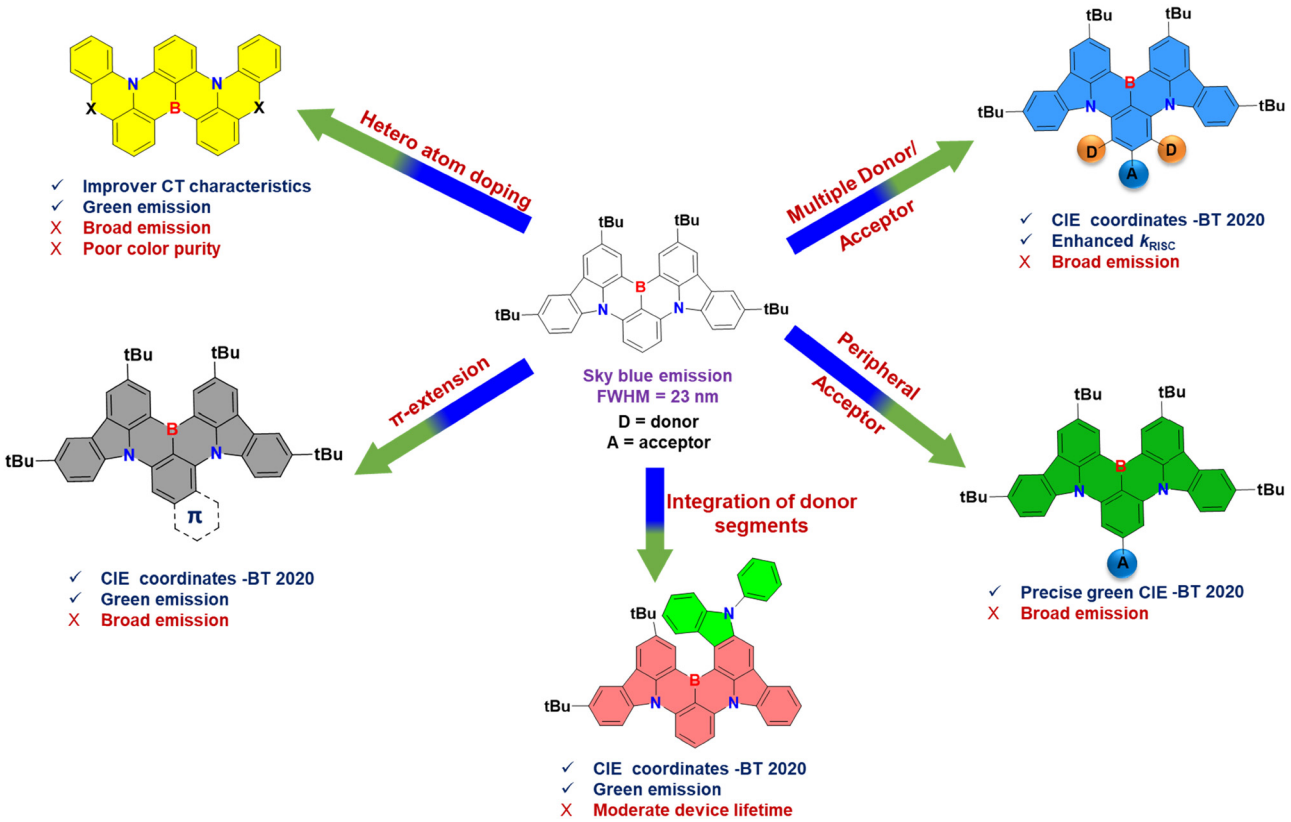

Fig. 12 Design strategies for developing green MR-TADF emitters.

Hatakeyama *et al.* introduced a novel green MR-TADF emitter, **OAB-ABP-1**, developed by fusing DOBNA and ADBNA core structures to extend the π-conjugation.[112] This design enhanced intramolecular charge delocalization, resulting in pure green emission ~506 nm with a narrow FWHM of 34 nm. The emitter also exhibited a small ΔE_{ST} of 0.12 eV, thereby promoting efficient RISC. To enable the fabrication of solution-processable devices, the researchers synthesized two custom polymers–polymer A (used as an interlayer) and polymer B, a bipolar host containing a triazine unit. These polymers were engineered to match the ionization potential and electron affinity of **OAB-ABP-1**, ensuring optimal charge balance in the device. OLEDs fabricated using this system delivered pure green EL at ~505 nm with a narrow FWHM of 33 nm, achieving a peak EQE of 21.8% and CIE coordinates of (0.12, 0.63). This work represents the first report of a solution-processed green MR-OLED and demonstrates notable device stability, highlighting the promise of this approach for efficient, color-pure OLED applications.

Wang *et al.* designed a narrowband green MR-TADF emitter, **DtBuPhCzB**, by extending the π-conjugation of the **BCz-BN** core through the introduction of *tert*-butylphenyl groups at the 3,6-positions of the carbazole unit.[113] For comparison, a structurally similar compound, **DtBuCzB**, lacking the phenyl extension, was also synthesized. In toluene, **DtBuPhCzB** exhibited a red-shifted emission (λ_{PL}) at 496 nm compared to 481 nm for **DtBuCzB**, while both maintained a narrow FWHM of 21 nm. **DtBuPhCzB** demonstrated a ΔE_{ST} of 0.09 eV *vs.* 0.13 eV for **DtBuCzB**, attributed to the stabilized singlet energy level from extended conjugation. This modification also led to an improved PLQY of 97% for **DtBuPhCzB** compared to 91% for **DtBuCzB**. In a 1 wt% doped mCBP film, **DtBuPhCzB** showed a slightly shorter τ_d of 61.3 μs than **DtBuCzB** (68.9 μs), consistent with its smaller ΔE_{ST}. In OLED devices using an mCBP host, **DtBuCzB** and **DtBuPhCzB** exhibited EL peaks at 488 nm and 501 nm, respectively, with FWHMs of 29 nm and 34 nm, and EQEs of 21.6% and 23.4%, respectively. However, both emitters exhibited significant efficiency roll-off at high luminance because of their long τ_d. To mitigate this, the device structure was optimized using an exciplex co-host system (TCTA: PIM-TRZ), which enhanced the EQE_{max} of **DtBuPhCzB** to 25.5% and yielded green emission with CIE(x, y) of (0.20, 0.65).

The same group proposed a new strategy called FMOE, which involved incorporating an auxiliary 3,6-di-*tert*-butylcarbazole (**DtBuCz**) unit at the *meta*-position relative to the boron atom in the **BCz-BN** core.[114] This modification aimed to extend the delocalization of the HOMO and lower its energy level, leading to a red-shift in emission. The resulting emitter, ***m*-Cz-BNCz**, featured a hybrid architecture combining a twisted D–A configuration with an MR framework. In toluene, ***m*-Cz-BNCz** showed a narrowband green emission centered at 519 nm with a FWHM of 38 nm and a high PLQY of 97%. The material also exhibited positive solvatochromism, indicating the presence of ICT in the excited state. An OLED device fabricated

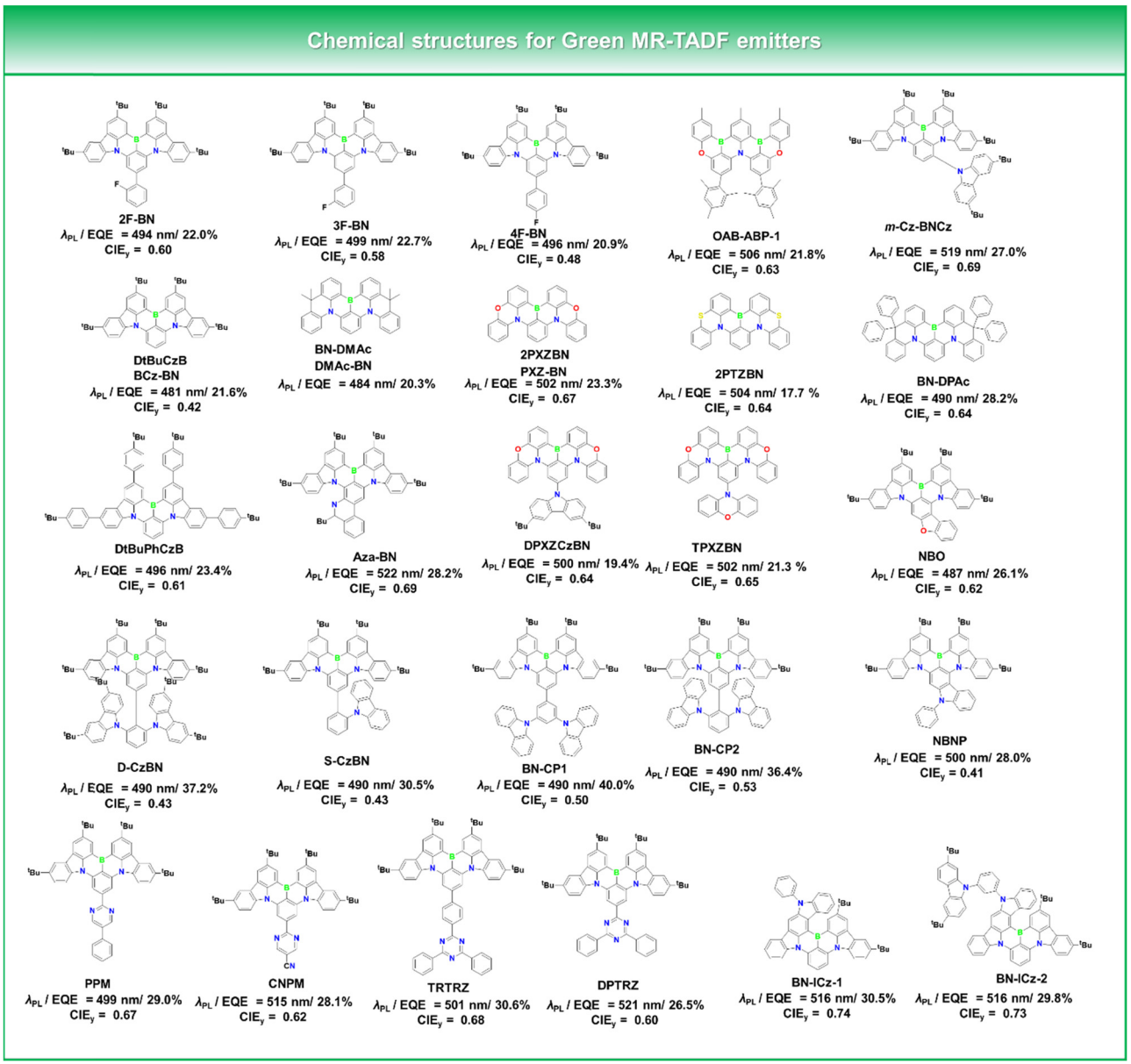

Chart 4 Chemical structure of green MR-TADF emitters.

using **PhCzBCz** as the host material and ***m*-Cz-BNCz** as the dopant displayed a sharp green emission and reached an EQE of approximately 26%. Notably, as the doping concentration increased, the emission spectrum underwent a slight red shift and the FWHM broadened, reflecting enhanced intermolecular interactions at higher concentrations.

Wang *et al.* designed a group of green MR-TADF emitters, **DPTRZ**, **TPTRZ**, **PPm**, and **CNPm**, by introducing various electron-withdrawing substituents at the *para*-position of the central phenyl ring relative to the boron atom.[115] This targeted modification effectively lowered the LUMO energy while maintaining the HOMO level, thereby reducing the bandgap and inducing a noticeable red-shift in the emission spectrum. The HOMO remained on the parent MR-core, whereas the LUMO extended onto the acceptor fragments, as confirmed by computational analysis. Photophysical characterization showed that these compounds emitted green light with peak wavelengths of 521 nm (**DPTRZ**), 501 nm (**TPTRZ**), 499 nm (**PPm**), and 515 nm (**CNPm**), each with narrow FWHM values of 24–36 nm. The emitters also featured small ΔE_{ST} ranging from 0.08 to 0.17 eV and high PLQY values between 93% and 97%. When employed in OLEDs, the emitters exhibited EL peaks at 532 nm (**DPTRZ**), 516 nm (**TPTRZ**), 508 nm (**PPm**), and 540 nm (**CNPm**), with corresponding FWHMs of 39, 38, 33, and 44 nm. These devices achieved high EQEs of 24.6%, 29.8%, 28.6%, and 25.0%, respectively. The results emphasize the efficacy of *para*-position functionalization in fine-tuning optoelectronic properties for high-performance green OLED applications.

Kido *et al.* designed two carbon- and oxygen-bridged MR-TADF emitters, **DMAc-BN** and **PXZ-BN**, by locking the rotation

of the phenyl groups in the **DABNA-1** structure.[116] This structural modification enhanced the electron-donating ability and π-conjugation of the molecules. Therefore, both emitters exhibited efficient green emission, with **DMAc-BN** and **PXZ-BN** emitting at 484 and 502 nm, respectively. Their emissions featured narrow FWHM values of 33 nm (**DMAc-BN**) and 38 nm (**PXZ-BN**), and high PLQY of 88% and 90%, respectively. The measured ΔE_{ST} were 0.16 eV for **DMAc-BN** and 0.17 eV for **PXZ-BN**. OLED devices incorporating these emitters delivered strong performance, achieving EQEs of 20.3% for **DMAc-BN** and 23.3% for **PXZ-BN**. The color coordinates were (0.18, 0.60) for **DMAc-BN** and (0.22, 0.67) for **PXZ-BN**, indicating bright green emission. Furthermore, both materials exhibited significantly lower efficiency roll-off than the original **DABNA-1**, highlighting their potential for stable, high-efficiency OLED applications.

Zheng *et al.* developed two new MR-TADF emitters, **TPXZBN** and **DPXZCZBN**, by modifying the **PXZ-BN** core structure with two phenoxazine groups attached to the B atom.[117] These phenoxazine units were positioned at the *para*-carbon of the central phenyl ring and were electronically decoupled from the MR core. This design increased the HOMO energy level while effectively narrowing the energy gap between the HOMO and LUMO, improving the TADF characteristics. Photoluminescence measurements revealed that **TPXZBN** and **DPXZCZBN** emitted green light with peak wavelengths of 537 and 527 nm, respectively, accompanied by narrow FWHM values of 33 and 32 nm, respectively. Both emitters displayed small $\Delta E_{ST} \leq 0.16$ eV and high PLQY $\geq$ 90%. OLED devices incorporating these materials in an mCBP host matrix showed green electroluminescence with peak wavelengths of 537 nm (FWHM $\sim$ 37 nm) for **TPXZBN** and 527 nm (FWHM $\sim$ 36 nm) for **DPXZCZBN**. The corresponding color coordinates were (0.16, 0.06) and (0.15, 0.64), indicating efficient green emission. These devices achieved maximum EQEs of 21.3% and 19.8%, respectively, and demonstrated reduced efficiency roll-off, making them promising candidates for high-performance green OLED applications.

Yang *et al.* introduced structural modifications to the known MR-TADF emitter DMAC-BN by replacing the two methyl groups on the acridine unit with phenyl groups, leading to the development of a new green emitter named **BN-DPAc**.[118] This modification was aimed at enhancing the SRCT effect, and **BN-DPAc** was directly compared to its precursor, **BN-DMAc**. Both **BN-DMAc** and **BN-DPAc** displayed red-shifted emissions relative to the benchmark compound **DABNA-1**, consistent with the stronger SRCT character. These emitters also showed reduced ΔE_{ST}, measured at 0.14 eV for **BN-DMAc** and 0.11 eV for **BN-DPAc**, and shorter τ_d of 13.9 μs and 11.6 μs, respectively. **BN-DPAc** exhibited a markedly enhanced k_{RISC} of 1.26×10^5 s^{-1}. OLED devices fabricated using these emitters delivered pure green electroluminescence, with emission peaks at 502 nm for **BN-DMAc** and 504 nm for **BN-DPAc**. The device incorporating **BN-DPAc** achieved a high EQE_{max} of 28.2%, attributed to its efficient triplet-to-singlet upconversion. When paired with a TADF-type exciplex host system, the EQE_{max} of the **BN-DPAc**-based device further increased to 30%, underscoring the effectiveness of host engineering in boosting device performance.

Subsequently, the same group developed a novel approach to enhance the efficiency of MR-TADF emitters by incorporating a heavy sulfur atom into the BN-PAHs framework, providing the advantage of boosting k_{RISC} without compromising the MR-effect. They synthesized two MR-TADF emitters, a phenothiazine derivative (**2PTZBN**) and a phenoxazine derivative (**2PXZBN**).[119] The PL emission spectra of **2PTZBN** and **2PXZBN** reveal narrowband green emission with FWHM less than 40 nm in toluene. Theoretical calculations indicate that the heavy atom effect induced by the sulfur atom leads to significant SOC values, shortened τ_d, and accelerated k_{RISC} rates. Both compounds demonstrate satisfactory device performance, emitting light in the green region with wavelengths of 522 and 528 nm. They achieve a maximum EQE of 17.7% and 25.5%, respectively, along with a reduced efficiency roll-off.

Duan *et al.* introduced a new molecular design that utilizes a sterically shielded MR core, enhanced by bulky substituents to minimize intermolecular interactions and effectively prevent aggregation-induced quenching of emission.[120] They synthesized two novel MR-TADF emitters, named **s-Cz-BN** and **d-Cz-BN** (Fig. 13), which incorporate one or two carbazole donor groups positioned at the *meta*-site relative to the boron atom in the **D*t*BuCzB** framework. DFT calculations revealed that these donor groups act as electronically passive components with minimal impact on the FMO distribution, thus preserving the core photophysical properties. Both emitters demonstrated slightly redshifted emission relative to **D*t*BuCzB**, along with narrower FWHM values, showcasing the success of this structural approach. Additionally, **s-Cz-BN** and **d-Cz-BN** exhibited low ΔE_{ST} and excellent PLQYs of 94% and 98%, respectively. Notably, even as the doping concentration increased, the emitters retained their narrow emission profiles and exhibited minimal spectral shift, particularly **d-Cz-BN**, which achieved a pristine film FWHM of 26 nm, which is significantly narrower than **s-Cz-BN** (40 nm) and the original **D*t*BuCzB** (60 nm)-highlighting the superior steric protection of **d-Cz-BN**. Crucially, both materials delivered high EQE_{max} ranging from 36.3% to 37.0% across a doping range of 1–20 wt%. They also showed reduced efficiency roll-off at high brightness levels, likely due to suppressed long-range delayed fluorescence and minimized aggregation-induced quenching, demonstrating their potential for high-performance OLED applications.

Yang *et al.* synthesized two new MR-TADF emitters, **BN-CP1** and **BN-CP2**. In **BN-CP1**, the two carbazole donors were positioned at the *ortho*-positions of the phenyl linker relative to the parent MR-TADF core, whereas in **BN-CP2**, the carbazole donor positions were shifted to the *meta*-position of the phenyl linker.[121] Both compounds displayed sky-blue emission with peak wavelengths (λ_{PL}) of 490 and 496 nm, respectively. **BN-CP2** in the neat film showed a significant red shift (λ_{PL} 521 nm), a broader FWHM of 48 nm, and a reduced PLQY of 25% compared to **BN-CP1**, which demonstrated a λ_{PL} of 502 nm, a narrow FWHM of 26 nm, and a high PLQY of 40%. The differences in behavior were attributed to the severe

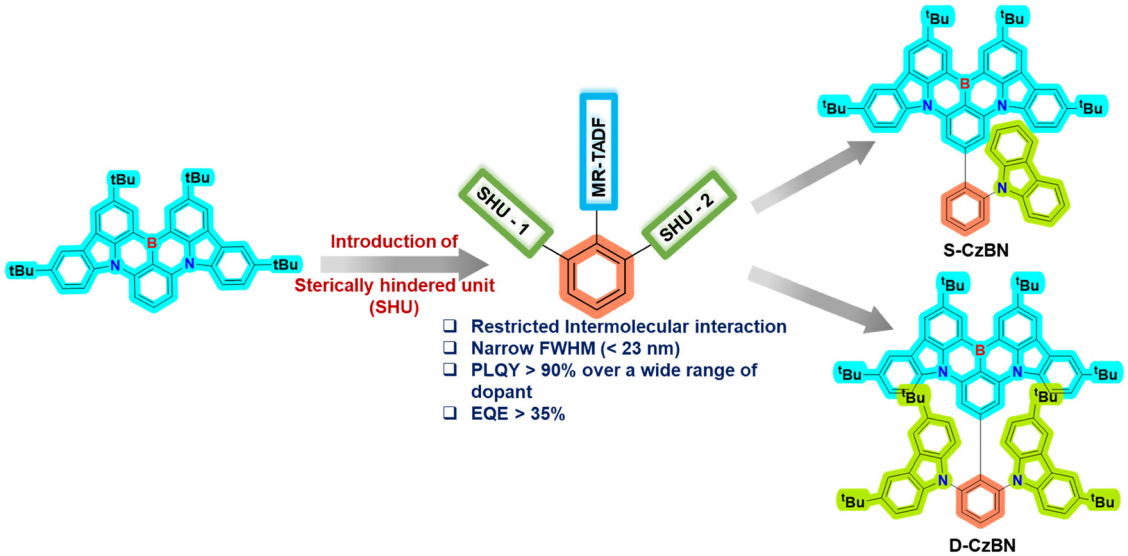

Fig. 13 Incorporation of a sterically hindered unit to control the ACQ.

aggregation in **BN-CP2** compared with **BN-CP1**. Additionally, both **BN-CP1** and **BN-CP2** exhibited short τ_d of 79.6 μs and 83.6 μs, and fast k_{RISC} of 1.56 × 10^4 s^{-1} and 1.43 × 10^5 s^{-1}, respectively, indicating their TADF nature. OLED performance analysis of these emitters was conducted in a DMIC-TRZ host. Despite an increase in the doping concentration from 1 to 30 wt%, the emission characteristics of **BN-CP1** remained unchanged, with an emission maximum at 496 nm and a FWHM of 25 nm. In contrast, **BN-CP2** exhibited a significant redshift with broadened emission due to the suppression of aggregation-caused emission quenching. **BN-CP1** maintained an EQE_{max} of 33–40% across the doping concentrations, whereas **BN-CP2** experienced a notable drop in EQE from 34% to 23% with increasing doping concentration. The optimized device using 5 wt% **BN-CP1** achieved the highest reported EQE_{max} of 40%.

Zheng *et al.* engineered an MR-TADF emitter by integrating rigid hole-transporting units, namely dibenzofuran (**NBO**) and carbazole (**NBNP**), with the MR-core.[122] The red-shifted emission was attributed to the effective expansion of the charge transfer dissociation domain within the B,N-framework, resulting in peak wavelengths of 489 nm and 500 nm, each with a FWHM of 27 nm and 29 nm for **NBO** and **NBNP**. Detailed DFT studies revealed that the HOMO orbitals of the compounds are fully delocalized across the entire molecular backbone, whereas the LUMO orbitals are mainly localized on the parent MR core. Consequently, this led to a reduction in the energy gap between the HOMO and LUMO, yielding low ΔE_{ST} values of 0.12 eV and 0.09 eV and high PLQY values of 92% and 93%, respectively. Additionally, the OLED devices based on these compounds exhibited a maximum EQE of 28.0% for **NBNP** and 26.5% for **NBO**, along with a reduced efficiency roll-off attributed to the fast k_{RISC}.

Duan *et al.* developed two ultrapure green MR-TADF emitters by fusing conventional PAHs to MR fragments, effectively suppressing the shoulder peak, thereby extending π-conjugation, enhancing molecular rigidity, and reducing vibrational frequency.[123] The synthesized fluorophores, **BN-ICz-1** and **BN-ICz-2**, exhibited emission in the green region with maximum wavelengths of 521 and 520 nm and narrow FWHM values of 20 and 21 nm, respectively, accompanied by PLQY of 99.2% and 98.3%. Both **BN-ICz-1** and **BN-ICz-2** exhibited low energy gap (ΔE_{ST}) values of 0.22 eV and 0.18 eV, respectively. Furthermore, OLED devices based on these compounds displayed similar narrowband green emission at a wavelength of 523 nm, FWHM of 23 nm, and CIE coordinates of (0.22, 0.74) and (0.23, 0.73). High EQE_{max} values of 30.5% and 29.8% were achieved, with reduced efficiency roll-off attributed to their short τ_d and high k_{RISC} values. To enhance the color purity of **BN-ICz-1**, a top-emitting OLED (TE-OLED) was fabricated using a phosphorescent sensitizer, $Ir(ppy)_2acac$. As anticipated, this configuration exhibited pure green emission at a wavelength of 525 nm, FWHM of 19 nm, and CIE color coordinates of (0.17, 0.78), achieving a high efficiency of 220 cd A^{-1}.

Wang *et al.* introduced a novel strategy by integrating a MR core with a polycyclic aromatic unit known as **BN-TP**, which features boron and nitrogen atoms arranged in a *para*-configuration within a six-membered ring.[124] The molecule exhibits a distinct absorption at 506 nm due to an ICT transition and emits bright green light with an emission maximum at 523 nm. The emission exhibited a small Stokes shift of 22 nm and a narrow FWHM of 34 nm, reflecting the high structural rigidity of **BN-TP** in its excited state. It also shows efficient TADF behavior, as evidenced by a small ΔE_{ST} of 0.14 eV, a high PLQY of 96%, and a k_{RISC} of 2.09 × 10^4 s^{-1}. When used as a dopant in the **PhCzBCz** host matrix, **BN-TP** achieved an impressive EQE_{max} of 35.1%, a CE of 139.3 cd A^{-1}, and an emission FWHM of 36 nm, along with green emission CIE(x, y) ∼ (0.26, 0.70).

Lu *et al.* designed four MR-TADF emitters by introducing phenyl-based substituents to protect the periphery of the MR framework.[125] This molecular design helps suppress the high-

frequency vibrational modes, resulting in significantly reduced emission bandwidths. The resulting compounds-**TW-BN**, **TPh-BN**, **pCz-BN**, and **mCz-BN**-emit narrow green light with a FWHM of approximately 20 nm and exhibit a small ΔE_{ST} of 0.11 eV in solution. Among them, **TPh-BN** showed outstanding performance when incorporated into an OLED device, achieving a high EQE of 28.9% and emitting green light with a narrow FWHM of 28 nm. Notably, the device exhibited a low efficiency roll-off of just 13% at practical luminance levels without the use of a dopant and demonstrated superior operational stability, with a half-lifetime (LT_{50}) of 36.5 hours at an initial brightness of 5000 cd m^{-1}.

Wang *et al.* proposed an innovative molecular design strategy for high-efficiency green MR-TADF emitters by implementing *para*-B–π–B and *para*-O–π–O configurations.[126] Their concept is built on two main principles: first, placing boron atoms in *para* positions within the central core-rather than the conventional *meta* arrangement to significantly boost electron-accepting ability and induce a red-shifted emission; and second, replacing *para*-arylated nitrogen atoms with *para*-arylated oxygen atoms, which possess lower atomic energy. This substitution limits the HOMO π-conjugation without significantly affecting the LUMO, thereby retaining the MR character and avoiding excessive red-shift. Additionally, the nearly planar molecular geometry and extended π-conjugation improve the horizontal orientation of the emitting dipoles, thereby enhancing light outcoupling efficiency. To validate this strategy, they synthesized a new emitter, **DBNO**, featuring a five-ring benzene structure with *para*-positioned B and O atoms in the central phenyl core. **DBNO** displayed green photoluminescence at 500 nm with an exceptionally narrow FWHM of 19 nm. When used as a dopant in an OLED device, **DBNO** achieved an EQE of 35.9% and a CE of 94.1 cd A^{-1}. The performance was further elevated to an EQE of 37.1% by adopting a hyperfluorescent device architecture using **5TCzBN** as the host.

Xu *et al.* recently developed two multi-resonance TADF emitters, **BO-N1** and **BO-N2**, by integrating a B-oxygen-based MR core with covalent B–N bonds.[127] These bonds were efficiently formed using an amine-directed borylation method, achieving a high yield of 90% (Fig. 14). To modulate the electronic properties, *tert*-butyl (**BO-N1**) and phenoxyl (**BO-N2**) groups were introduced at the *para* positions relative to the oxygen atoms, offering varying degrees of electron donation and steric effects that influence ICT. Although the B–N bond did not disrupt the MR characteristics, it reduced the boron atom's electron-accepting strength, thereby weakening the SRCT. This design resulted in a minimal Stokes shift and a narrow emission bandwidth. **BO-N1** and **BO-N2** exhibited sharp green emissions with peak wavelengths at 488 and 496 nm, FWHM of 20 and 21 nm, and identical small Stokes shifts of 9 nm. Their PLQYs were 85% and 90%, respectively. **BO-N2** demonstrated superior device performance, delivering bright green light with an FWHM of 29 nm and reaching peak values of CE ~ 36.4 cd A^{-1}, PE ~ 41.9 lm W^{-1}, and EQE ~ 20.1%.

Wang *et al.* recently developed a novel MR-TADF material (**BNBO**) by combining two MR-TADF cores.[128] The B–O-based core contributes to electron-accepting ability, while the B–N-based core acts as both an electron-withdrawing and electron-accepting entity, resulting in red-shifted emission (Table S3, ESI†). The MR-effect and rigidity of the B–N core significantly facilitate highly efficient narrowband emission for **BNBO**, exhibiting λ_{PL} at 500 nm with a FWHM of 25 nm and a small ΔE_{ST} of 0.14 eV. Furthermore, the corresponding OLED device demonstrates narrow emission in the green region, with a peak wavelength of 508 nm, FWHM of 36 nm, and maximum efficiencies (EQE/PE) of 24.3%/62.3 lm W^{-1}, respectively.

Choi *et al.* developed a dual MR-TADF emitter, **FICzBN-BO**, with high solubility by combining two MR components, *t*DOBNA and FICzBN, using an oxygen bridge.[129] The organic emitter, **FICzBN-BO**, has a lower LUMO energy level due to the hybridization of the LUMOs from both MR components, which results in a decreased HOMO–LUMO energy gap. Moreover, the lower LUMO level of **FICzBN-BO** results in a red-shifted emission, a narrow FWHM, and a high PLQY. Additionally, the phenyl-fluorene-based peripheral units induce structural distortion, which leads to a reduced ΔE_{ST} and enhances both k_{RISC} and radiative decay. Photoluminescence studies indicate that the compound demonstrates a narrowband green emission (λ_{PL}/FWHM = 507 nm/24 nm) with a PLQY of 92% and an ΔE_{ST} of 0.05 eV. Furthermore, solution-processed OLEDs utilizing **FICzBN-BO** as the emissive layer displayed a green emission at 504 nm and a FWHM of 31 nm, achieving a maximum EQE of 16.26%. Owing to the steric shielding effect of the fluorene-based unit, the emitter exhibited reduced sensitivity to the doping concentration.

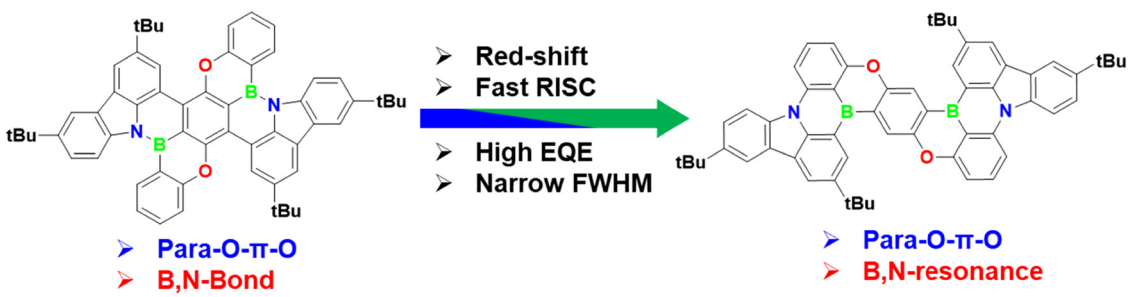

Fig. 14 Switching of the B–N to B–C bond to produce green MR-emitters.

Recently, Su *et al.* developed two MR-based TADF emitters, **TCZBAC** and **TCZBAO**, based on a carbonyl-reinforced SRCT strategy to achieve a red shift in emission and decreased ICT.[130] In this approach, the carbonyl group was fused with B,N-doped PAH to construct a boron/nitrogen/carbonyl MR-TADF emitter (**TCZBAO**). The photophysical properties confirmed a bathochromic shift following the incorporation of the carbonyl group. **TCZBAO** exhibited green emission (λ_{PL}/FWHM) at 507 nm/30 nm, whereas the carbonyl-free **TCZBAC** demonstrated emission at 492 nm/35 nm. In an OLED device utilizing **TCZBAO** as a terminal emitter and the TADF material, DspiroAc-TRZ as an assistant host, an EQE of 36.1% and a FWHM of 39 nm were achieved, with reduced efficiency roll-off. In contrast, the **TCZBAC**-based OLED device exhibited an EQE of 32.4% with a FWHM of 46 nm. Thus, the differential behavior of **TCZBAC** and **TCZBAO** is attributed to the addition of the carbonyl group.

Zheng *et al.* developed three green emitters, ***p*-ICz-BNCz**, ***m*-ICz-BNCz**, and ***dm*-ICz-BNCz**, by integrating the **D*t*BuCzB** core with indolocarbazole (ICz) units either *para* or *meta*-relative to the central B-atom on the phenyl ring.[131] In the *meta*-substituted derivatives, ***m*-ICz-BNCz** and ***dm*-ICz-BNCz**, the repulsion between the bulky ICz unit and the MR core resulted in a twisted conformation, yielding k_{RISC} values three times higher than those of the *para*-substituted compound, ***p*-ICz-BNCz**. Photophysical studies revealed that all three emitters displayed green emission with peak wavelengths, FWHM, and PLQY of 484 nm, 24 nm, and 94.5% for ***p*-ICz-BNCz**; 508 nm, 38 nm, and 90.3% for ***m*-ICz-BNCz**; and 526 nm, 41 nm, and 93.6% for ***dm*-ICz-BNCz**, respectively. The ***dm*-ICz-BNCz** displayed a significant red shift compared to its congener ***m*-ICz-BNCz**, which was attributed to the improved ICT characteristics; however, it showed broad emission attributed to vibronic coupling. The estimated k_{RISC} of the compounds ***p*-ICz-BNCz**, ***m*-ICz-BNCz**, and ***dm*-ICz-BNCz** were 2.14×10^4, 5.69×10^4, and 6.81×10^4 s^{-1}, respectively. OLED devices based on these emitters produced sharp EL peaks at 494, 516, and 534 nm with corresponding FWHM values of 31, 40 and 46 nm. All three devices demonstrated strong performance, achieving high maximum CE of 77.8 cd A^{-1}, 107.0 cd A^{-1}, and 138.2 cd A^{-1}, EQE_{max} values of 32.5%, 28.0%, and 32.9%, and maximum PE of 90.3 lm W^{-1}, 81.9 lm W^{-1}, and 105.8 lm W^{-1}, respectively.

Wang *et al.* recently developed a pure-green, solution-processable MR-TADF emitter named **3CzSF-BN** by integrating a bulky spirobifluorene unit into the MR framework (**D*t*BuCz**) and attaching a carbazole donor group to the central phenyl ring, positioned *para* to the nitrogen atom.[132] The carbazole donor effectively shifted the emission into the green region, while the steric hindrance from the spirobifluorene moiety helped suppress molecular aggregation and enhanced the emitter's solubility. Photophysical analysis revealed that **3CzSF-BN** emitted green light with a λ_{em} of 520 nm and a narrow FWHM of 30 nm in solution, and 527 nm with a 37 nm FWHM in thin film. The compound achieved an exceptional PLQY of 100% in solution and 87.5% in film. When used in a bottom-emitting, solution-processed OLED, **3CzSF-BN** delivered narrowband green emission with an EQE of 20.3% using a single host. This efficiency was further boosted to 23.1% with the introduction of a TADF sensitizer, maintaining a high EQE of 21.3% at 1000 cd m^{-2}. The device exhibited precise green emission with CIE coordinates of (0.214, 0.716).

Based on a molecular orbital engineering strategy, Kwon *et al.* developed two symmetrical green MR-TADF materials, **BpIC-DPA** and **BpIC-Cz**.[133] A rigid *p*-ICz donor is used as a scaffold in the parent core, which enhances the rigidity of the molecules and improves charge transfer localization by extending their conjugation.[133] **BpIC-DPA** features bis(4-(*tert*-butyl)phenyl)amine (*t*DPA), while **BpIC-Cz** includes TBCz donors. Both compounds exhibited ultrapure green emissions with λ_{PL} of 527 nm for **BpIC-DPA** and 534 nm for **BpIC-Cz**, a narrow FWHM below 25 nm and a high PLQY exceeding 83%. When fabricated into OLED devices, the DIC-TRZ:2 wt% **BpIC-DPA** device demonstrated a narrow green emission at a maximum wavelength of 536 nm and a FWHM of 22 nm, achieving an EQE_{max} of 22.0%. In comparison, the DIC-TRZ:4 wt% **BpIC-Cz** device emitted light at 544 nm with a FWHM of 32 nm and an EQE_{max} of 25.7%. Both devices exhibited reduced efficiency roll-off (Table S4, ESI†). Furthermore, the **BpIC-Cz**-based devices, featuring TBCz, displayed superior operational stability, achieving a lifetime (LT_{90}) of 291.5 hours at an initial luminance of 1000 cd m^{-2}, compared to 156.1 hours for the **BpIC-DPA**-based devices.

To achieve the RISC, Zhang *et al.* designed a connecting D–A type CT core to the MR core.[134] ***t*CzBN-PQ** integrates the secondary acceptor 4-phenylquinazoline (PQ) at the *para* position relative to the B-atom of *t*CzBN, imparting LRCT characteristics (Chart 5). In contrast, ***t*CzBN-PQCz** incorporates the secondary D–A phenyl-3-(quinazolin-4-yl)-9*H*-carbazole (PQCz) in the same position, resulting in dual LRCT properties. Both compounds demonstrate a hybrid of SRCT and LRCT characteristics. The PL spectra measured in toluene show sharp emission peaks at 515 nm (FWHM ~ 31 nm) for ***t*CzBN-PQ** and 511 nm (FWHM ~ 30 nm) for ***t*CzBN-PQCz**, both exhibiting bathochromic shifts compared to *t*CzBN (λ_{PL} ~ 485 nm). The ***t*CzBN-PQ** achieves a high k_{RISC} of 5.9×10^5 s^{-1} and a PLQY of 89%, while ***t*CzBN-PQCz** demonstrates an even higher k_{RISC} of 7.3×10^5 s^{-1} and a PLQY of 95%, which are significantly higher than the parent MR-core. This is attributed to the improved SOC of the quinazoline derivatives. When fabricated OLED devices at a concentration of 3 wt% for both ***t*CzBN-PQ** and ***t*CzBN-PQCz** show emission in the green region with maximum wavelengths of 524 and 516 nm, respectively. Consequently, both ***t*CzBN-PQ** and ***t*CzBN-PQCz** achieved EQE values of 30.2% and 35.1%, respectively, with minimal efficiency roll-off.

Wang *et al.* synthesized two MR-TADF compounds, **BN-TPP** and **BN-DPBQ**, by incorporating the electron acceptor 2,4,6-triphenylpyrimidine (TPP) into DtCzB.[135] The steric hindrance effect of TPP caused **BN-TPP** to exhibit PL emission in the green region, with a wavelength of 496 nm and a FWHM of 20 nm in dilute solution. In contrast, **BN-DPBQ** showed a further red-shifted emission in the yellow-green region at 539 nm, with a

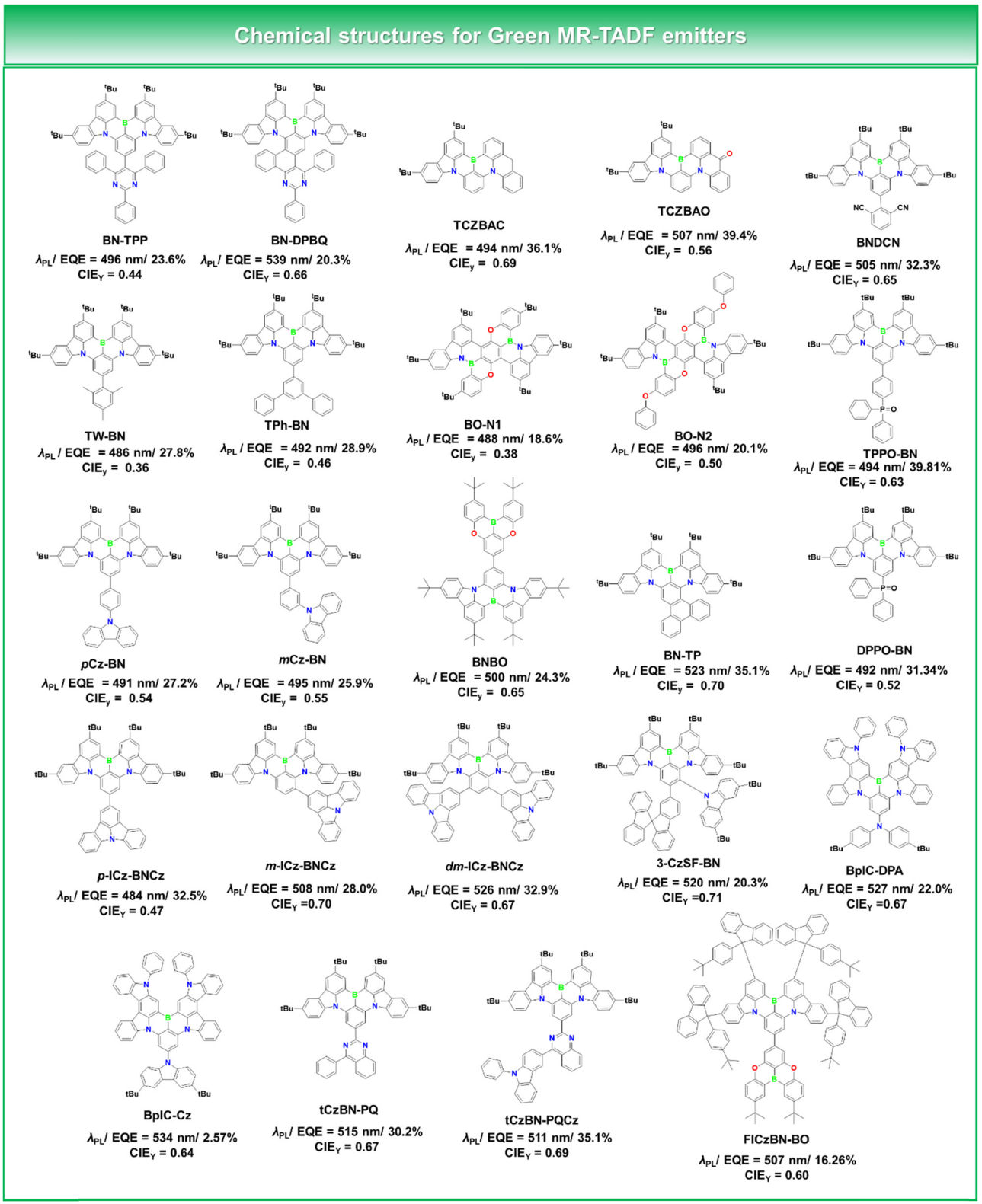

Chart 5 Chemical structure of green MR-TADF emitters.

FWHM of 32 nm, due to an extended conjugation system and LRCT transitions. The **BN-TPP** and **BN-DPBQ** films exhibited emission peaks at 495 and 539 nm, respectively, with FWHMs of 25 and 35 nm, respectively. The PLQYs for **BN-TPP** and **BN-DPBQ** doped in PhCzBCz were determined to be 87% and 67%, respectively. The corresponding OLED devices for **BN-TPP** and

BN-DPBQ exhibited sharp emission peaks at 494 and 538 nm, respectively, with narrow FWHMs of 25 and 34 nm, and CIE chromaticity coordinates of (0.080, 0.443) and (0.321, 0.660), respectively. The maximum EQEs for these devices were 23.6% and 20.3%. However, both devices displayed relatively low luminance and significant efficiency roll-offs at higher current densities, primarily due to fluorescence quenching.

Xiao *et al.* developed an emitter **D-BNDCN** that benefits from both SRCT and through-space charge transfer (TSCT) effects due to the introduction of *m*-dicyanobenzene into the parent skeleton, BBCz-B.[136] The photophysical characteristics of **D-BNDCN** reveal an emission peak at 506 nm with a narrow FWHM of 27 nm and a PLQY of 90%. The presence of two charge transfer processes results in a small ΔE_{ST} of 0.06 eV and τ_d of 16.0 μs, along with a k_{RISC} value of 0.8×10^5 s^{-1}. The corresponding OLED device exhibits green emission with a maximum wavelength of 507 nm (FWHM ~ 30 nm) and a maximum EQE of 32.3%. Additionally, the OLED's CIE coordinates are (0.13, 0.65), which fall within the green emission range as defined by the NTSC.

Zhang *et al.* synthesized two similar MR-TADF emitters by incorporating benzophenone (BP) and 9-fluorenone (FP) into the **DtBuCzB** MR skeleton, resulting in **TCzBN-BP** and **TCzBN-FP**.[137] Despite their structural similarities, these emitters exhibit different photophysical and EL properties due to the varying contributions of LRCT and SRCT electronic transitions. SRCT excitation predominates in **TCzBN-BP**, leading to narrowband emission, a fast k_r, and ultimately more efficient exciton harvesting. Conversely, in **TCzBN-FP**, LRCT transitions play a significant role, which adversely affects the emission bandwidth and increases singlet exciton energy loss *via* IC. The λ_{PL} for **TCzBN-BP** and **TCzBN-FP** were observed at 497 and 516 nm, respectively, with the spectral FWHM increasing from 29 nm for **TCzBN-BP** to 37 nm for **TCzBN-FP**. In doped films using 2-(9,9′-spirobi[fluoren]-3-yl)-4,6-diphenyl-1,3,5-triazine (SF3TRZ) as the host, **TCzBN-BP** and **TCzBN-FP** both exhibit green emissions with peaks at 508 and 542 nm, respectively. The FWHM of **TCzBN-BP** is notably narrower at 33 nm (0.16 eV) than that of **TCzBN-FP**, which has an FWHM of 56 nm (0.23 eV). Additionally, **TCzBN-BP** demonstrates a significantly higher PLQY of 97.6%, in contrast to **TCzBN-FP**, which has a PLQY of 75.3%. Furthermore, an OLED using **TCzBN-BP** as the emitter features a narrowband EL spectrum with a peak at 512 nm and an FWHM of 35 nm (0.16 eV), achieving an EQE_{max} of 35.6%. This performance is markedly superior to that of the OLED based on **TCzBN-FP**, which has an EQE_{max} of 27.2% and FWHM of 56 nm (0.23 eV).

To enable multiple exciton-harvesting pathways and to enhance the k_{RISC}, Colman *et al.* developed two novel emitters, **DtCzBN-CNBT1** and **DtCzBN-CNBT2**.[138] These compounds integrate isomeric D–A-type TADF units, CNBT1 and CNBT2, derived from bis(benzothienocarbazol-5-yl)benzonitrile, onto a D*t*CzBN-based MR-TADF core (Fig. 15). The resulting molecules adopt a highly twisted molecular conformation. In toluene, both emitters exhibited narrow green emissions, with peak wavelengths of 498 nm for **DtCzBN-CNBT1** and 492 nm for **DtCzBN-CNBT2**. Among the two, **DtCzBN-CNBT2** demonstrates superior exciton dynamics due to the favourable properties of the CNBT2 moiety. In a 15 wt% doped film in PhCzBCz, **DtCzBN-CNBT2** achieves a rapid k_{RISC} of 1.1×10^5 s^{-1}, a short τ_d of 15.3 μs, and a high PLQY of 97%. In contrast, **DtCzBN-CNBT1** exhibited a slower k_{RISC} of 2.0×10^4 s^{-1}, a longer τ_d of 75.5 μs, and a PLQY of 92%. Vacuum-deposited OLEDs using 15 wt% **DtCzBN-CNBT2** in PhCzBCz show a narrow green EL at

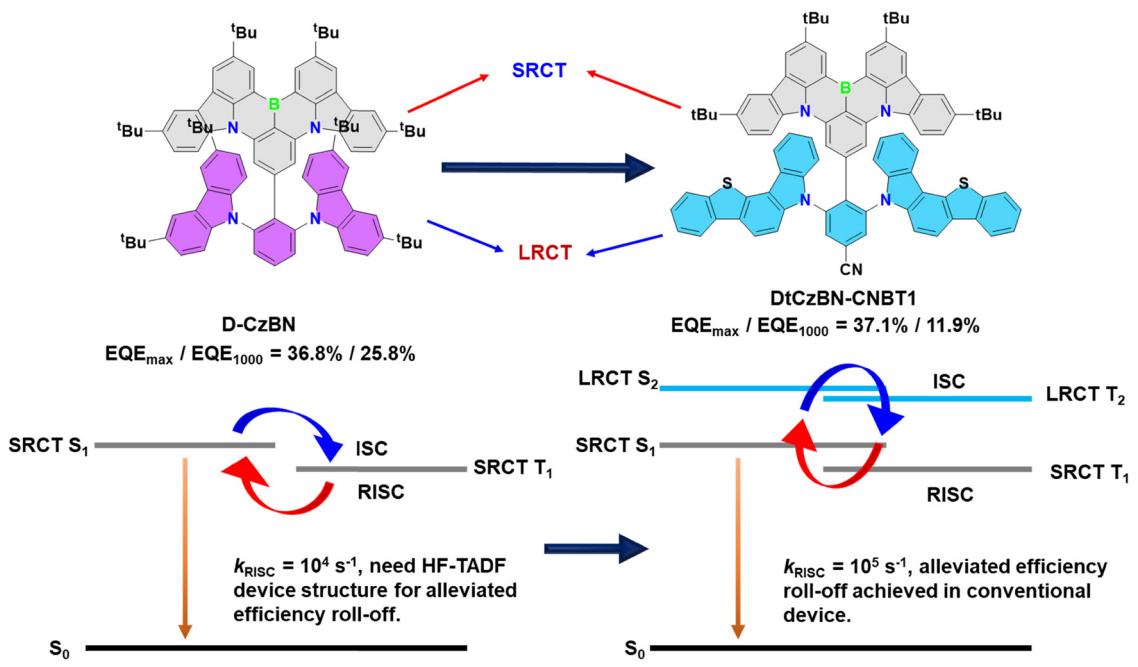

Fig. 15 Merging SRCT and LRCT to accelerate RISC.

508 nm (FWHM = 37 nm), with CIE coordinates of (0.17, 0.67), achieving a high maximum EQE of 40.2% and maintaining 20.7% at 1000 cd m^{-2}. In comparison, devices with **D*t*CzBN-CNBT1** emit at 507 nm (FWHM = 38 nm) and reach a peak EQE of 37.1%, but suffer from significant efficiency roll-off, with EQE dropping to 11.9% at 1000 cd m^{-2} due to the slower k_{RISC}. Additionally, solution-processed devices replicate the narrow emission profile of their vacuum-deposited counterparts but show lower efficiency retention. For **D*t*CzBN-CNBT2**, the solution-processed OLED achieved a maximum EQE of 24.4%, which decreased to 5.6% at 1000 cd m^{-2}. The **D*t*CzBN-CNBT1**-based solution device followed a similar trend, with an EQE peaking at 22.3% and declining to 4.8% at 1000 cd m^{-2}.

Sasabe *et al.* developed a series of π-extended phenoxazine-based asymmetric MR-TADF emitters, namely **PXZ-*t*CzBN**, **PhPXZ-*t*CzBN** and **MesPXZ-*t*CzBN**.[139] To increase the energy transfer efficiency and overall device performance, the molecular design is focused on extending the π-conjugation to enhance the spectral overlap with the phosphorescent sensitizer *fac*-tris(2-phenylpyridinato-C2,N)iridium(III) ($Ir(ppy)_3$). The photophysical properties reveal that in the solution state, these compounds exhibit green emission with maximum wavelengths (FWHM) of 510 nm (37 nm), 514 nm (41 nm) and 518 nm (43 nm) and PLQY of 88%, 85% and 80% for **PXZ-*t*CzBN**, **MesPXZ-*t*CzBN** and **PhPXZ-*t*CzBN**, respectively. In the solid state, these emitters showed efficient energy transfer for $Ir(ppy)_3$, as proved by solid-state PLQY of 63%, 85%, and 75%, respectively, along with a significantly shorter lifetime of ~10 μs, indicating the efficient Förster energy transfer (FRET). Furthermore, phosphorescent-sensitized OLEDs based on these MR-TADF emitters achieve maximum PE of 102.0 lm W^{-1}, 145.4 lm W^{-1}, and 150.3 lm W^{-1}, along with maximum EQEs of 20.7%, 27.3%, and 27.6%, and long LT_{95} of over 130, 59, and 3000 h at 1000 cd m^{-2} for **PXZ-*t*CzBN**, **MesPXZ-*t*CzBN**, and **PhPXZ-*t*CzBN**, respectively.

Lu *et al.* designed a series of MR-TADF materials, **Cz-CN-BN**, **TPA-CN-BN** and **PTZ-CN-BN**, utilizing a "hybridized long-short axis (HLSA)" molecular design strategy.[140] The hybridization combines the LRCT characteristics of high-lying triplet excited states and SRCT feature along the long axis skeleton of singlet states, which facilitates the spin–flip processes, enables narrowband emission, high PLQY, and fast RISC (Fig. 16). Compared to the typical MR-TADF molecule, **BCzBN**, the **Cz-CN-BN**, **TPA-CN-BN** and **PTZ-CN-BN** exhibit smaller ΔE_{ST} of 0.08 eV, 0.06 eV and 0.06 eV, and remarkably increased k_{RISC} of 1.1 × 10^5 s^{-1}, 1.4 × 10^5 s^{-1}, and 1.0 × 10^5 s^{-1}. The photoluminescence spectrum shows narrowband green emission with wavelengths of 496 nm (21 nm), 493 nm (23 nm) and 495 nm (26 nm) and PLQY of nearly 100% for **Cz-CN-BN**, **TPA-CN-BN** and **PTZ-CN-BN**. In addition, the sensitizer-free OLEDs using **Cz-CN-BN**, **TPA-CN-BN** and **PTZ-CN-BN** show narrowband green emission with maximum EQEs of 35.7%, 37.9%, and 33.7%, respectively, with reduced efficiency roll-off, with EQEs remaining at 32.1%, 34.8%, and 25.2% at a high luminance of 100 cd m^{-2}.

Lu *et al.* designed a simple MR-TADF emitter, **Cz-2PTz-BN**, by introducing *tert*-butyl carbazole at the *para*-position of the B-atom, which can reduce the π–π stacking and intermolecular interactions between B/N atoms.[141] Further introduction of the PTZ unit with sulfur atom, which facilitates the spin-flipping in the fused B/N skeleton (Chart 6). The photophysical properties show that the compound **Cz-2PTz-BN** exhibits green emission at a maximum wavelength of 505 nm with a PLQY of 86% and an enhanced RISC rate of 9.41 × 10^4 s^{-1} in toluene. The corresponding OLED device with 3 wt% doped with PhCzBCz exhibits an emission maximum of 520 nm, CIE color

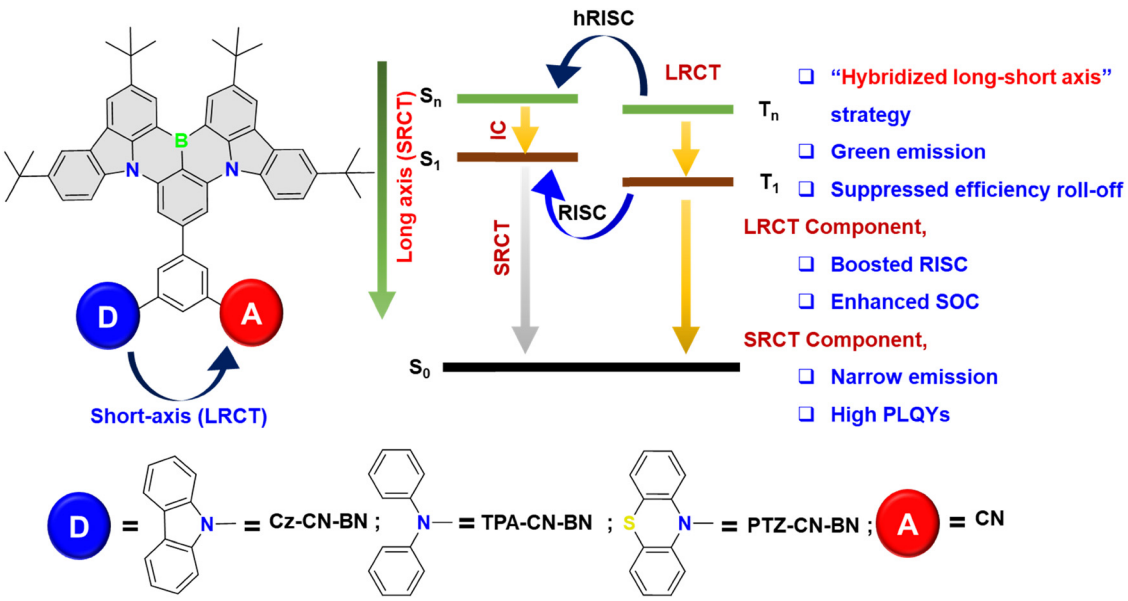

Fig. 16 Hybridized long-short axis (HLSA) molecular design for efficient MR-TADF emitters.

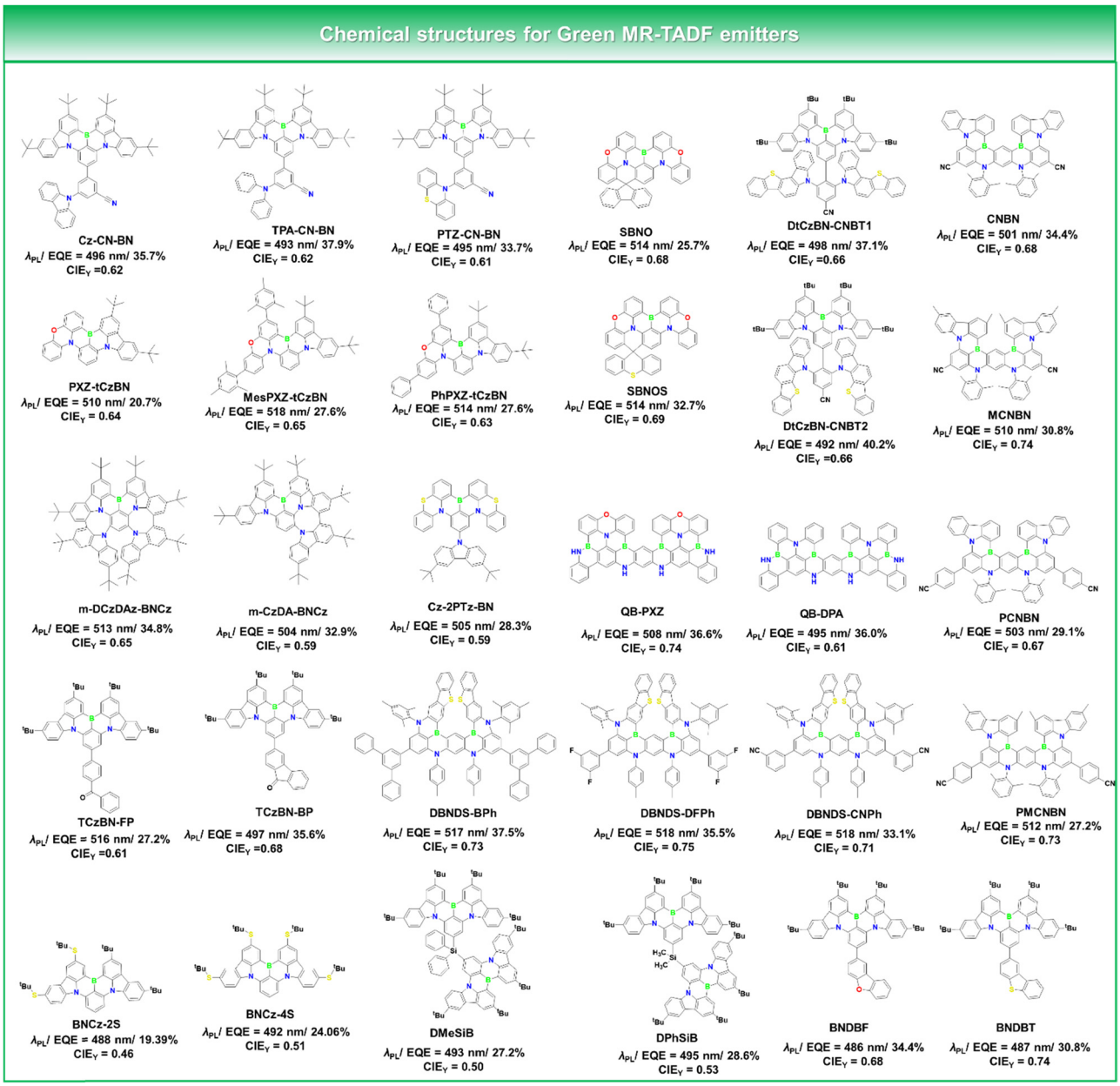

Chart 6 Chemical structure of green MR-TADF emitters.

coordinates of (0.30, 0.60), and a maximum EQE of 28.3% and the compound shows reduced efficiency roll-off.

To achieve ultrapure green emission and accelerate RISC in MR-TADF emitters, Yang *et al.* developed two quadrupole-borylated MR-TADF emitters, **QB-DPA** and **QB-PXZ**, using a π-extension and peripheral locking strategy in blue MR-TADF core (**ν-DABNA**).[142] The photophysical properties reveal that both compounds are bathochromically shifted compared to **ν-DABNA**, with the wavelength (FWHM) of 495 nm (15 nm) for **QB-DPA** and 508 nm (15 nm) for **QB-PXZ** in toluene. Due to the extended π-framework, the PLQY in the solid state was nearly unity of 98% for **QB-DPA** and 97% for **QB-PXZ**, enhanced k_{RISC} values of 2.5×10^5 s^{-1} for **QB-DPA** and 2.0×10^5 s^{-1} for **QB-PXZ** and perfect horizontal ratios of emitting dipole orientation ($\Theta_{\parallel}$). The corresponding sensitizer-free OLED devices based on **QB-DPA** and **QB-PXZ** exhibited narrowband green emission with maximum wavelengths (FWHM) of 502 nm (17 nm) and 516 nm (20 nm), CIE color coordinates of (0.10, 0.61) and (0.18, 0.74), and maximum EQE of 36% and 36.6%, respectively, with reduced efficiency roll off.

Wang *et al.* proposed a method to modulate the charge transfer excited states of MR emitters through intramolecular covalent bond locking (Fig. 17), which facilitates the conversion of strong ICT states to weak ICT states, thereby narrowing the FWHM, resulting in ***m*-CzDAz-BNCz** and ***m*-DCzDAz-BNCz**.[143] The photophysical properties reveal that the compounds show

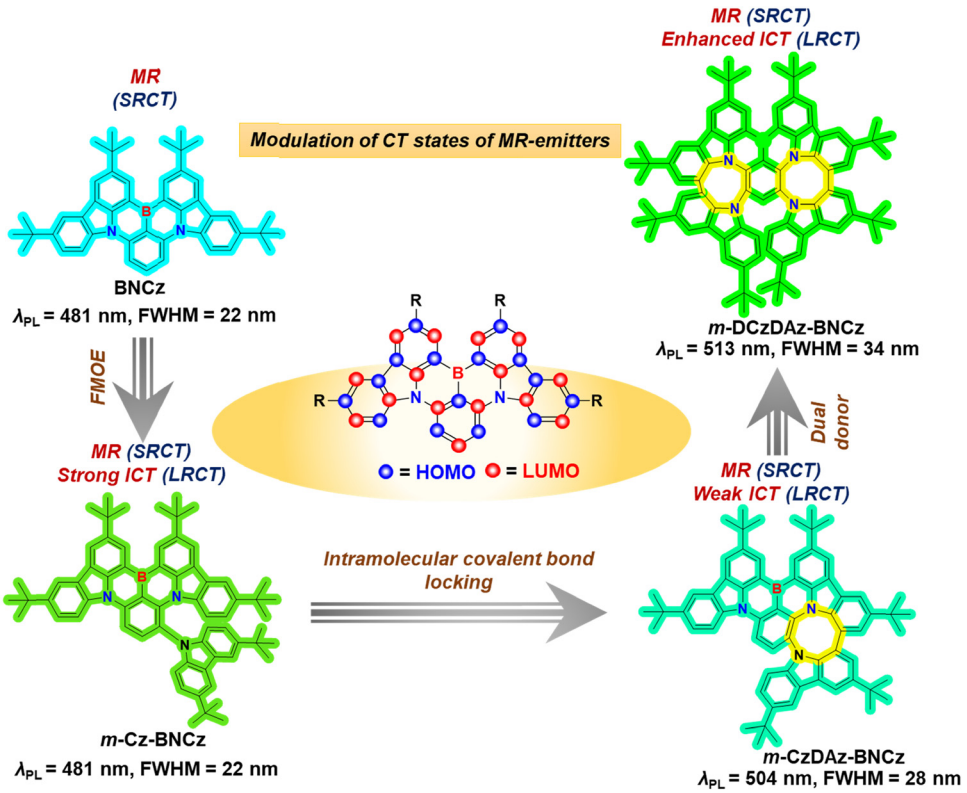

Fig. 17 Ring expansion strategy for the construction of efficient green MR-emitters.

an emission maximum of 504 nm (FWHM ~ 28 nm) and PLQY of 98% for ***m*-CzDAz-BNCz**, whereas 513 nm (FWHM ~ 89 nm) and PLQY of 89% for ***m*-DCzDAz-BNCz**. The slight red shift of ***m*-DCzDAz-BNCz** is due to the presence of a dual donor (*t*Cz) leads to enhancement of ICT. Both compounds show similar ΔE_{ST} values of 0.14 eV, which favors exciton upconversion. The sensitized OLEDs based on ***m*-CzDAz-BNCz** and ***m*-DCzDAz-BNCz** emitters exhibit a narrow EL emission at maximum wavelengths (FWHM) of 504 nm (30 nm) and 512 nm (35 nm) with CIE color coordinates of (0.12, 0.59) and (0.17, 0.65), respectively. Both compounds show maximum EQE values of 32.9% for ***m*-CzDAz-BNCz** and 34.8% for ***m*-DCzDAz-BNCz**, respectively, with reduced efficiency roll-off.

Li *et al.* synthesized two orthorhombic asymmetric conformational materials, **SBNO** and **SBNOS**, by adding a spirocarbon bridge in the "bay area" of an MR-TADF compound (BNO).[144] ACQ is successfully minimized by the orthogonal arrangement, which decreases intermolecular interactions between the chromophores of nearby molecules. Furthermore, these compounds' rigid structure aids in reducing vibrational relaxation. The photophysical properties of both materials show similar emission peaks at 514 nm with a FWHM of 30 nm. **SBNO** and **SBNOS** have PLQY of 89% and 93%, respectively. For **SBNO**-doped films, the lifespan ratios (τ_p/τ_d) are 7.38 ns/164.49 μs, whereas for **SBNOS**, they are 7.03 ns/154.45 μs. Furthermore, OLED devices fabricated with **SBNO** and **SBNOS** emitters had maximum EQEs of 32.7% and 25.7%, respectively, with severe efficiency roll-off.

Li *et al.* proposed a parallel "bifunctional group" modulation method to control the emission wavelength and FWHM. They synthesized three B/N-based green emitters, **DBNDS-TPh**, **DBNDS-DFPh**, and **DBNDS-CNPh**, by modifying the chlorine substituent in the *ortho* positions of two B-atoms in the novel B/N core, DBNDS-DC1, with triphenyl, 1,3-difluorobenzene and benzonitrile.[145] The photophysical studies of **DBNNDS-TPh**, **DBNDS-DFPh** and **DBNDS-CNPh** compounds in dilute toluene solution showed narrowband green emission peaks at 517, 518 and 518 nm with FWHM of 16, 16.4 and 16.6 nm and PLQY > 90%. Meanwhile, all the compounds show ΔE_{ST} of about 0.06, 0.08 and 0.08 eV, which promotes their enhanced k_{RISC} and decay rate. Furthermore, the conventional non-sensitized pure-green OLEDs utilizing **DBNDS-TPh** and **DBNDS-DFPh** showed EQE_{max} values of 35.0% and 34.5%, respectively, with corresponding CIE coordinates of (0.18, 0.75) and (0.17, 0.76) at a concentration of 1 wt%. The OLED corresponding to **DBNDS-DFPh** marks the first instance of a green OLED in a bottom-emitting device configuration achieving a CIE_y value above 0.75, reaching as high as 0.76, according to existing literature. Additionally, at a concentration of 3 wt%, the non-sensitized pure-green OLEDs based on **DBNDS-TPh** and **DBNDS-DFPh** attained peak EQE_{max} values of 35.2% and 36.0%, with CIE coordinates of (0.17, 0.75) and (0.19, 0.75), respectively.

Zheng *et al.* developed two silicic linkage-based dual-core MR-TADF emitters, **DMeSiB** and **DPhSiB**, in which two **D*t*BuCzB** units were incorporated with dichlorodimethylsilane (**DMeSiB**) and dichlorodiphenylsilane (**DPhSiB**) using a steric

hinderance strategy that suppresses both concentration quenching and spectral broadening.[146] Photophysical studies revealed that both **DMeSiB** and **DPhSiB** exhibited blue-green narrow emission with peak wavelengths at 493 and 495 nm and FWHM of 21 and 22 nm, respectively, indicating minimal structural relaxation between S_0 and S_1 states. Additionally, they also exhibit small ΔE_{ST} values ($\sim$0.2 eV) and high PLQY ($\sim$92%). The corresponding OLED device fabricated based on **DMeSiB** and **DPhSiB** exhibited maximum EQE of 27.2% and 28.6%, respectively, at 5 wt% doped concentration, and also exhibited narrow EL emission with wavelengths of λ_{EL} = 495 nm (FWHM = 25 nm) for **DMeSiB** and λ_{EL} = 496 nm (FWHM = 24 nm) for **DPhSiB**. When the doping concentration was increased to 20 wt%, **DMeSiB** and **DPhSiB** exhibited maximum EQE of 19.2% and 19.3%, respectively, while maintaining narrow emission with 2–3 nm broadening compared to 5 wt% doped devices. The device exhibits severe efficiency roll-off.

To enhance SOC and solution-processed methods, Fei *et al.* developed two MR-TADF emitters using an alkylthio-substituted carbazole building block, resulting in **BNCz-2S** and **BNCz-4S**.[147] As the number of sulfur atoms increases, **BNCz-4S** exhibits a superior PLQY of 99%, a smaller ΔE_{ST} of 0.07 eV, reorganization energy, a larger SOC constant, which facilitates the spin–flip of triplet excitons and a higher k_{RISC} of 7.88×10^4 s^{-1} as compared to **BNCz-2S**, PLQY of 93%, a smaller ΔE_{ST} of 0.11 eV and k_{RISC} of 3.68×10^4 s^{-1}. Furthermore, these compounds show emission at 488 nm and 492 nm with FWHM of 26 nm and 30 nm for **BNCz-2S** and **BNCz-4S**. The corresponding solution-processed OLED device based on **BNCz-2S** and **BNCz-4S** shows a sharp emission peak (λ_{EL}) at 492 and 496 nm with FWHM of 43 and 34 nm, and CIE color coordinates of (0.11, 0.46) and (0.14, 0.51), respectively. Furthermore, they demonstrated superior device efficiencies (CE_{max}/PE_{max}/EQE_{max}) of 16.30 cd A^{-1}/33.20 lm W^{-1}/19.39% for **BNCz-2S** and 2.94 cd A^{-1}/46.88 lm W^{-1}/24.06% for **BNCz-4S**, respectively.

Yang *et al.* developed a series of MR-TADF emitters featuring sky-blue double boron MR-skeletons with rigid cyano (**CNBN** and **MCNBN**) and 4-cyanophenyl (**PCNBN** and **PMCNBN**) acceptor groups.[148] Photophysical studies revealed that all the compounds emitted green light, with peak wavelengths ranging from 500 to 519 nm. Cyano derivatives exhibited a narrower FWHM than the 4-cyanophenyl derivatives. The 4-cyanophenyl derivatives showed a slight red shift in emission, which was attributed to the combined effects of electron-withdrawing characteristics and enhanced π-conjugation. OLED devices based on these emitters demonstrated excellent EL performance, with narrowband pure green emission. The maximum EQE_{max} for the devices was 34.4%, 30.8%, 29.1%, and 27.2% for **CNBN**, **MCNBN**, **PCNBN**, and **PMCNBN**, respectively. Notably, the OLED incorporating **MCNBN** achieved ultrapure green emission at 517 nm, with CIE coordinates of (0.17, 0.74), which perfectly matches the BT.2020 green OLED standard.

Lu *et al.* developed two MR-TADF emitters, **BNDBF** and **BNDBT**,[149] in which electron-deficient dibenzofuran (DBF) and dibenzothiophene (DBT) were attached to the MR-skeleton through a single bond using a phenyl linker. In the toluene solution, both compounds exhibited green emission with wavelength peaking (λ_{PL}/FWHM) at (486 nm/21 nm) for **BNDBF** and (487 nm/22 nm) for **BNDBT** with high PLQY of 84% and 86%, respectively. Due to the presence of a heavy S-atom in **BNDBT**, it shows a shortened delayed fluorescence lifetime of 33.21 μs and rapid k_{RISC} of 6.02×10^4 s^{-1} compared to **BNDBT** due to the larger SOC in **BNDBT**. Furthermore, the OLED device based on BNDBF and **BNDBT** exhibits narrowband green emission with a maximum EQE of 32.6% for **BNDBF** and 35.5% for BNDBT.

4. Challenges and strategies in yellow MR-TADF materials

Konidena *et al.* recently proposed a novel design by incorporating an additional indole unit into the parent MR-core, creating the compound **CzCzB**.[150] This structure features *para*-N–π–N conjugation between one of the carbazole units of the MR core and the outer carbazole unit, which significantly enhances charge delocalization throughout the B,N-PAH framework. This increased delocalization stabilizes the S_1 and T_1 energy levels, leading to a notable bathochromic shift of approximately $\sim$70 nm compared with that of the original parent core, **CzB** (Table S5, ESI†). Although its FWHM was slightly broader around 48 nm, **CzCzB** emitted yellow light with a peak at 558 nm. The OLED device using **CzCzB** exhibited solid performance, achieving an EQE of 19% and CIE coordinates of (0.43, 0.56).

As at continuation, Wang *et al.* recently synthesized two MR-TADF materials based on FMOE to achieve red-shifted emission, **BN-Cz** and **BN-Cb**.[151] They replaced the Me-group in the outer carbazole unit of **CzCzB** with a butyl group to create the **BN-Cz** emitter (Chart 7). To fine-tune the photophysical characteristics of **BN-Cz**, they employed the nitrogen embedding molecular engineering (NEME) technique to develop **BN-Cb**. Both the **BN-Cz** and **BN-Cb** compounds exhibit yellow emissions with peak wavelengths of 551 nm, representing a blue shift of approximately 7 nm compared with the **CzCzB** compound. The FWHM values for **BN-Cz** and **BN-Cb** are 49 and 41 nm, respectively, with Stokes shifts of 33 and 29 nm, respectively. The corresponding OLED device based on these compounds exhibits bright yellow emission with maximum wavelengths (FWHM) of 560 nm (49 nm) and 556 nm (45 nm) with CIE color coordinates of (0.44, 0.55) and (0.43, 0.56) for **BN-Cz** and **BN-Cb**, respectively. Moreover, the maximum efficiencies for EQE/CE/PE are remarkable, with **BN-Cz** achieving 32.9%/114.0 cd A^{-1}/130.8 lm W^{-1} and **BN-Cb** achieving 29.7%/113.1 cd A^{-1}/131.6 lm W^{-1}, respectively.

Duan *et al.* developed two narrowband yellow MR-TADF emitters, **DBN-ICz** and **BN-DICz**, utilizing a multi-fusion molecular design strategy.[152] This strategy enables simultaneous extension of π-conjugation, improved structural rigidity, and reduced vibrational frequency compared to their parent green emitter, BN-Cz. In toluene solution, these compounds exhibit yellow emission with peak wavelengths (FWHM) of 533 nm

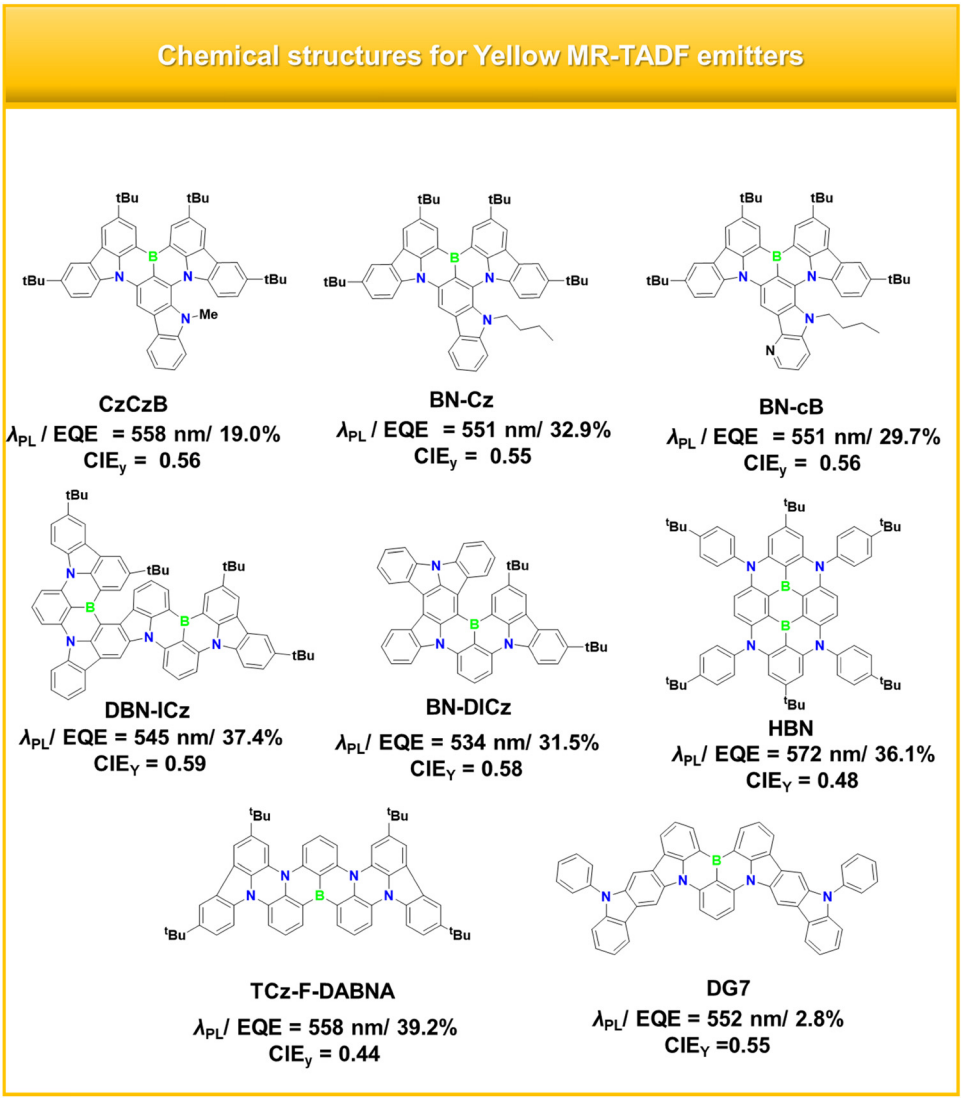

Chart 7 Chemical structure of the yellow MR-TADF emitters.

(20 nm) for **DBN-ICz** and 542 nm (18 nm) for **BN-DICz**, demonstrating nearly unity PLQY. When incorporated into OLEDs as 3 wt% dopants, **DBN-ICz** and **BN-DICz** displayed narrowband yellow emission with maximum efficiencies (EQE_{max}/CE/PE) of 37.4%/136.6 cd A^{-1}/119.2 lm W^{-1} and 31.5%/123.3 cd A^{-1}/88.6 lm W^{-1}, respectively.

Sini *et al.* recently developed an indolocarbazole-based MR-TADF emitter (**DG7**), which demonstrates distinctive optical characteristics in toluene solution.[153] It exhibits greenish-yellow PL and EL emissions with a FWHM of 20 nm and a PLQY of 100% in degassed and sonicated samples; however, it does not display TADF behavior. The observed increase in PL intensity is primarily attributed to reduced singlet state quenching by dissolved oxygen and the presence of remaining microaggregates in toluene solution, in contrast with the more commonly reported triplet exciton quenching by oxygen. In the thin-film state, **DG7** shows yellow emission with a (FWHM of 30 nm and a PLQY of only 4%, a result of strong π–π interactions that lead to aggregation-induced quenching. The lack of TADF behavior is due to the minimal SOC between the singlet (S_1) and triplet (T_1) states (0.02 cm^{-1}) and the significant energy gap between T_1 and T_2 states, which hinders RISC. However, a weak TADF effect was observed in a guest–host mixture, attributed to a reduced T_1–T_2 energy gap caused by the structural distortion of the emitter. The EL properties of this compound reveal a low EQE of 2.8% and substantial efficiency roll-off, largely due to its limited ability to utilize triplet excitons, resulting in yellow emission at 559 nm with an FWHM of 23 nm (Table S6, ESI†).

In contrast to previous strategies such as FMOE, *para*-E–π–E (E = N, S, or O), and *para*-B–π–B, Zhang *et al.* introduced a novel molecular design approach by extending conjugation through fused carbazole donors on the DABNA core.[154] The resulting compound, **TCZ-F-DABNA**, exhibited a significant bathochromic shift of approximately 96 nm compared to **DABNA**, which was attributed to the extended molecular orbital distribution and longer π-conjugation. Thus, **TCZ-F-DABNA** exhibited narrow yellow emission with a peak wavelength of 558 nm and a FWHM of

38 nm. The compound displayed minimal concentration quenching, achieving an exceptionally high PLQY of 99%. Solvatochromic studies indicated a moderate red shift with increasing solvent polarity, suggesting a mild ICT character while preserving dominant MR features. Transient photoluminescence measurements revealed a short τ_d of 20 μs due to a small ΔE_{ST} of approximately 0.12 eV. OLED devices incorporating **TCZ-F-DABNA** achieved a record-high EQE of 39% in the long-wavelength region, primarily due to its high PLQY and a high $\Theta_{\parallel} \approx 96\%$.

Zheng *et al.* designed a tetraazacyclophane-based structure (**HBN**) to achieve long-wavelength ultra-narrowband emission.[155] This strategy enhances the ICT characteristics and promotes small SRCT, which facilitates the ultra-narrowband long wavelength emission. Therefore, the compound **HBN** demonstrates yellow emission wavelength peaking at 572 nm with a FWHM of 17 nm in dilute toluene, whereas emission was slightly red-shifted and broadened in doped films. Furthermore, the corresponding phosphor-sensitized OLED device with 2 wt% **HBN**:30 wt% Bt2Ir(acac) in the mCBP-based device exhibited a yellow emission peak at 581 nm with a FWHM of 25 nm, a maximum EQE of 36.1% with low efficiency roll-off and luminescence exceeding 40 000 cd m^{-2}.

5. Challenges and strategies for orange MR-TADF emitters

Bin *et al.* introduced **CNCz-BNCz**, the first orange-emitting MR-TADF compound, by incorporating a simple CN acceptor group onto the central phenyl ring of **BBCz-Y** in a position *para* to the boron atom.[156] This modification combines the effects of *para*-N–π–D and *para*-B–π–A interactions in **CNCz-BNCz**, resulting in a significant bathochromic shift (Fig. 18). As expected, **CNCz-BNCz** exhibited orange emission with a λ_{PL} of 583 nm, indicating a redshift of **BBCz-Y**. Due to the minimal structural relaxation of the simple CN acceptor group in the excited state, the compound maintained a FWHM of approximately 42 nm, which was identical to that of **BBCz-Y**. **CNCz-BNCz** also demonstrated a small ΔE_{ST} and an impressive PLQY of 96%. Moreover, its k_{RISC} was significantly enhanced compared with that of the reference material, highlighting its strong TADF characteristics. When incorporated into an OLED, **CNCz-BNCz** displayed orange-red emission at λ_{EL}/FWHM ≈ 584 nm/49 nm and achieved an EQE of 23%. However, it experienced notable efficiency roll-off at high brightness levels. To address this, a TADF-hosted OLED was fabricated, which achieved a maximum EQE of 33.3% with a much-reduced efficiency roll-off.

Yang *et al.* recently introduced a novel molecular design by incorporating the indolophenazine (IPz) building block, a strong donor, into B/N-doped PAHs (Chart 8). This design aimed to shift the emission spectrum toward longer wavelengths through enhanced molecular conjugation and strengthened ICT while maintaining narrowband emission due to the rigid structure of IPz, which preserves the intrinsic MR characteristics. To explore this concept, they developed a series of symmetrical and asymmetrical MR-TADF emitters based on IPz, paired with secondary electron-donating segments: **BNIP-*t*BuCz**, **BNIP-*t*BuDAPC**, **BNIP-CzDPA**, and **BNDIP**.[157] Photophysical analysis revealed that the electron-donating strength of the donor segments significantly

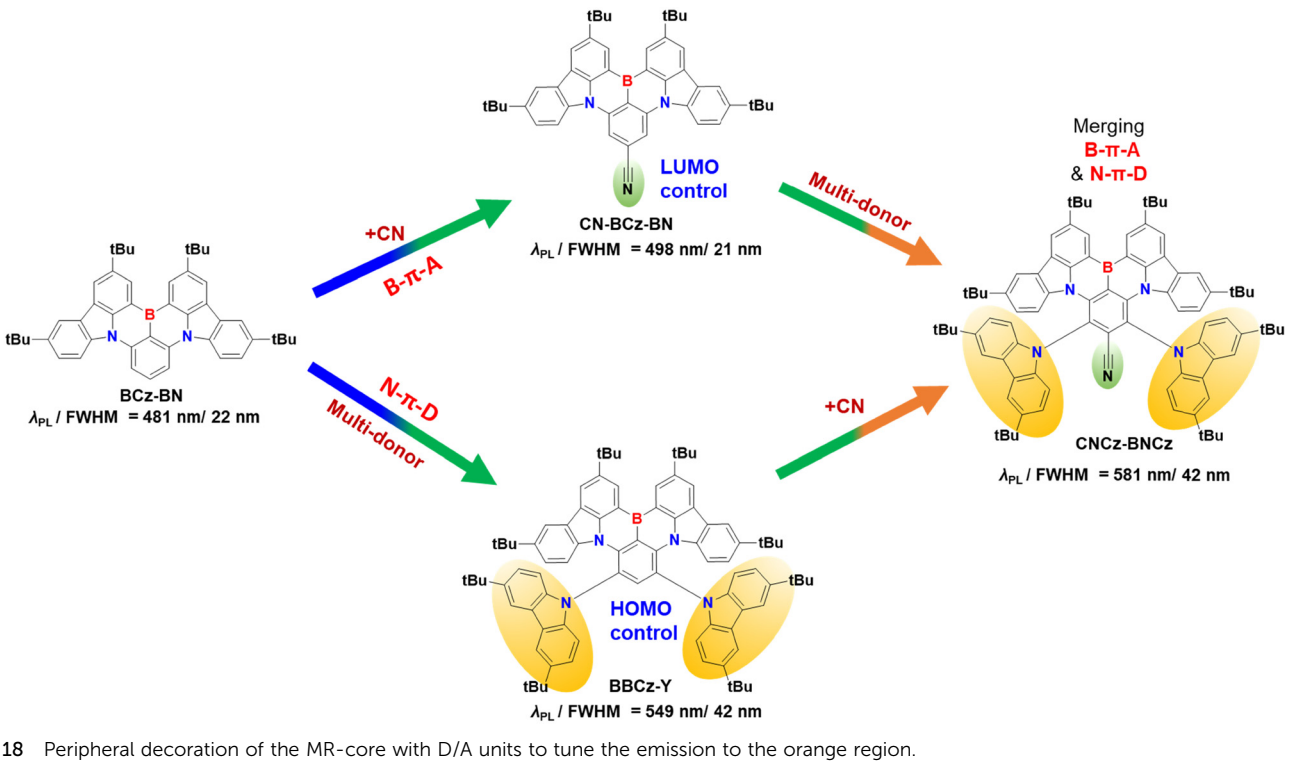

Fig. 18 Peripheral decoration of the MR-core with D/A units to tune the emission to the orange region.

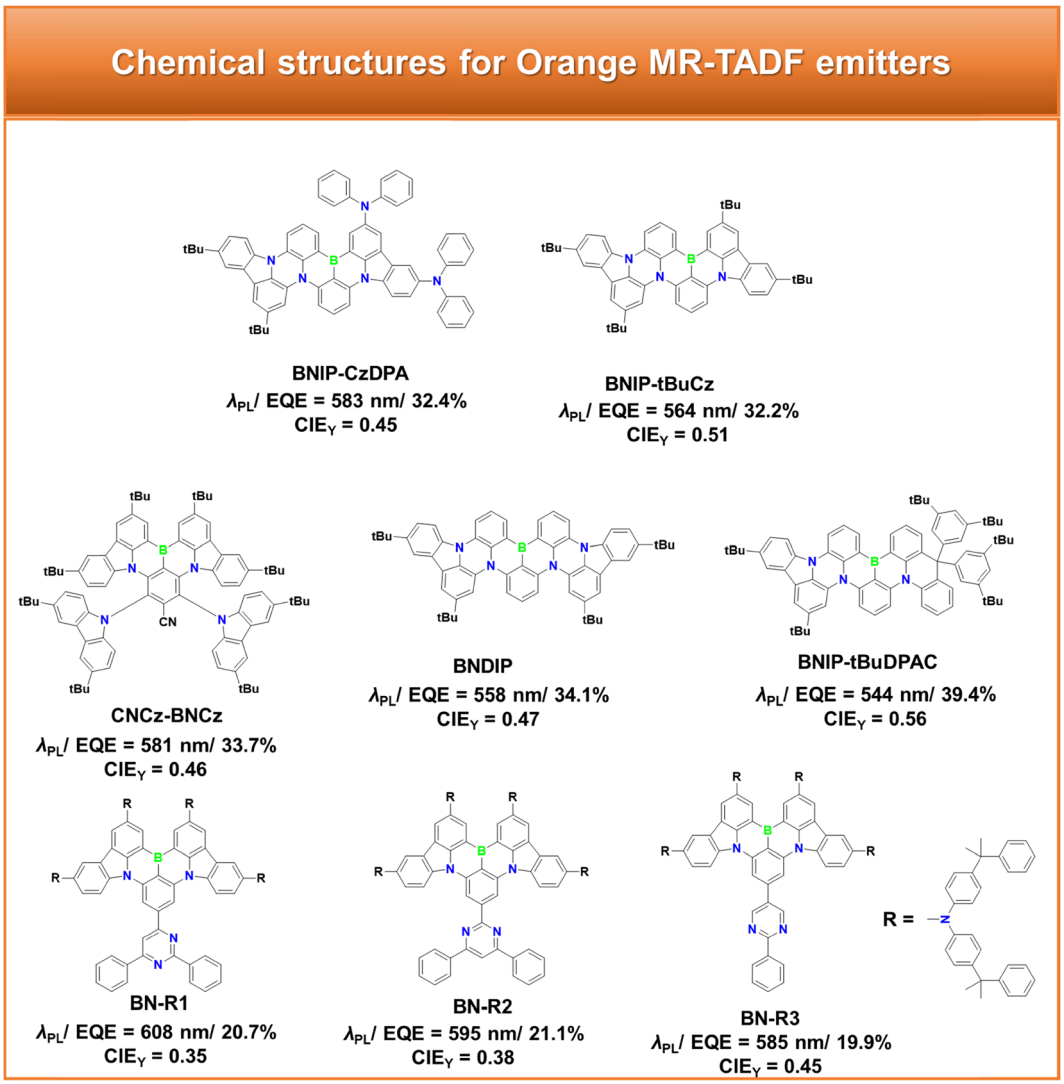

Chart 8 Chemical structure of orange MR-TADF emitters.

influenced the emission wavelength and TADF properties. These materials exhibited a combination of long-range ICT and MR-induced charge transfer. **BNIP-*t*BuCz** (λ_{PL} ~ 564 nm) exhibited a 20 nm red shift relative to **BNIP-*t*BuDAPC** (λ_{PL} ~ 544 nm), though with broader emission (FWHM ~ 60 nm), as the large donor difference in **BNIP-*t*BuCz** favours long-range CT-dominant emission. **BNIP-CzDPA** exhibited the most red-shifted emission in the series (λ_{PL} ~ 583 nm) while maintaining a narrower profile (FWHM ~ 49 nm) due to an extended HOMO over its terminal carbazole segments. **BNDIP**, on the other hand, displayed a blue-shifted emission at λ_{PL} ~ 558 nm. All materials achieved near-total $\Theta_{\parallel}$ ~ 100% and near-unity PLQY. In OLED devices, the emitters exhibited yellow-orange emissions with the following characteristics: **BNIP-*t*BuCz** (λ_{EL}/FWHM/EQE = 566 nm/69 nm/32.8%), **BNIP-*t*BuDAPC** (λ_{EL}/FWHM/EQE = 554 nm/58 nm/39.4%), **BNIP-CzDPA** (λ_{EL}/FWHM/EQE = 584 nm/62 nm/32.4%), and **BNDIP** (λ_{EL}/FWHM/EQE = 582 nm/67 nm/34.4%). The high EQE of **BNIP-*t*BuDAPC** is largely attributed to its high $\Theta_{\parallel}$ (~ 98%). The **BNDIP**-based device exhibited an extended operational lifetime, with an LT_{99} exceeding 110 hours at an initial luminance (L_0) of 3000 cd m^{-2}.

Zhuang *et al.* developed an orange-red MR-TADF emitter with suppressed aggregation-induced quenching by utilizing the FMOE strategy, modifying a set of pyrimidine derivatives (**BN-R1**, **BN-R2**, and **BN-R3**).[158] By incorporating different pyrimidine units with varying electron-donating abilities into the LUMO position of the yellow MR-TADF emitter, BN-Y, they successfully achieved red-shifted emission in the solid state compared to the solution state. This was attributed to the effective suppression of aggregation-induced quenching and spectral broadening, which was facilitated by steric hindrance from the electronically inert terminal substituents. In the solution state, **BN-R1**, **BN-R2**, and **BN-R3** exhibited PL emissions with peak wavelengths (λ_{PL}/FWHM) of 608 nm/43 nm, 595 nm/36 nm, and 585 nm/40 nm, respectively (Table S7, ESI†). In contrast, in the solid state, the emissions were further red-shifted to 618 nm/48 nm, 607 nm/45 nm, and 591 nm/

48 nm. These newly synthesized compounds were incorporated as sensitizers in solution-processed OLED devices, producing high-color-purity orange-red light with peak wavelengths (λ_{EL}/FWHM) of 611 nm/44 nm, 601 nm/41 nm, and 587 nm/44 nm. The corresponding CIE color coordinates were (0.64, 0.35), (0.60, 0.39), and (0.55, 0.44) for **BN-R1**, **BN-R2**, and **BN-R3**, respectively. The maximum efficiencies of the devices using **BN-R1**, **BN-R2**, and **BN-R3** were 19.0%, 20.4%, and 20.4%, respectively, demonstrating their promising performance in OLED applications (Table S8, ESI†).

6. Challenges and strategies in red and near-infrared (NIR) MR-TADF materials

Duan *et al.* further refined the *para*-N–π–N and *para*-B–π–B molecular design strategy to create deep-red and NIR MR-TADF emitters, named **R-BN** and **R-TBN**.[159] This was achieved by incorporating two *para*-N–π–N and one *para*-B–π–B conjugated pathways within a PAH framework, through the integration of four carbazole units and two boron atoms. The presence of strong N and B elements effectively stabilized the HOMO and LUMO levels, resulting in a significantly reduced bandgap of $\leq$1.7 eV. Consequently, **R-BN** and **R-TBN** exhibited deep-red and NIR emission, with peak wavelengths at 662 and 696 nm, respectively, while maintaining the MR character (Table S9, ESI†). Both compounds demonstrated short τ_d and moderate k_{RISC} around 10^4 s^{-1}. OLED devices incorporating these emitters-using $Ir(mphmq)_2tmd$ as a sensitizer-delivered deep-red EL with λ_{EL}/FWHM/EQE values of 664 nm/48 nm/28.1% for **R-BN** and 686 nm/49 nm/27.6% for **R-TBN**. The devices also achieved saturated red color with CIE coordinates of (0.71, 0.28) for **R-BN** and (0.72, 0.27) for **R-TBN**. Both devices exhibited excellent operational lifetimes, with LT_{90} values of approximately 125 hours (**R-BN**) and 151 hours (**R-TBN**) at an initial luminance of 2000 cd m^{-2}. These findings highlight the effectiveness of combining *para*-N–π–N and *para*-B–π–B conjugation in designing high-performance deep-red MR-TADF materials.

Recently, Wang *et al.* developed two NIR MR-TADF emitters, **PXZ-R-BN** and **BCz-R-BN**, by incorporating 10*H*-phenoxazine (PXZ) and 7*H*-dibenzo[*c*,*g*]carbazole (BCz) units in a BN-PAH core to enhance electron donating and extending the π-conjugation.[160] Their rigid, butterfly-like structures resulted in high PLQYs, favorable $\Theta_{\parallel}$, and narrow emission spectra in the NIR region. Photophysical studies revealed λ_{PL}/FWHM of 688 nm/49 nm for **PXZ-R-BN** and 715 nm/43 nm for **BCz-R-BN**. The slight blue shift observed in **PXZ-R-BN** compared to the parent core, **R-TBN** (692 nm), can be attributed to the distorted π-conjugation in the phenoxazine core. Additionally, a 1 wt% PMMA film exhibited PL emissions at 697 nm and 718 nm, with narrow FWHM values of 55 nm (0.14 eV) and 52 nm (0.12 eV), respectively. The phosphorescence sensitized OLEDs based on **PXZ-R-BN** achieved an exceptional maximum EQE of 29.3% with an EL peak at 693 nm and a narrow FWHM of 59 nm. The EQE of the **BCz-R-BN**-based OLEDs was 24.2%, with an EL peak at 713 nm and a FWHM of 56 nm. The **PXZ-R-BN** OLED device demonstrated long operational stability with LT_{97} of 39 084 hours at an initial radiance of 1000 mW sr^{-1} m^{-2}, while the **BCz-R-BN** OLED exhibited operational stability with LT_{90} values of 309 hours and 697 hours at initial radiances of 1614 mW sr^{-1} m^{-2} and 1000 mW sr^{-1} m^{-2}, respectively (Table S10, ESI†). This study offers an effective molecular design strategy for narrowband NIR MR-TADF emitters and underscores the potential for high-performance NIR OLEDs with outstanding efficiency and extended operational lifetimes.

Yang *et al.* developed a series of pure red MR-TADF emitters, **BNO1–BNO3**, by replacing one of the *para*-N–π–N configurations with *para*-O–π–O. This modification was designed to reduce the electron-donating strength, as oxygen is a weaker donor than nitrogen, resulting in a hypsochromic shift in the optical properties compared to **R-TBN**.[161] The emission wavelengths and TADF characteristics of these materials were fine-tuned by decorating the O atom with various aryl groups. Despite the weaker electron-donating capability of oxygen, all emitters exhibited λ_{PL} above 600 nm and maintained a narrow emission profile, with FWHM under 33 nm. Notably, **BNO3** displayed a pure red emission with λ_{PL} at 616 nm and an FWHM of 33 nm. Photophysical studies showed that these materials possessed a high PLQY of 95% or higher and demonstrated good TADF characteristics, indicated by their narrow ΔE_{ST} and short τ_d. Initially, TADF-hosted OLED devices using these emitters achieved low EQEs under 15% and showed significant efficiency roll-off. However, the series showed marked improvement upon incorporating phosphorescent sensitization **BNO3**, in particular, achieved a maximum EQE of 36.1% with minimal roll-off, retaining an EQE of 28.6% at a luminance of 10 000 cd m^{-2}. All materials consistently exhibited pure red emission with CIE_x coordinates of approximately 0.64–0.67. The **BNO1**-based device displayed an operational lifetime with LT_{90} of approximately 49.8 hours.

They further introduced two new red MR-TADF emitters, **RBNO1** and **RBNO2**, designed by embedding three nitrogen atoms and one oxygen atom into a double boron-containing PAH framework.[162] This structural modification enhanced π-conjugation and strengthened SRCT, leading to red-shifted emissions compared to the earlier BNO series (Fig. 19). Both **RBNO1** and **RBNO2** displayed pure red emission with narrow spectral profiles, exhibiting λ_{PL}/FWHM values at 631/39 and 645/39 nm, respectively. These emitters also achieved a high PLQY of approximately 95% and maintained a small ΔE_{ST} above 0.23 eV. Temperature-dependent transient PL measurements confirmed TADF activity, with τ_d of 26.4 ms for **RBNO1** and 25.3 ms for **RBNO2**-markedly shorter than that of **BNO1** (90.1 ms). This indicates that carbazole functions as a more effective resonance partner than phenol in promoting efficient delayed fluorescence in MR-TADF systems. When employed in phosphorescent-sensitized OLEDs, **RBNO1** and **RBNO2** delivered outstanding device performance. They achieved high EQE_{max} values of 33.1% and 34.1% and exhibited minimal efficiency roll-off under high luminance conditions. Both emitters produced vivid red electroluminescence with emission peaks/FWHM of 645/48 nm (**RBNO1**) and 648/49 nm (**RBNO2**).

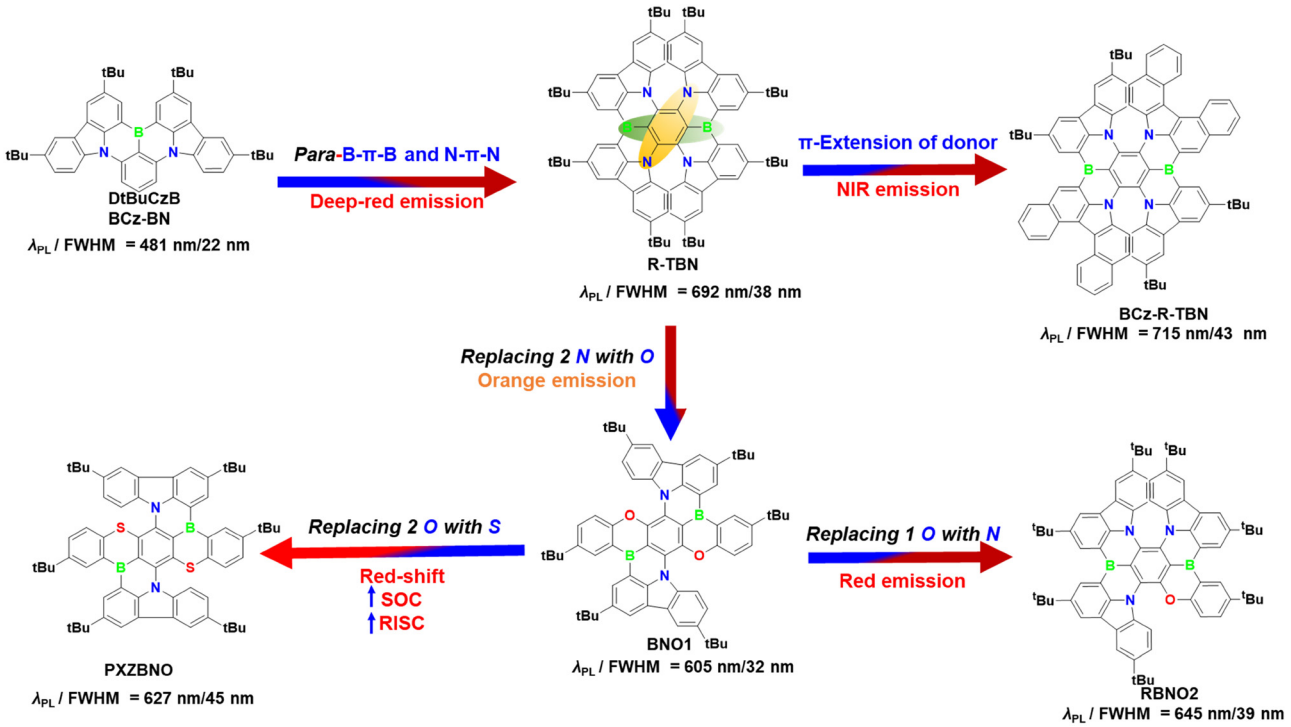

Fig. 19 Design strategies for developing efficient red MR-TADF emitters.

Notably, the CIE coordinates for **RBNO2** (0.70, 0.29) are in close alignment with the BT.2020 red color standard, underscoring the promise of this molecular design for high-fidelity red OLED applications.

Wang *et al.* advanced the design of red MR-TADF emitters by applying FMO engineering to a parent BN core. They introduced an electron-donating DPA unit at the HOMO-dominant positions on the carbazole moiety and an electron-accepting triazine group at the LUMO-dominant carbon on the central phenyl ring, located *para* to the B atom. This configuration created a *para*-N–π–D and *para*-B–π–A framework, leading to the development of two emitters: **BN-Y** and **BN-R**.[163] DFT calculations confirmed that the DPA donor and triazine acceptor in **BN-R** effectively contributed to the HOMO and LUMO, respectively, while preserving the MR nature of the core. This molecular tuning stabilized both frontier orbitals, resulting in a narrowed bandgap and red-shifted emission. **BN-R** exhibited red emission at ~624 nm, whereas **BN-Y** emitted yellow light at ~567 nm. Despite the bathochromic shifts, both compounds maintained narrow emission bandwidths with FWHM values under 46 nm, consistent with MR-based emission profiles. Photophysical studies revealed high PLQYs exceeding 94%, small $\Delta E_{ST} < 0.12$ eV, and short τ_d, confirming efficient TADF behaviour. The presence of methyl groups on the donor segments also enhanced solubility, enabling solution processing. OLEDs fabricated using **BN-R** as a dopant achieved red emission with λ_{EL}/FWHM at 621 nm/46 nm and a maximum EQE of 22%. However, the device experienced notable efficiency roll-off, attributed to **BN-R** relatively slow k_{RISC} and short τ_d. To mitigate this, sensitized OLEDs were constructed using **BN-R** as the terminal emitter. These devices retained the emission characteristics of **BN-R** while significantly reducing efficiency roll-off. Importantly, the LT_{50} improved dramatically-from 118 hours to 1030 hours at an initial luminance of 1000 cd m^{-2}. This work represents a significant milestone in achieving both high efficiency and extended device lifetimes for solution-processed, long-wavelength MR-TADF OLEDs.

Zou *et al.* modified **BNO1** by replacing two *t*-Bu-carbazole units with electron-rich phenothiazine and phenoxazine (Chart 9), resulting in **PXZBNO** and **PTZBNO**.[164] This modification enhanced the donor strength due to the presence of phenothiazine and phenoxazine, leading to further red-shifted emissions with λ_{PL}/FWHM values of 612/45 nm for **PXZBNO** and 627/45 nm for **PTZBNO**. Both emitters exhibited nearly unity PLQY and high k_r around 10^7 s^{-1}. Their ΔE_{ST} and τ_d were measured as 0.27 eV/27 μs for **PTZBNO** and 0.30 eV/60 μs for **PXZBNO**, with **PTZBNO**'s shorter τ_d attributed to the sulfur heavy atom effect. Phosphorescent-sensitized OLED devices were fabricated using these emitters as dopants. **PTZBNO** demonstrated the highest performance, achieving an EQE_{max} of 34.5% with red EL at approximately 618 nm. Notably, **PTZBNO** showed suppressed efficiency roll-off at high brightness, attributed to its fast RISC rate, enhancing its suitability for high-performance OLED applications.

Wang *et al.* further advanced the BNO-based MR-TADF framework by replacing the oxygen atom in the tri-decacyclic aromatic skeleton with sulfur, resulting in the development of two red-emitting MR-TADF compounds: **DBNS** and **DBNS-*t*Bu**.[165] This substitution introduced a heavy atom effect from

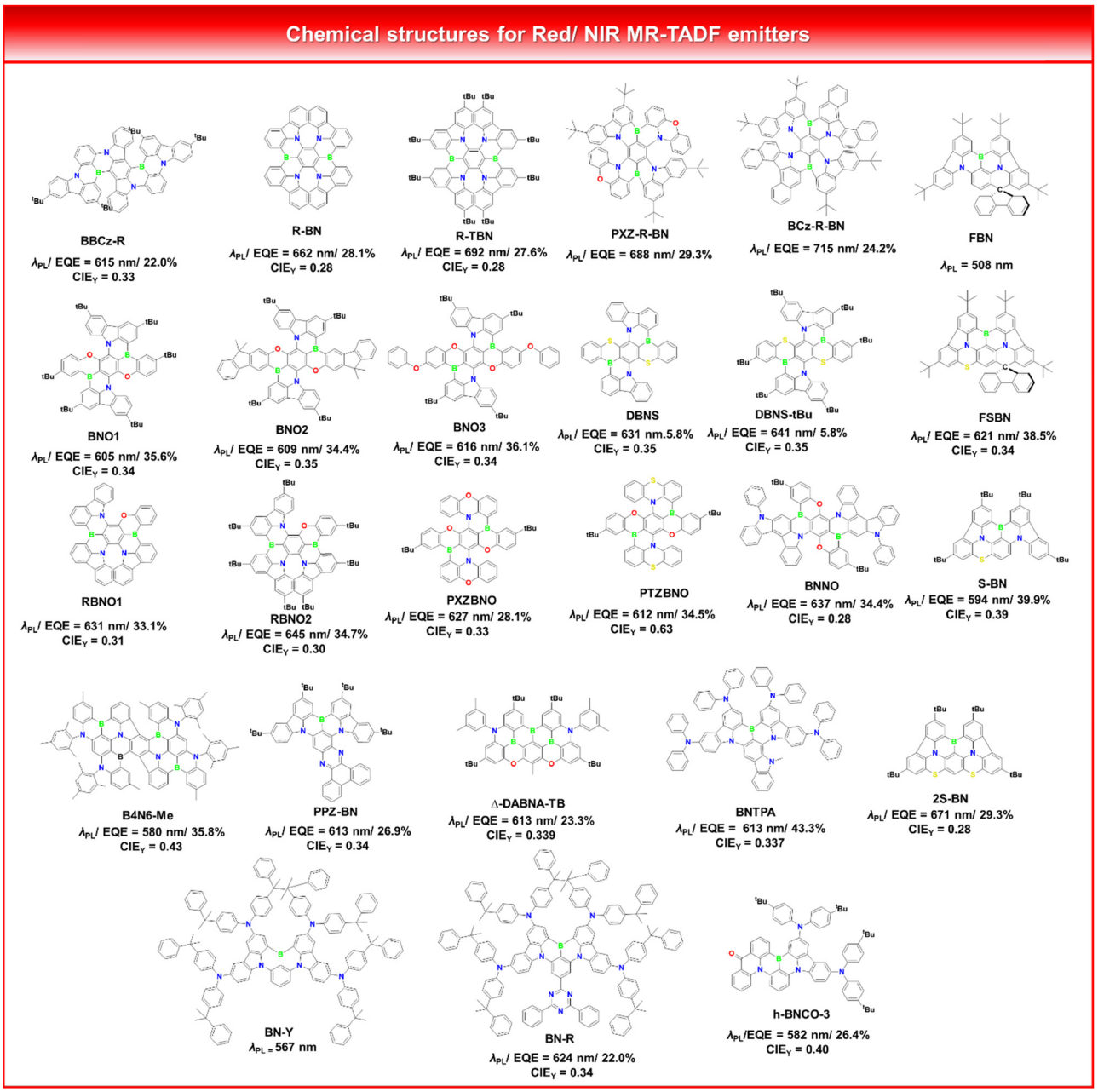

Chart 9 Chemical structure of red MR-TADF emitters.

sulfur, which contributed to enhanced SOC and promoted more efficient RISC. Both emitters exhibited red emission, with λ_{PL} at 631 nm for **DBNS** and 641 nm for **DBNS-*t*Bu**. Although their emission profiles remained relatively narrow, their FWHM values were slightly broader (around 40 nm) than those of conventional oxygen-containing BNO-type emitters. The presence of sulfur notably increased the SOC between the T_2 and S_1 states, with values exceeding 1.38 cm^{-1}. This led to accelerated RISC, particularly in **DBNS-*t*Bu**, which demonstrated a high k_{RISC} of 2.2 $\times$ 10^5 s^{-1}. A solution-processed OLED incorporating **DBNS-*t*Bu** as the emitter achieved a maximum EQE of 7.8%, highlighting the role of sulfur in boosting RISC efficiency and enabling red-shifted emission while preserving the MR-TADF characteristics.

Zhang and Duan *et al.* recently developed a novel red-emitting MR-TADF material, **BNNO**, by modifying the established BNO framework through the replacement of two carbazole units with rigid, strongly electron-donating indolocarbazole (23CICz) moieties.[166] The 23CICz units were chosen due to their *para*-N–π–N conjugation, which significantly enhances electron donation, and their extended planar structure, which boosts π-conjugation across the MR core while limiting structural distortion and vibrational relaxation in the excited state. As a result of these structural refinements, **BNNO**

exhibited a pronounced bathochromic shift, delivering deep red emission with a λ_{PL} of 637 nm and a narrow FWHM of just 32 nm, indicative of excellent color purity. Computational studies revealed an increased oscillator strength ($f \sim 0.30$) relative to the parent **BNO** compound ($f \sim 0.24$), owing to enhanced conjugation and greater molecular polarizability. Additionally, **BNNO** demonstrated a lower reorganization energy (0.13 eV) than **BNO** (0.19 eV), further supporting its efficient radiative transitions and narrow emission bandwidth. BNNO also showed a high PLQY of 95%, a small ΔE_{ST} of 0.09 eV, and a short τ_d of 69 μs, with a k_{RISC} of 1.4×10^4 s^{-1}. When integrated into a phosphorescent-sensitized OLED device, **BNNO** achieved an EQE of 34.4% and red EL at 644 nm with a FWHM of 42 nm. Importantly, the device maintained high efficiency even at 1000 cd m^{-2}, attributed to the material's high PLQY and favorable $\Theta_{\parallel}$. The CIE(x, y) ∼ (0.70, 0.29) closely approached the BT.2020 red standard, underscoring **BNNO's** potential for ultra-pure red OLED applications.

Zhang *et al.* introduced an innovative molecular design strategy to develop orange/red MR-TADF emitters with extremely narrow emission bands (FWHM < 20 nm).[167] This was achieved by inserting B and N atoms into a rigid PAH framework, utilizing *para*-N–π–N/*para*-B–π–B and **ν-DABNA** structural motifs. The resulting compound, **B4N6-Me**, is a quadruple-borylated orange-red MR-TADF emitter with the largest π-conjugated MR core among the **ν-DABNA** derivatives, with four B atoms and two N atoms. In **B4N6-Me**, the core structure is arranged with B and N atoms in a *para*-N–π–N/*para*-B–π–B configuration, while additional peripheral B and N atoms form a *para*-B–π–N pattern. This dual configuration synergistically combines the narrow emission of *para*-B–π–N with the red-shifted emission of *para*-N–π–N/*para*-B–π–B, resulting in **B4N6-Me** orange-red emission at $\lambda_{em} \sim 580$ nm with a FWHM of just 19 nm. The compound exhibited excellent TADF properties, including a τ_d of 138 μs and a high PLQY of 98%. In a phosphorescent-sensitized OLED, **B4N6-Me** achieved an EQE of 34%, emitting at λ_{EL}/FWHM ∼ 580 nm/27 nm, demonstrating its potential for high-efficiency OLED applications.

Zhang *et al.* recently proposed an innovative approach for developing red MR-TADF emitters by integrating phenanthrol[9,10-*b*]pyrazine (PPZ) into a CB-based MR core, resulting in the compound **PPZ-BN**.[168] The introduction of PPZ enhances π-conjugation and CT characteristics, while the electronegative nitrogen atoms effectively localize the HOMO and LUMO, leading to a significant bathochromic shift. The fully fused structure ensures a narrowband emission and high PLQY. The HOMO is predominantly located on the CB core with some contribution from the PPZ unit, while the LUMO is mainly centered on the electron-withdrawing **PPZ** and extends into the CB core, indicating pronounced CT features while maintaining the MR characteristics. Therefore, PPZ-BN exhibits deep-red emission with a peak at $\lambda_{PL} \sim 613$ nm and a FWHM of 38 nm, representing a bathochromic shift of over 128 nm compared to the original CB core. The TADF properties of **PPZ-BN** include a ΔE_{ST} of 0.25 eV, a τ_d of 50 μs, and a PLQY of 88%. In a phosphorescent-sensitized OLED, **PPZ-BN** produced red emission with an EQE of 26%, λ_{EL}/FWHM of 613 nm/53 nm, and CIE coordinates of (0.67, 0.33). Notably, the **PPZ-BN**-based OLED demonstrated excellent operational stability with an LT_{99} of 43 hours at an initial luminance of 10 000 cd m^{-2}.

Wang *et al.* proposed a spiro-carbon-locking and sulfur-embedding strategy to modify the parent MR-TADF framework (DtCzB) (Fig. 20), resulting in **FBN** and **FSBN** exhibiting red-shifted emission.[169] The **FSBN** showed pure red emission with a wavelength peaking at 621 nm, a FWHM of 55 nm and a PLQY of 98% in toluene. Additionally, **FSBN** exhibits a small ΔE_{ST} value of 0.05 eV, which is beneficial for the efficient RISC process. The steric effect of the bulky fluorene moiety enables **FSBN** to maintain a stable emission spectrum across a wide range of doping concentrations. The corresponding OLED device shows pure red emission with a wavelength peak at 624 nm and CIE coordinates of (0.67, 0.33). Based on the advantage of high PLQY (98%) and high horizontal molecular orientation ratio (87%) of the emitter, the single-host OLED device exhibits a maximum EQE of 37.5% and a PE of 50.1 lm W^{-1}.

Hatakeyama *et al.* introduced a B/N "core–shell" design strategy by strategically adding a B-atom at the *ortho*-position of the two existing B-atoms in **ν-DABNA-O2-TB**, which enhances the concentration and stabilization of the LUMO wave function density.[170] The resulting compound, **Δ-DABNA-TB**, features a condensed B-core that facilitates relatively strong ICT with the surrounding HOMO on a rigid platform, resulting in a bathochromic shift from 447 nm (in **ν-DABNA-O2-TB**) to 624 nm (in

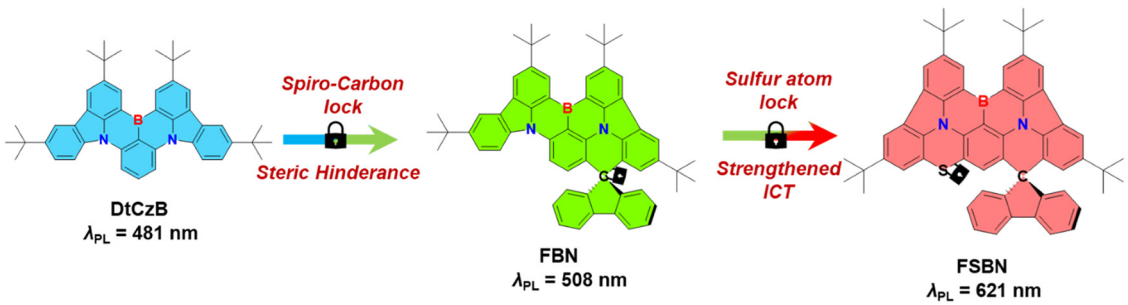

Fig. 20 Design strategy to develop red MR-emitter by interlocking with spiro-C and S atoms.

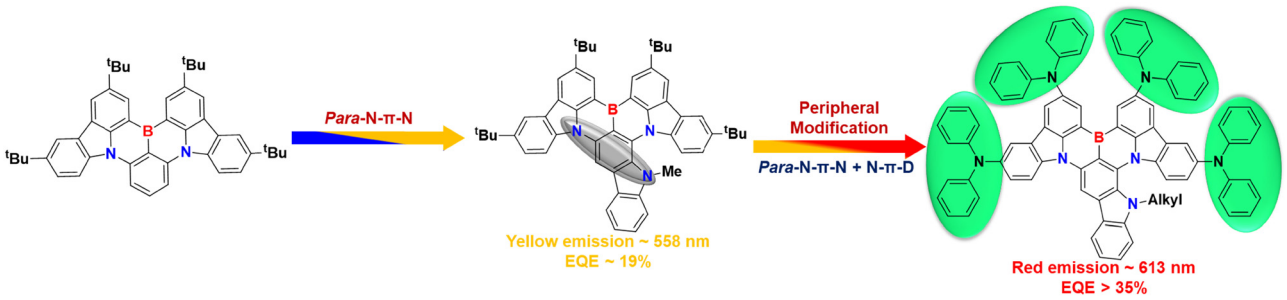

Fig. 21 π-Extension and peripheral decoration strategy to tune the MR-TADF emitters to the long-wavelength region.

Δ-DABNA-TB) in solution. The slow RISC rate of 8.5×10^2 s^{-1} for **Δ-DABNA-TB** is attributed to triplet accumulation and related annihilation. In an OLED device incorporating the TADF molecule 4CzTPN as host with 1.0 wt% of **Δ-DABNA-TB**, a red emission peak was observed at 624 nm (FWHM = 42 nm) and a maximum EQE of 23.3% was achieved. Additionally, **Δ-DABNA-TB** demonstrates remarkable device stability, maintaining 99% of the initial luminance at 1000 cd m^{-2} after 441 h for 0.5 wt% and 293 h for 1.0 wt% of **Δ-DABNA-TB**, with an initial driving voltage of ~6.5 V.

Cui *et al.* developed a pure-red MR-TADF molecule, **BNTPA**, by integrating the secondary electron-donating units (DPA) and extending the π-skeleton into MR molecules (Fig. 21).[171] The compound exhibited bright and saturated red emission with a maximum wavelength of 613 nm, FWHM of 42 nm and PLQY of 94%. The ΔE_{ST} of **BNTPA** is 0.10 eV, which is smaller than the reported red MR-TADF emitters. Furthermore, an OLED device based on 0.5 wt% of **BNTPA** exhibits saturated red emission with an EL peak at 617 nm and a narrow FWHM of 48 nm with CIE coordinates of (0.657, 0.343), respectively. The EQE_{max} of 35.2% and EQE_{1000} of 30.1% showed reduced efficiency roll-off. Additionally, the phosphor-sensitized OLED exhibits EQE_{max} of 43.3% and EQE_{5000} of 31.3% with suppressed efficiency roll-off and an exceptional long-term operational lifetime (LT_{98}) of over 322 h at an initial luminance of 1000 cd m^{-2}.

Zhang *et al.* proposed the hybridization of organoboron–nitrogen and carbonyl (h-BNCO) strategy to develop an MR system.[172] Significantly, the carbonyl group to B/N-based skeleton leads to n–π* contribution to the triplet excited state, thereby promoting the SOC and accelerating the k_{RISC}. The synthesized MR-TADF emitter, **h-BNCO-3**, was obtained by modifying the green **h-BNCO-2** skeleton with diphenylamine, which effectively narrows the energy gap without affecting the MR properties. Furthermore, it achieves a red-shifted emission of approximately 76 nm with λ_{PL} at 582 nm and a FWHM of 45 nm. Additionally, the compound shows ΔE_{ST} of 0.07 eV and k_{RISC} over 10^5 s^{-1}. In OLEDs, **h-BNCO-3** exhibits EQE_{max} of 26.4% with severe efficiency roll-off. To enhance device performance, phosphor-sensitized OLEDs were fabricated, which help to harvest triplet excitons, achieving an EQE_{max} of 38.0% and an EQE_{1000} of 31.2%, indicating reduced efficiency roll-off. These devices exhibited electroluminescence emission at 608 nm with a FWHM of 60 nm and CIE coordinates of (0.61, 0.39).

7. Challenges and strategies for full-color MR-TADF emitters

Yasuda *et al.* introduced an approach for developing full-color, narrowband, and high-efficiency MR-TADF emitters by integrating tri-coordinate boron and carbazole moieties.[173] They utilized **BBCz-SB** as the core structure (Fig. 22). By placing a B-atom at the *para*-carbon position relative to the N-atom in the central core, they reduced the donating ability of the N-atom. Similarly, positioning an N-atom *para* to the B-atom diminished the acceptor strength of the B-atom. Thus, the compound **BBCz-DB** exhibited a larger bandgap and blue-shifted emission. On the other hand, in **BBCz-R**, the N- and B-atoms were placed parallel to each other within a fused PAH framework, resulting in a smaller bandgap and a red-shifted emission. They also synthesized two D–A-type MR-TADF emitters by combining the **BBCz-SB** core with either three or two carbazole units, producing **BBCz-G** and **BBCz-Y**. The series of compounds exhibited tunable emission colors, ranging from deep-blue to deep-red, with emission wavelengths of 446, 489, 517, 549, and 615 nm (Table S11, ESI†). Among them, compounds **BBCz-DB** and **BBCz-R** exhibited narrow FWHM values of 16 and 21 nm, respectively, due to their fully fused molecular structures. All compounds exhibited high PLQY, low ΔE_{ST}, and high k_{RISC}, making them ideal candidates for use as dopants in OLEDs. OLED devices doped with these emitters in an mCBP host exhibited tunable colors from deep-blue to red. The color coordinates for the compounds **BBCz-DB**, **BBCz-G**, and **BBCz-R** closely match the primary colors: blue (0.12, 0.18), green (0.26, 0.68), and red (0.67, 0.30), respectively. The EQE values for compounds **BBCz-DB**, **BBCz-SB**, **BBCz-G**, **BBCz-Y** and **BBCz-R** were 29.3%, 27.8%, 31.8%, 29.3%, and 22.0%, respectively.

Subsequently, the same research group demonstrated a strategy involving the incorporation of electron-withdrawing imine and electron-donating amine moieties into the boron-embedded 1,3-bis(carbazol-9-yl)benzene (**Cz-B**) framework, resulting in a significant blue shift and red shift of narrowband emissions.[174] In this series, the imine derivative (**y-Cb-B**) exhibited deep-blue emission attributed to the imine N-atom's influence on the carbon atom distributed in the HOMO, which diminished the HOMO energy and increased the HOMO–LUMO energy gap. Conversely, the carbazole (**TCz-B**) and diphenylamine (**DACz-B**) derivatives displayed more red-shifted emission due to their ability to stabilize the HOMO

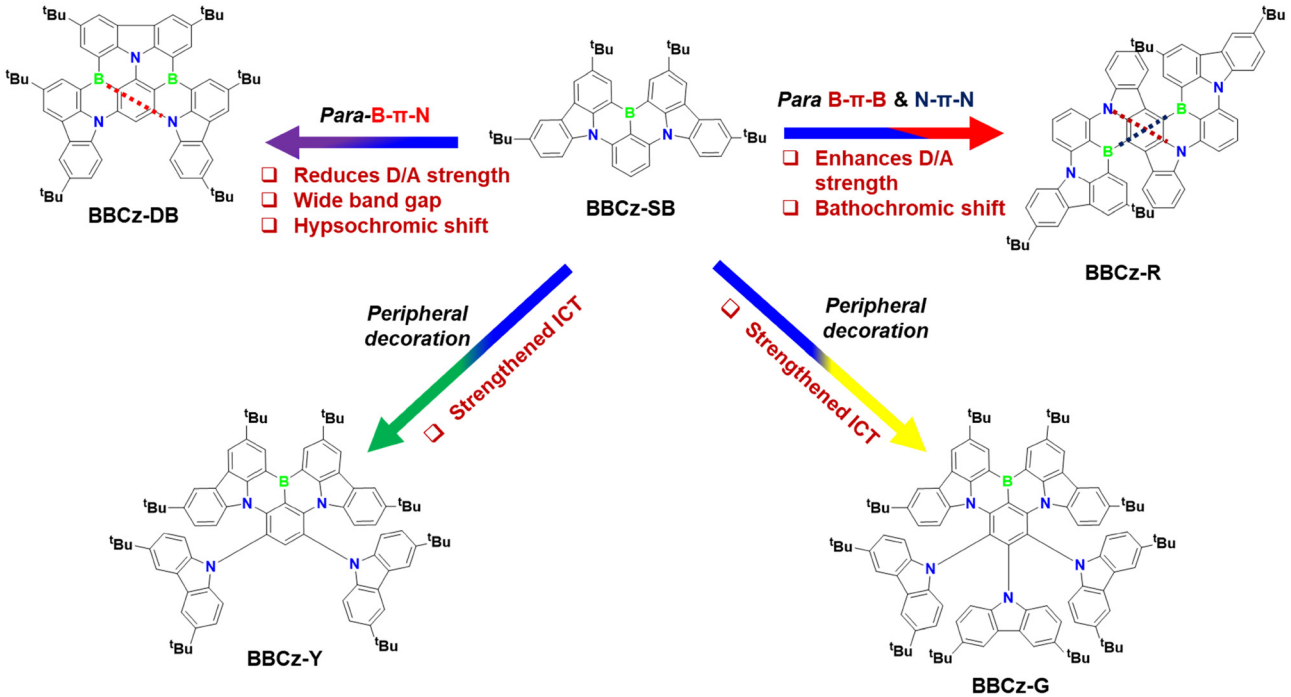

Fig. 22 Design strategies for full-color MR-TADF emitters.

energy and reduce the bandgap. The diphenylamine derivative (**DACz-B**) exhibited a greater degree of red shift owing to its robust donor strength. All the compounds displayed narrow emissions with a FWHM of 35 nm or less, as well as low ΔE_{ST} values. Subsequently, OLED devices based on these emitters with mCBP hosts were investigated. Among these compounds, the carbazole (**TCz-B**) derivative exhibited superior device performance, achieving a maximum EQE of 29.2% and CE of 100.7 cd A^{-1}, respectively.

Yang *et al.* also detailed a peripheral decoration strategy for the MR-fragment using strong electron donors (Chart 10). They altered the well-established **CzB** core by incorporating carbazole (**BN1**), mono-diphenylamine (**BN2**), and di-diphenylamine (**BN3**) units.[175] This modification enabled the tuning of the emission wavelengths of the compounds from blue (λ_{PL} = 496 nm) to yellow (λ_{PL} = 562 nm) based on the donor strength and the number of appended chromophores. Within the series, **BN3** exhibited a yellow emission and a low ΔE_{ST}. These findings underscore the effectiveness of the peripheral decoration strategy in fine-tuning the color of MR-TADF emitters without affecting the MR properties. Upon utilizing these materials as dopant emitters in OLEDs, **BN3** demonstrated superior performance, achieving a maximum EQE of 24.7% and CE of 92.6 cd A^{-1} in the yellow region, with CIE color coordinates of (0.47, 0.52).

Zheng *et al.* developed a series of full-color MR-TADF materials using a straightforward strategy to create four ternary B/N-based PAH emitters: **SBON**, **SBSN**, **DBON**, and **DBSN**.[176] These materials exhibited emission across the full color spectrum, from pure blue (λ_{PL} ~ 463 nm) to yellow (λ_{PL} ~ 553 nm), by modifying the coordination between B/N and heteroatoms (O or S) to enhance charge transfer delocalization.[176] This design resulted in narrowband emissions for all the compounds, with FWHM values ≤28 nm. The diboron-containing derivatives, **DBON** and **DBSN**, exhibited a high PLQY of 98%, which was attributed to their extended π-conjugation and reduced nonradiative deactivation. The S-based materials, **SBSN** and **DBSN**, exhibited high k_{RISC} values of 1.5 × 10^5 s^{-1} and 1.9 × 10^5 s^{-1}, respectively, due to enhanced SOC from the sulfur heavy-atom effect, outperforming the oxygen-based derivatives, **SBON** and **DBON**. Among the series, the OLED device using **DBON** achieved the best performance, with an EQE_{max} of 26.7% and CIE(x, y) of (0.17, 0.68) (Table S12, ESI†).

8. Summary and outlook

Since their first demonstration by Hatakeyama *et al.*, B-based MR-TADF emitters have attracted significant interest owing to their exceptional color purity (FWHM < 40 nm) and high EQE > 35%. Over the past decade, extensive research has been conducted to understand their structure–function relationships, leading to the development of numerous MR-TADF materials. Although these materials have addressed the key limitations of traditional D–A-type TADF emitters, several challenges remain, including low k_{RISC}, efficiency roll-off, poor operational stability, and aggregation-caused emission quenching (Fig. 23). Additionally, achieving ultrawide color gamut emitters remains a significant challenge from a molecular design perspective.

To overcome these limitations, various design strategies have been explored:

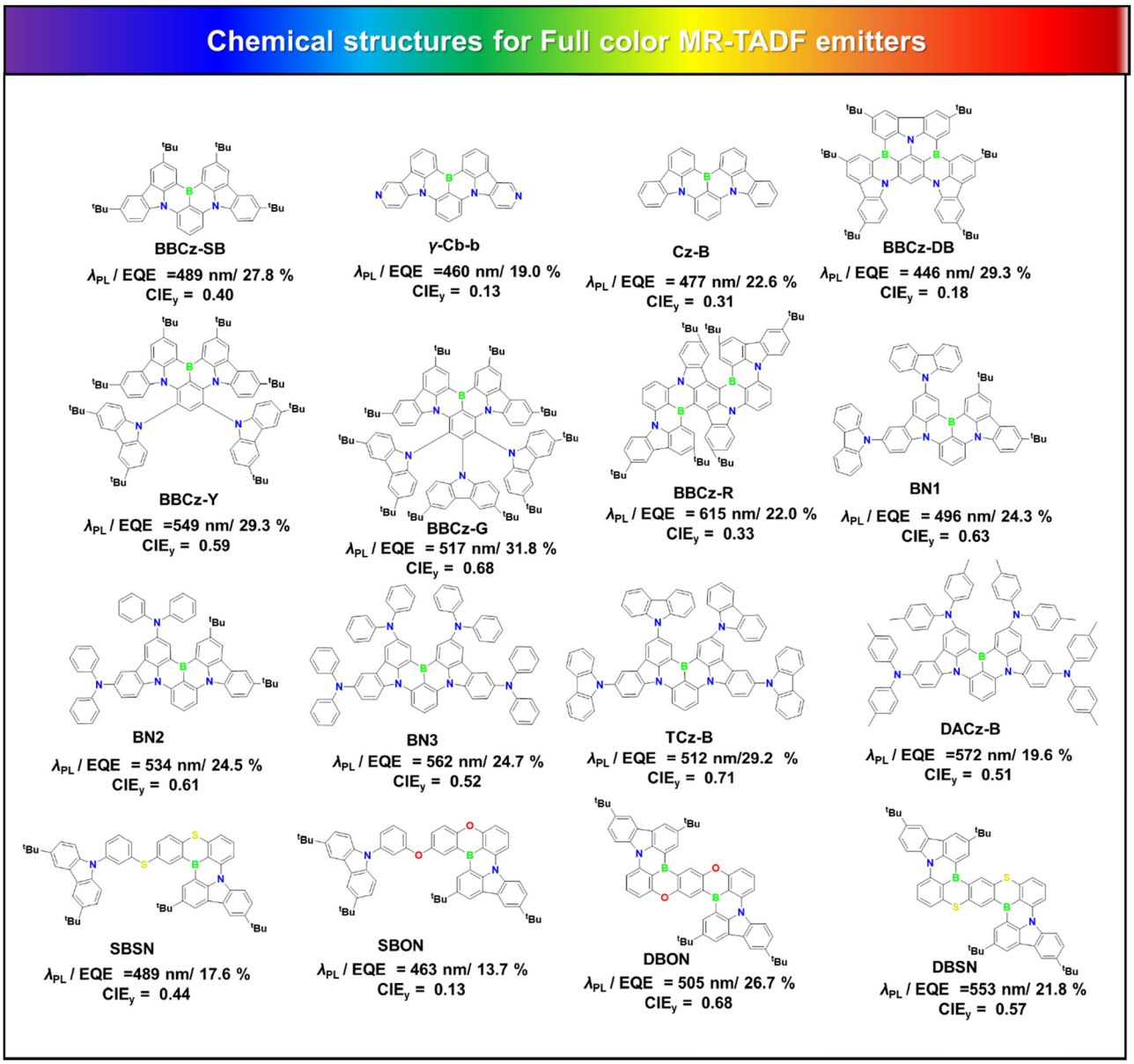

Chart 10 Chemical structure of the full-color MR-TADF emitters.

• Narrowband emission: to enhance the color purity of MR-TADF OLEDs, it is essential to maintain an intrinsically narrow emission spectrum by suppressing solid-state π–π stacking and ensuring an optimal intermolecular distance. Additionally, rigidifying the core structure helps to minimize vibrational modes in the emissive state, reducing spectral broadening. Furthermore, controlling the CT characteristics by the LRCT component in MR-TADF molecules ensures sharper emission profiles. These design strategies collectively contribute to achieving high color purity while maintaining efficient photophysical properties.

• Enhanced k_{RISC}: using the heavy atom effect (S, Se, Te) can significantly enhance the k_{RISC} of MR-TADF molecules, effectively reducing efficiency roll-off under strong SOC. However, the incorporation of heavy atoms also induces greater structural relaxation, resulting in emission broadening. Therefore, a careful structural design is required to balance the narrowband emission and k_{RISC} enhancement. Additionally, the weaker BDE between heavy atoms and carbon may compromise the stability of the emitters. Alternatively, k_{RISC} can be accelerated by linearly extending the π-skeleton and incorporating multiple B atoms, facilitating efficient triplet harvesting while maintaining emission sharpness.

• Long-wavelength MR-emitters: the limited availability of long-wavelength (>550 nm) MR-TADF emitters remains a challenge that must be addressed. The emission can be precisely tuned using the following strategies: (i) peripheral modification of MR-TADF emitters with donor or acceptor core units, enabling FMO engineering to achieve a red-shifted emission while ensuring a narrow FWHM for high color purity.

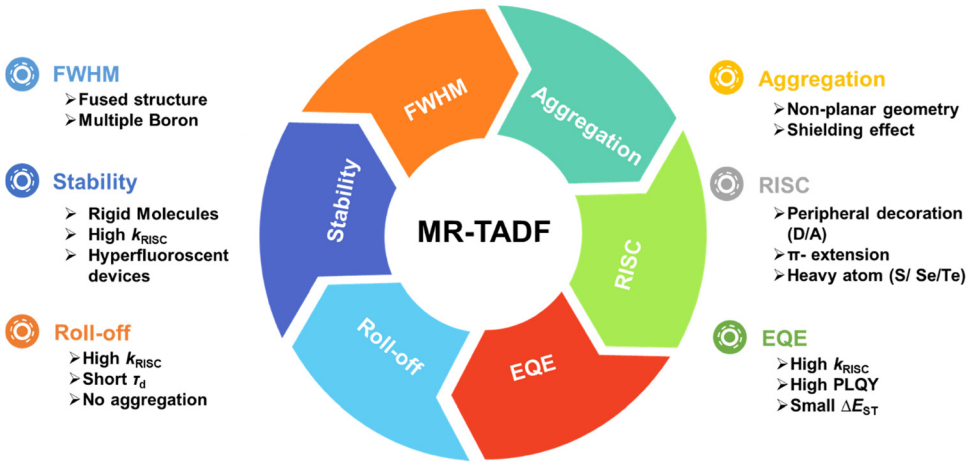

Fig. 23 Challenges and key design aspects of MR-TADF emitters.

(ii) Incorporating *para*-X–π–X (X = O, S, N) and B–π–B configurations within a rigid PAH framework, which effectively stabilizes the HOMO and LUMO energy levels, facilitating a red-region emission without compromising spectral sharpness.

• Aggregation control: the planar nature of the MR core makes most emitters prone to ACQ. This issue can be effectively mitigated through the following strategies: (i) employing a shielding effect, where the MR core is protected by rigid aromatic units. (ii) Disrupting core planarity by introducing non-planar geometries, which help reduce undesirable π–π stacking, thereby maintaining emission efficiency in the solid state.

• Efficiency roll-off reduction: to reduce roll-off and sustain high EQE at high brightness, it is essential to enhance the RISC rate to efficiently harness triplet excitons. It is critical to minimize triplet exciton accumulation, which can otherwise lead to undesirable TTA and TPA. From a molecular design perspective, these challenges can be addressed by incorporating heavy atoms, extending the π-conjugation, and controlling aggregation effects to ensure stable and efficient emission.

• Improved operational lifetime: achieving long-lifetime OLED devices is essential for advancing display and lighting technologies. The stability of MR-OLEDs can be significantly improved by designing rigid PAH cores with high BDE of C–N and B–C bonds, thereby enhancing the chemical stability of the emitters. Additionally, optimizing the k_{RISC} and maintaining a τ_d helps suppress triplet exciton accumulation, thereby minimizing TTA or TPQ. Another effective approach is the integration of MR emitters as terminal dopants in triplet host-sensitized (hyperfluorescent) devices, which enhances operational lifetime by promoting efficient energy transfer and exciton management. These molecular design strategies are critical for ensuring the long-term stability and performance of MR-TADF-based OLEDs.

Despite significant progress, challenges, such as limited red/NIR emission tuning (>550 nm), slow k_{RISC}, and sub-optimal device lifetimes, still hinder their commercial viability. Thus, innovative emitter designs are essential for enhancing the structural diversity and functional performance of MR-TADF materials. Besides OLED applications, MR-TADF emitters possess immense potential for interdisciplinary applications in biomedicine, photocatalysis, and laser technologies due to their unique photophysical properties. Their integration into photodynamic therapy (PDT), bioimaging, and NIR-emitting photosensitizers could revolutionize biomedical applications. Given the rapid advancements in MR-TADF research, these materials are poised to become a core technology for next-generation ultrawide color gamut OLED displays and beyond, with the potential to significantly impact various scientific and industrial fields.

Conflicts of interest

There are no conflicts to declare.

Data availability

No primary research results, software or code has been included and no new data were generated or analysed as part of this review.

References

1 C. W. Tang and S. A. VanSlyke, *Appl. Phys. Lett.*, 1987, **51**, 913–915.
2 C. Adachi, M. A. Baldo, S. R. Forrest, S. Lamansky, M. E. Thompson and R. C. Kwong, *Appl. Phys. Lett.*, 2001, **78**, 1622–1624.
3 C. Adachi, S. Tokito, T. Tsutsui and S. Saito, *Jpn. J. Appl. Phys.*, 1988, **27**, L269.
4 Y. Chi and P.-T. Chou, *Chem. Soc. Rev.*, 2010, **39**, 638–655.
5 H. Cho, S.-H. Jeong, M.-H. Park, Y.-H. Kim, C. Wolf, C.-L. Lee, J. H. Heo, A. Sadhanala, N. Myoung, S. Yoo, S. H. Im, R. H. Friend and T.-W. Lee, *Science*, 2015, **350**, 1222–1225.

6 M. A. Baldo, C. Adachi and S. R. Forrest, *Phys. Rev. B:Condens. Matter Mater. Phys.*, 2000, **62**, 10967–10977.
7 M.-C. Tang, C.-H. Lee, S.-L. Lai, M. Ng, M.-Y. Chan and V. W.-W. Yam, *J. Am. Chem. Soc.*, 2017, **139**, 9341–9349.
8 X. Yang, G. Zhou and W.-Y. Wong, *Chem. Soc. Rev.*, 2015, **44**, 8484–8575.
9 C. Poriel and J. Rault-Berthelot, *Acc. Mater. Res.*, 2022, **3**, 379–390.
10 X. Cai and S. Su, *Adv. Funct. Mater.*, 2018, **18**, 1802558.
11 C.-T. Chen, *Chem. Mater.*, 2004, **16**, 4389–4400.
12 H. Sasabe and J. Kido, *J. Mater. Chem. C*, 2013, **1**, 1699.
13 P. L. Burn, S.-C. Lo and I. D. W. Samuel, *Adv. Mater.*, 2007, **19**, 1675–1688.
14 K. Tuong Ly, R.-W. Chen-Cheng, H.-W. Lin, Y.-J. Shiau, S.-H. Liu, P.-T. Chou, C.-S. Tsao, Y.-C. Huang and Y. Chi, *Nat. Photonics*, 2017, **11**, 63–68.
15 M. A. Baldo, D. F. O'Brien, Y. You, A. Shoustikov, S. Sibley, M. E. Thompson and S. R. Forrest, *Nature*, 1998, **395**, 151–154.
16 S. Madayanad Suresh, D. Hall, D. Beljonne, Y. Olivier and E. Zysman-Colman, *Adv. Funct. Mater.*, 2020, **30**, 1908677.
17 S. K. Jeon, H. L. Lee, K. S. Yook and J. Y. Lee, *Adv. Mater.*, 2019, **31**, 1803524.
18 D. Zhang, L. Duan, C. Li, Y. Li, H. Li, D. Zhang and Y. Qiu, *Adv. Mater.*, 2014, **26**, 5050–5055.
19 W.-C. Chen, Y. Yuan, S.-F. Ni, Q.-X. Tong, F.-L. Wong and C.-S. Lee, *Chem. Sci.*, 2017, **8**, 3599–3608.
20 R. K. Konidena, K. H. Lee and J. Y. Lee, *J. Mater. Chem. C*, 2020, **8**, 2491–2499.
21 I. E. Serdiuk, C. H. Ryoo, K. Kozakiewicz, M. Mońka, B. Liberek and S. Y. Park, *J. Mater. Chem. C*, 2020, **8**, 6052–6062.
22 J. Song, H. Lee, E. G. Jeong, K. C. Choi and S. Yoo, *Adv. Mater.*, 2020, **32**, 1907539.
23 P. Keerthika and R. K. Konidena, *Adv. Opt. Mater.*, 2023, **11**, 2301732.
24 K. R. Naveen, R. K. Konidena and P. Keerthika, *Chem. Rec.*, 2023, **23**, e202300208.
25 R. K. Konidena and K. R. Naveen, *Adv. Photonics Res.*, 2022, **3**, 2301732.
26 Y. Xu, P. Xu, D. Hu and Y. Ma, *Chem. Soc. Rev.*, 2021, **50**, 1030–1069.
27 H. Nakanotani, T. Higuchi, T. Furukawa, K. Masui, K. Morimoto, M. Numata, H. Tanaka, Y. Sagara, T. Yasuda and C. Adachi, *Nat. Commun.*, 2014, **5**, 4016.
28 A. Endo, M. Ogasawara, A. Takahashi, D. Yokoyama, Y. Kato and C. Adachi, *Adv. Mater.*, 2009, **21**, 4802–4806.
29 D. Zhang, Y. Wada, Q. Wang, H. Dai, T. Fan, G. Meng, J. Wei, Y. Zhang, K. Suzuki, G. Li, L. Duan and H. Kaji, *Adv. Sci.*, 2022, **9**, 2106018.
30 P. Han, C. Lin, K. Wang, Y. Qiu, H. Wu, A. Qin, D. Ma and B. Z. Tang, *Mater. Horiz.*, 2022, **9**, 376–382.
31 M. A. Baldo, D. F. O'Brien, M. E. Thompson and S. R. Forrest, *Phys. Rev. B:Condens. Matter Mater. Phys.*, 1999, **60**, 14422–14428.
32 L. Bergmann, G. J. Hedley, T. Baumann, S. Bräse and I. D. W. Samuel, *Sci. Adv.*, 2016, **2**, e1500889.
33 H. Uoyama, K. Goushi, K. Shizu, H. Nomura, C. Adachi, W.-C. Chen, C.-S. Lee and Q.-X. Tong, *J. Mater. Chem. C*, 2015, **492**, 234–238.
34 D. Zhang, Y. Wada, Q. Wang, H. Dai, T. Fan, G. Meng, J. Wei, Y. Zhang, K. Suzuki, G. Li, L. Duan and H. Kaji, *Adv. Sci.*, 2022, **9**, 4802–4804.
35 S. Lamansky, P. Djurovich, D. Murphy, F. Abdel-Razzaq, H.-E. Lee, C. Adachi, P. E. Burrows, S. R. Forrest and M. E. Thompson, *J. Am. Chem. Soc.*, 2001, **123**, 4304–4312.
36 H. Xu, R. Chen, Q. Sun, W. Lai, Q. Su, W. Huang and X. Liu, *Chem. Soc. Rev.*, 2014, **43**, 3259–3302.
37 K. Kim, C. Moon, J. Lee, S. Kim and J. Kim, *Adv. Mater.*, 2014, **26**, 3844–3847.
38 J. Li, P. I. Djurovich, B. D. Alleyne, M. Yousufuddin, N. N. Ho, J. C. Thomas, J. C. Peters, R. Bau and M. E. Thompson, *Inorg. Chem.*, 2005, **44**, 1713–1727.
39 M. A. Baldo, S. Lamansky, P. E. Burrows, M. E. Thompson and S. R. Forrest, *Appl. Phys. Lett.*, 1999, **75**, 4–6.
40 A. B. Tamayo, B. D. Alleyne, P. I. Djurovich, S. Lamansky, I. Tsyba, N. N. Ho, R. Bau and M. E. Thompson, *J. Am. Chem. Soc.*, 2003, **125**, 7377–7387.
41 R. Ieuji, K. Goushi and C. Adachi, *Nat. Commun.*, 2019, **10**, 5283.
42 H.-T. Feng, J. Zeng, P.-A. Yin, X.-D. Wang, Q. Peng, Z. Zhao, J. W. Y. Lam and B. Z. Tang, *Nat. Commun.*, 2020, **11**, 2617.
43 H. Min, I. S. Park and T. Yasuda, *Adv. Opt. Mater.*, 2022, **10**, 2200290.
44 P. Rajamalli, N. Senthilkumar, P.-Y. Huang, C.-C. Ren-Wu, H.-W. Lin and C.-H. Cheng, *J. Am. Chem. Soc.*, 2017, **139**, 10948–10951.
45 M. Godumala, S. Choi, M. J. Cho and D. H. Choi, *J. Mater. Chem. C*, 2016, **4**, 11355–11381.
46 L. Cui, H. Nomura, Y. Geng, J. U. Kim, H. Nakanotani and C. Adachi, *Angew. Chem., Int. Ed.*, 2017, **56**, 1571–1575.
47 Z. Yang, Z. Mao, Z. Xie, Y. Zhang, S. Liu, J. Zhao, J. Xu, Z. Chi and M. P. Aldred, *Chem. Soc. Rev.*, 2017, **46**, 915–1016.
48 V. Jankus, C. Chiang, F. Dias and A. P. Monkman, *Adv. Mater.*, 2013, **25**, 1455–1459.
49 H. Lim, H. J. Cheon, S. Woo, S. Kwon, Y. Kim and J. Kim, *Adv. Mater.*, 2020, **32**, 2004083.
50 R. Braveenth, H. Lee, J. D. Park, K. J. Yang, S. J. Hwang, K. R. Naveen, R. Lampande and J. H. Kwon, *Adv. Funct. Mater.*, 2021, **31**, 2105805.
51 Y. Liu, C. Li, Z. Ren, S. Yan and M. R. Bryce, *Nat. Rev. Mater.*, 2018, **3**, 18020.
52 Y. Wada, S. Kubo and H. Kaji, *Adv. Mater.*, 2018, **30**, 1705641.
53 D. Zhang, X. Song, A. J. Gillett, B. H. Drummond, S. T. E. Jones, G. Li, H. He, M. Cai, D. Credgington and L. Duan, *Adv. Mater.*, 2020, **32**, 1908355.
54 K. R. Naveen, H. Lee, R. Braveenth, D. Karthik, K. J. Yang, S. J. Hwang and J. H. Kwon, *Adv. Funct. Mater.*, 2022, **32**, 2110356.

55 Y. H. Lee, S. Park, J. Oh, S. Woo, A. Kumar, J. Kim, J. Jung, S. Yoo and M. H. Lee, *Adv. Opt. Mater.*, 2018, **6**, 1800385.
56 S. Hirata, Y. Sakai, K. Masui, H. Tanaka, S. Y. Lee, H. Nomura, N. Nakamura, M. Yasumatsu, H. Nakanotani, Q. Zhang, K. Shizu, H. Miyazaki and C. Adachi, *Nat. Mater.*, 2015, **14**, 330–336.
57 M. Yokoyama, K. Inada, Y. Tsuchiya, H. Nakanotani and C. Adachi, *Chem. Commun.*, 2018, **54**, 8261–8264.
58 J. Guo, X.-L. Li, H. Nie, W. Luo, R. Hu, A. Qin, Z. Zhao, S.-J. Su and B. Z. Tang, *Chem. Mater.*, 2017, **29**, 3623–3631.
59 J. Chen, K. Wang, C. Zheng, M. Zhang, Y. Shi, S. Tao, H. Lin, W. Liu, W. Tao, X. Ou and X. Zhang, *Adv. Sci.*, 2018, **5**, 1800436.
60 T. J. Penfold, F. B. Dias and A. P. Monkman, *Chem. Commun.*, 2018, **54**, 3926–3935.
61 K. R. Naveen, K. Prabhu CP, R. Braveenth and J. Hyuk Kwon, *Chem. – Eur. J.*, 2022, **28**, e202103532.
62 X. Chen, Y. Tsuchiya, Y. Ishikawa, C. Zhong, C. Adachi and J. Brédas, *Adv. Mater.*, 2017, **29**, 1702767.
63 H. Shin, Y. H. Ha, H. Kim, R. Kim, S. Kwon, Y. Kim and J. Kim, *Adv. Mater.*, 2019, **31**, 1808102.
64 Q. Zhang, J. Li, K. Shizu, S. Huang, S. Hirata, H. Miyazaki and C. Adachi, *J. Am. Chem. Soc.*, 2012, **134**, 14706–14709.
65 K. R. Naveen, S. J. Hwang, H. Lee and J. H. Kwon, *Adv. Electron. Mater.*, 2022, **8**, 2101114.
66 S. M. Cho, K. M. Youn, H. I. Yang, S. H. Lee, K. R. Naveen, D. Karthik, H. Jeong and J. H. Kwon, *Org. Electron.*, 2022, **105**, 106501.
67 Y. Wada, H. Nakagawa, S. Matsumoto, Y. Wakisaka and H. Kaji, *Nat. Photonics*, 2020, **14**, 643–649.
68 E. Peli, ITU-R Recommendation BT, 2020: Parameter Values for Ultrahigh Definition Television Systems for Production and International Programme Exchange, International Telecommunication Union, ITU, Geneva 2012.
69 H. Hirai, K. Nakajima, S. Nakatsuka, K. Shiren, J. Ni, S. Nomura, T. Ikuta and T. Hatakeyama, *Angew. Chem., Int. Ed.*, 2015, **54**, 13581–13585.
70 Y. Kondo, K. Yoshiura, S. Kitera, H. Nishi, S. Oda, H. Gotoh, Y. Sasada, M. Yanai, T. Hatakeyama, H. Hirai, K. Nakajima, S. Nakatsuka, K. Shiren, J. Ni, S. Nomura, T. Ikuta and T. Hatakeyama, *Nat. Photonics*, 2019, **54**, 678–682.
71 T. Hatakeyama, K. Shiren, K. Nakajima, S. Nomura, S. Nakatsuka, K. Kinoshita, J. Ni, Y. Ono and T. Ikuta, *Adv. Mater.*, 2016, **28**, 2777–2781.
72 Y. Kondo, K. Yoshiura, S. Kitera, H. Nishi, S. Oda, H. Gotoh, Y. Sasada, M. Yanai and T. Hatakeyama, *Nat. Photonics*, 2019, **13**, 678–682.
73 H. Tanaka, S. Oda, G. Ricci, H. Gotoh, K. Tabata, R. Kawasumi, D. Beljonne, Y. Olivier and T. Hatakeyama, *Angew. Chem., Int. Ed.*, 2021, **60**, 17910–17914.
74 K. Rayappa Naveen, H. Lee, R. Braveenth, K. Joon Yang, S. Jae Hwang and J. Hyuk Kwon, *Chem. Eng. J.*, 2022, **432**, 134381.
75 I. S. Park, M. Yang, H. Shibata, N. Amanokura and T. Yasuda, *Adv. Mater.*, 2022, **34**, 1–9.
76 J. Jin, S. Wang, H. Jiang, L. Wang and W. Y. Wong, *Adv. Opt. Mater.*, 2024, **12**, 2302354.
77 S. Oda, B. Kawakami, Y. Yamasaki, R. Matsumoto, M. Yoshioka, D. Fukushima, S. Nakatsuka and T. Hatakeyama, *J. Am. Chem. Soc.*, 2022, **144**, 106–112.
78 H. J. Cheon, Y. S. Shin, N. H. Park, J. H. Lee and Y. H. Kim, *Small*, 2022, **18**, 2107574.
79 S. H. Han, J. H. Jeong, J. W. Yoo and J. Y. Lee, *J. Mater. Chem. C*, 2019, **7**, 3082–3089.
80 J. Park, K. J. Kim, J. Lim, T. Kim and J. Y. Lee, *Adv. Mater.*, 2022, **34**, 1–7.
81 J. M. Jin, D. Liu, W. C. Chen, C. Shi, G. Chen, X. Wang, L. Xing, W. Ying, S. Ji, Y. Huo and S. J. Su, *Angew. Chem., Int. Ed.*, 2024, **63**, e202401120.
82 Y. Wang, Y. Duan, R. Guo, S. Ye, K. Di, W. Zhang, S. Zhuang and L. Wang, *Org. Electron.*, 2021, **97**, 106275.
83 S. Oda, B. Kawakami, R. Kawasumi, R. Okita and T. Hatakeyama, *Org. Lett.*, 2019, **21**, 9311–9314.
84 M. Nagata, H. Min, E. Watanabe, H. Fukumoto, Y. Mizuhata, N. Tokitoh, T. Agou and T. Yasuda, *Angew. Chem., Int. Ed.*, 2021, **60**, 20280–20285.
85 I. S. Park, H. Min and T. Yasuda, *Angew. Chem., Int. Ed.*, 2022, **61**, e202205684.
86 J. Park, J. Lim, J. H. Lee, B. Jang, J. H. Han, S. S. Yoon and J. Y. Lee, *ACS Appl. Mater. Interfaces*, 2021, **13**, 45798–45805.
87 J. Han, Z. Huang, X. Lv, J. Miao, Y. Qiu, X. Cao and C. Yang, *Adv. Opt. Mater.*, 2022, **10**, 2102092.
88 Y. Qiu, H. Xia, J. Miao, Z. Huang, N. Li, X. Cao, J. Han, C. Zhou, C. Zhong and C. Yang, *ACS Appl. Mater. Interfaces*, 2021, **13**, 59035–59042.
89 J. Bian, S. Chen, L. Qiu, R. Tian, Y. Man, Y. Wang, S. Chen, J. Zhang, C. Duan, C. Han and H. Xu, *Adv. Mater.*, 2022, **34**, 2110547.
90 T. Hua, J. Miao, H. Xia, Z. Huang, X. Cao, N. Li and C. Yang, *Adv. Funct. Mater.*, 2022, **32**, 2201032.
91 X. Lv, J. Miao, M. Liu, Q. Peng, C. Zhong, Y. Hu, X. Cao, H. Wu, Y. Yang, C. Zhou, J. Ma, Y. Zou and C. Yang, *Angew. Chem.*, 2022, **134**, e202201588.
92 Y. K. Qu, D. Y. Zhou, F. C. Kong, Q. Zheng, X. Tang, Y. H. Zhu, C. C. Huang, Z. Q. Feng, J. Fan, C. Adachi, L. S. Liao and Z. Q. Jiang, *Angew. Chem., Int. Ed.*, 2022, **61**, e202201886.
93 H. Lee, R. Braveenth, J. Do Park, C. Y. Jeon, H. S. Lee and J. H. Kwon, *ACS Appl. Mater. Interfaces*, 2022, **14**, 36927–36935.
94 S. Madayanad Suresh, L. Zhang, D. Hall, C. Si, G. Ricci, T. Matulaitis, A. M. Z. Slawin, S. Warriner, Y. Olivier, I. D. W. Samuel and E. Zysman-Colman, *Angew. Chem., Int. Ed.*, 2022, **62**, e202215522.
95 R. W. Weerasinghe, S. Madayanad Suresh, D. Hall, T. Matulaitis, A. M. Z. Slawin, S. Warriner, Y. T. Lee, C. Y. Chan, Y. Tsuchiya, E. Zysman-Colman and C. Adachi, *Adv. Mater.*, 2024, **36**, 2402289.
96 J. J. Hu, Y. Wei, X. Z. Wang, X. Liang, X. J. Liao, L. Yuan, H. X. Ni and Y. X. Zheng, *Adv. Opt. Mater.*, 2024, **12**, 2302987.

97 K. R. Naveen, H. Lee, L. H. Seung, Y. H. Jung, C. P. Keshavananda Prabhu, S. Muruganantham and J. H. Kwon, *Chem. Eng. J.*, 2023, **451**, 138498.
98 X. Xiong, J. Q. Li, T. F. Chen, X. C. Fan, Y. C. Cheng, H. Wang, F. Huang, H. Wu, J. Yu, X. K. Chen, K. Wang and X. H. Zhang, *Adv. Funct. Mater.*, 2024, **34**, 2313726.
99 Y. Hu, X. Fan, F. Huang, Y. Shi, H. Wang, Y. Cheng, M. Chen, K. Wang, J. Yu and X. Zhang, *Adv. Opt. Mater.*, 2023, **11**, 2202267.
100 X. Cai, Y. Pan, C. Li, L. Li, Y. Pu, Y. Wu and Y. Wang, *Angew. Chem.*, 2024, **136**, e202408522.
101 Q. Wu, J. Li, D. Liu, Y. Mei, B. Liu, J. Wang, M. Xu and Y. Li, *Dyes Pigm.*, 2023, **217**, 111421.
102 J. Jin, M. Chen, H. Jiang, B. Zhang, Z. Xie and W.-Y. Wong, *ACS Mater. Lett.*, 2024, **6**, 3246–3253.
103 M. Xing, G. Chen, S. Wang, X. Yin, J. Liu, Z. Xue, N. Li, J. Miao, Z. Huang and C. Yang, *Adv. Funct. Mater.*, 2024, **35**, 2414635.
104 D. Wan, J. Zhou, Y. Yang, G. Meng, D. Zhang, L. Duan and J. Ding, *Adv. Mater.*, 2024, **36**, 2409706.
105 W. Yuan, Q. Jin, M. Du, L. Duan and Y. Zhang, *Adv. Mater.*, 2024, **36**, 2410096.
106 K. Xu, N. Li, Z. Ye, Y. Guo, Y. Wu, C. Gui, X. Yin, J. Miao, X. Cao and C. Yang, *Chem. Sci.*, 2024, **15**, 18076–18084.
107 J. Jin, Z. He, D. Liu, Y. Mei, J. Wang, H. Wan and J. Li, *Chem. Sci.*, 2024, **15**, 18135–18145.
108 Z. Huang, H. Xie, J. Miao, Y. Wei, Y. Zou, T. Hua, X. Cao and C. Yang, *J. Am. Chem. Soc.*, 2023, **145**, 12550–12560.
109 Z. Xue, Z. Xiao, Y. Zou, Z. Chen, J. Liu, Z. Huang and C. Yang, *Chem. Sci.*, 2025, **16**, 3655–3661.
110 Y. Zhang, D. Zhang, J. Wei, Z. Liu, Y. Lu and L. Duan, *Angew. Chem., Int. Ed.*, 2019, **58**, 16912–16917.
111 Y. Zhang, D. Zhang, J. Wei, X. Hong, Y. Lu, D. Hu, G. Li, Z. Liu, Y. Chen and L. Duan, *Angew. Chem., Int. Ed.*, 2020, **132**, 17652–17656.
112 N. Ikeda, S. Oda, R. Matsumoto, M. Yoshioka, D. Fukushima, K. Yoshiura, N. Yasuda and T. Hatakeyama, *Adv. Mater.*, 2020, **32**, 2004072.
113 Y. Xu, Z. Cheng, Z. Li, B. Liang, J. Wang, J. Wei, Z. Zhang and Y. Wang, *Adv. Opt. Mater.*, 2020, **8**, 1902142.
114 Y. Xu, C. Li, Z. Li, Q. Wang, X. Cai, J. Wei and Y. Wang, *Angew. Chem., Int. Ed.*, 2020, **59**, 17442–17446.
115 Y. Xu, C. Li, Z. Li, J. Wang, J. Xue, Q. Wang, X. Cai and Y. Wang, *CCS Chem.*, 2022, **4**, 2065–2079.
116 G. Liu, H. Sasabe, K. Kumada, A. Matsunaga, H. Katagiri and J. Kido, *J. Mater. Chem. C*, 2021, **9**, 8308–8313.
117 J. J. Hu, X. F. Luo, Y. P. Zhang, M. X. Mao, H. X. Ni, X. Liang and Y. X. Zheng, *J. Mater. Chem. C*, 2022, **10**, 768–773.
118 P. Jiang, L. Zhan, X. Cao, X. Lv, S. Gong, Z. Chen, C. Zhou, Z. Huang, F. Ni, Y. Zou and C. Yang, *Adv. Opt. Mater.*, 2021, **9**, 2100825.
119 T. Hua, L. Zhan, N. Li, Z. Huang, X. Cao, Z. Xiao, S. Gong, C. Zhou, C. Zhong and C. Yang, *Chem. Eng. J.*, 2021, **426**, 131169.
120 Y. Zhang, J. Wei, D. Zhang, C. Yin, G. Li, Z. Liu, X. Jia, J. Qiao and L. Duan, *Angew. Chem., Int. Ed.*, 2022, **61**, e202113206.
121 P. Jiang, J. Miao, X. Cao, H. Xia, K. Pan, T. Hua, X. Lv, Z. Huang, Y. Zou and C. Yang, *Adv. Mater.*, 2022, **34**, 2106954.
122 X. F. Luo, H. X. Ni, H. L. Ma, Z. Z. Qu, J. Wang, Y. X. Zheng and J. L. Zuo, *Adv. Opt. Mater.*, 2022, **10**, 2102513.
123 Y. Zhang, G. Li, L. Wang, T. Huang, J. Wei, G. Meng, X. Wang, X. Zeng, D. Zhang and L. Duan, *Angew. Chem., Int. Ed.*, 2022, **61**, e202202380.
124 Y. Xu, Q. Wang, J. Wei, X. Peng, J. Xue, Z. Wang, S. J. Su and Y. Wang, *Angew. Chem., Int. Ed.*, 2022, **61**, e202204652.
125 F. Liu, Z. Cheng, L. Wan, Z. Feng, H. Liu, H. Jin, L. Gao, P. Lu and W. Yang, *Small*, 2022, **18**, 2106462.
126 X. Cai, J. Xue, C. Li, B. Liang, A. Ying, Y. Tan, S. Gong and Y. Wang, *Angew. Chem., Int. Ed.*, 2022, **61**, e202200337.
127 C. Wang, N. Hu, Z. Chen, Y. Chen, P. Chang, C. Han, X. Cao and H. Xu, *Chem. Eng. J.*, 2024, **488**, 150785.
128 Z. Wang, C. Qu, J. Liang, X. Zhuang, Y. Liu and Y. Wang, *Molecules*, 2024, **29**, 841.
129 N. Y. Kwon, C. W. Koh, S. H. Park, H. Kwak, H. Y. Kim, C. Y. Park, N. Peethani, J. Y. Park, S. Kim, K. Jin, C. S. Hong, M. J. Cho, S. Park and D. H. Choi, *Chem. Eng. J.*, 2025, **506**, 160139.
130 Z. Yang, G. X. Yang, S. Jiang, M. Li, W. Qiu, X. Peng, C. Shen, Y. Gan, K. Liu, D. Li and S. J. Su, *Adv. Opt. Mater.*, 2024, **12**, 2301711.
131 S. Q. Song, C. F. Yip, Q. M. Liu, X. S. Zhong, Y. Wang and Y. X. Zheng, *Adv. Opt. Mater.*, 2024, **12**, 2400200.
132 X. Zhuang, B. Liang, C. Jiang, S. Wang, H. Bi and Y. Wang, *Adv. Opt. Mater.*, 2024, **12**, 2400490.
133 P. Palanisamy, O. P. Kumar, H. U. Kim, K. R. Naveen, J. Y. Kim, J. H. Baek, M. Y. Chae and J. H. Kwon, *Chem. Eng. J.*, 2024, **481**, 148781.
134 X. Song, S. Shen, S. Zou, Y. Wang, F. Guo, S. Gao and Y. Zhang, *Chem. Eng. J.*, 2024, **481**, 148794.
135 X. Song, Y. Nie, C. Jiang, B. Liang, J. Liang, X. Zhuang, H. Bi and Y. Wang, *Org. Electron.*, 2024, **125**, 106973.
136 X. F. Luo, L. Shen, J. Y. Wang and X. Xiao, *Chem. Commun.*, 2024, **60**, 574–577.
137 F. Huang, X. C. Fan, Y. C. Cheng, Y. Xie, S. Luo, T. Zhang, H. Wu, X. Xiong, J. Yu, D. D. Zhang, X. K. Chen, K. Wang and X. H. Zhang, *Adv. Opt. Mater.*, 2023, **11**, 2201950.
138 D. Chen, H. Wang, D. Sun, S. Wu, K. Wang, X. H. Zhang and E. Zysman-Colman, *Adv. Mater.*, 2024, **36**, 2412761.
139 H. Nemma, Y. Kori, N. Meguro, R. Mimura, Y. Chiba, J. Kido and H. Sasabe, *Adv. Opt. Mater.*, 2024, **13**, 2402131.
140 F. Liu, Z. Cheng, W. Dong, Y. Yan, Y. Xu, Z. Su, Y. Hu, L. Wan and P. Lu, *Angew. Chem., Int. Ed.*, 2024, **64**, e202416154.
141 Z. Cheng, F. Liu, L. Wan, Y. Hu, X. Ma, Y. Xu, Z. Su and P. Lu, *J. Phys. Chem. C*, 2024, **128**, 13756–13762.
142 S. Xiao, X. Cao, G. Chen, X. Yin, Z. Chen, J. Miao and C. Yang, *Angew. Chem., Int. Ed.*, 2024, **64**, e202418348.

143 T. Huang, Y. Xu, X. Lu, Y. Qu, J. Wei and Y. Wang, *Angew. Chem., Int. Ed.*, 2024, **63**, e202411268.
144 H. Z. Li, F. M. Xie, J. Y. Bai, K. Zhang, H. N. Shi, J. Y. Liu, X. Li, J. X. Tang and Y. Q. Li, *Small*, 2024, **20**, 2407220.
145 Z. G. L. Wu, Z. Xin, D. Liu, D. Li, J. Zhang, Y. Zhou, S. Wu, T. Wang, S. Su and W. Li, *Adv. Mater.*, 2025, **37**, 2416224.
146 Y. Z. H. Ni, J. Hu, J. Zhu, S. Xing and L. Yuan, *Adv. Opt. Mater.*, 2025, 2403139.
147 S. Li, M. Li, Y. Li, S. Chu, Y. Gao, X. Yao, W. Ji, G. Li, Z. Ren and Z. Fei, *Adv. Opt. Mater.*, 2025, 2403566.
148 C. Y. Z. Xue, Y. Hu, S. Xiao, J. Liu and J. Miao, *Angew. Chem., Int. Ed.*, 2025, **64**, e202500108.
149 P. L. L. Wan, Z. Cheng, X. Ma, Y. Jiang, Z. Yan, Y. Yan, Z. Su and F. Liu, *Chem. – Eur. J.*, 2025, **19**, e202404653.
150 R. K. Konidena, M. Yang and T. Yasuda, *Chem. Commun.*, 2023, **59**, 10251–10254.
151 Q. Wang, T. Huang, Y. Qu, X. Song, Y. Xu and Y. Wang, *ACS Appl. Mater. Interfaces*, 2024, **16**, 4948–4957.
152 Y. Zhang, J. Wei, L. Wang, T. Huang, G. Meng, X. Wang, X. Zeng, M. Du, T. Fan, C. Yin, D. Zhang and L. Duan, *Adv. Mater.*, 2023, **35**, 2005630.
153 R. Keruckiene, A. A. Vaitusionak, M. I. Hulnik, I. A. Berezianko, D. Gudeika, S. Macionis, M. Mahmoudi, D. Volyniuk, D. Valverde, Y. Olivier, K. L. Woon, S. V. Kostjuk, S. Reineke, J. V. Grazulevicius and G. Sini, *J. Mater. Chem. C*, 2024, **12**, 3450–3464.
154 Y. C. Cheng, X. C. Fan, F. Huang, X. Xiong, J. Yu, K. Wang, C. S. Lee and X. H. Zhang, *Angew. Chem., Int. Ed.*, 2022, **61**, e202212575.
155 J. Hu, X. Liang, Z. Yan, J. Liang, H. Ni, L. Yuan, J. Zuo and Y. X. Zheng, *Angew. Chem., Int. Ed.*, 2025, **10**, e202421102.
156 Y. Liu, X. Xiao, Y. Ran, Z. Bin and J. You, *Chem. Sci.*, 2021, **12**, 9408–9412.
157 W. Yang, J. Miao, F. Hu, Y. Zou, C. Zhong, S. Gong and C. Yang, *Adv. Funct. Mater.*, 2023, **23**, 2213056.
158 X. Cai, Y. Pan, X. Song, C. Li, Y. Pu, X. Zhuang, H. Bi and Y. Wang, *Adv. Opt. Mater.*, 2024, **12**, 2302811.
159 Y. Zhang, D. Zhang, T. Huang, A. J. Gillett, Y. Liu, D. Hu, L. Cui, Z. Bin, G. Li, J. Wei and L. Duan, *Angew. Chem., Int. Ed.*, 2021, **60**, 20498–20503.
160 T. Hua, N. Li, Z. Huang, Y. Zhang, L. Wang, Z. Chen, J. Miao, X. Cao, X. Wang and C. Yang, *Angew. Chem., Int. Ed.*, 2024, **63**, e202318433.
161 Y. Zou, J. Hu, M. Yu, J. Miao, Z. Xie, Y. Qiu, X. Cao and C. Yang, *Adv. Mater.*, 2022, **34**, 2201442.
162 Y. Zou, J. He, N. Li, Y. Hu, S. Luo, X. Cao and C. Yang, *Mater. Horiz.*, 2023, **10**, 3712–3718.
163 X. Cai, Y. Xu, Y. Pan, L. Li, Y. Pu, X. Zhuang, C. Li and Y. Wang, *Angew. Chem., Int. Ed.*, 2022, **7**, e202216473.
164 J. He, Y. Xu, S. Luo, J. Miao, X. Cao and Y. Zou, *Chem. Eng. J.*, 2023, **471**, 144565.
165 Y. Wang, K. Zhang, F. Chen, X. Wang, Q. Yang, S. Wang, S. Shao and L. Wang, *Chin. J. Chem.*, 2022, **40**, 2671–2677.
166 T. Fan, M. Du, X. Jia, L. Wang, Z. Yin, Y. Shu, Y. Zhang, J. Wei, D. Zhang and L. Duan, *Adv. Mater.*, 2023, **35**, e2301018.
167 X. C. Fan, F. Huang, H. Wu, H. Wang, Y. C. Cheng, J. Yu, K. Wang and X. H. Zhang, *Angew. Chem., Int. Ed.*, 2023, **62**, e202305580.
168 H. Chen, T. Fan, G. Zhao, D. Zhang, G. Li, W. Jiang, L. Duan and Y. Zhang, *Angew. Chem., Int. Ed.*, 2023, **62**, e202300934.
169 Y. Pu, X. Cai, Y. Qu, W. Cui, L. Li, C. Li, Y. Zhang and Y. Wang, *Angew. Chem., Int. Ed.*, 2024, **8**, e202420253.
170 M. Hayakawa, X. Tang, Y. Ueda, H. Eguchi, M. Kondo, S. Oda, X.-C. Fan, G. N. Iswara Lestanto, C. Adachi and T. Hatakeyama, *J. Am. Chem. Soc.*, 2024, **146**, 18331–18340.
171 L. Ge, W. Zhang, Y. H. Hao, M. Li, Y. Liu, M. Zhou and L. S. Cui, *J. Am. Chem. Soc.*, 2024, **146**, 32826–32836.
172 Y. C. Cheng, R. Walia, T. Zhang, H. Wang, X. Xiong, J. Yu, X. Fan, X. Chen, K. Wang and X. H. Zhang, *Adv. Opt. Mater.*, 2025, 2402891.
173 M. Yang, I. S. Park and T. Yasuda, *J. Am. Chem. Soc.*, 2020, **142**, 19468–19472.
174 M. Yang, S. Shikita, H. Min, I. S. Park, H. Shibata, N. Amanokura and T. Yasuda, *Angew. Chem., Int. Ed.*, 2021, **60**, 23142–23147.
175 Y. Qi, W. Ning, Y. Zou, X. Cao, S. Gong and C. Yang, *Adv. Funct. Mater.*, 2021, **31**, 2102017.
176 X. F. Luo, H. X. Ni, A. Q. Lv, X. K. Yao, H. L. Ma and Y. X. Zheng, *Adv. Opt. Mater.*, 2022, **10**, 2200504.
177 P. Ma, Y. Chen, Y. Man, Q. Qi, Y. Guo, H. Wang, Z. Li, P. Cheng, Q. Qu, C. Han and H. Xu, *Angew. Chem., Int. Ed.*, 2024, **63**, e202316479.
178 Y. Shi, H. Gou, H. Wu, S. Wan, K. Wang, J. Yu, X. Zhang and C. Ye, *J. Phys. Chem. Lett.*, 2024, **15**, 4647–4654.

